DYNAMIC AND THERMODYNAMIC MECHANISMS FOR THE ONSET OF THE SOUTHEASTERN UNITED STATES CONVECTIVE SEASON

by

Hannah C. Wells

July, 2018

Director of Thesis: Thomas M. Rickenbach, Ph.D.

Major Department: Geography, Planning, and Environment

The southeastern United States (SE US) receives ample precipitation year-round. In the winter, precipitation primarily comes from synoptic-scale baroclinic systems and cold fronts. Meanwhile, precipitation in the summer over the SE US is primarily the result of convection. With this shift from the winter to summertime precipitation regimes, spring is the transition period to the convective season, and this transition occurs rather abruptly. This shift can be described as a sudden increase in precipitation from isolated precipitation features (IPF) while precipitation from mesoscale precipitation features (MPF) stays relatively unchanged over the SE US. IPF is defined as small, short-lived, and spatially heterogeneous features while MPF is defined as larger, well-organized, and generally longer-lived precipitating features.

To study the springtime transition to the convective season, the SE US was split into twenty-seven 2°x2° boxes. Precipitation data for March-August from the National Mosaic and Multi-Sensor Quantitative Precipitation Estimation (QPE) (NMQ) for the years 2009-2012 is used to determine onset using an objective method based on IPF precipitation in each of the twenty-seven boxes for each year and for the four-year average. Meteorological data from the

North American Regional Reanalysis (NARR) is analyzed to determine potential dynamic and thermodynamic mechanisms that cause onset of the convective season in the SE US. Thermodynamic variables analyzed include convective available potential energy (CAPE), surface temperature, and specific humidity. Dynamic variables analyzed include 500 hPa geopotential height, mean sea level pressure (MSLP), and 850 hPa wind speed and direction. Daily composites of NARR are generated for May and June, while pentad average composites are generated for April-July for each year. Pentad averages of IPF will be created using the NMQ dataset to determine the pentad of onset. Three different sensitivity tests are also conducted to determine how sensitive onset is to the threshold criteria used to determine onset.

It was found that the timing of onset varies from year to year, and there is no regional progression of onset in the SE US. Along with that, IPF behavior varies quite greatly across the SE US. Despite this variation in onset timing within the four years and variation in IPF behavior across the SE US, there are similarities in meteorological conditions in the pentads immediately leading up to and during onset. The North Atlantic Subtropical High (NASH) becomes established over the SE US one to two pentads before onset, priming the atmosphere for onset by bringing warm air and moisture from the Gulf of Mexico into the SE US. As the NASH becomes established, CAPE and specific humidity increase over the SE US, providing instability and moisture for IPF precipitation to develop over the SE US. At 500 hPa, either a ridge or zonal flow is present over the SE US at the time of onset, which aids in the NASH staying established over the SE US. The results of this research have begun to provide a new framework to better understand precipitation variability in the SE US.

DYNAMIC AND THERMODYNAMIC MECHANISMS FOR THE ONSET OF THE SOUTHEASTERN UNITED STATES CONVECTIVE SEASON

A Thesis

Presented To the Faculty of the Department of Geography, Planning, and Environment

East Carolina University

In Partial Fulfillment of the Requirements for the Degree

M. S. Geography

by

Hannah C. Wells

July, 2018

DYNAMIC AND THERMODYNAMIC MECHANISMS FOR THE ONSET OF THE SOUTHEASTERN UNITED STATES CONVECTIVE SEASON

by

Hannah C. Wells

APPROVED BY:

DIRECTOR OF
THESIS: _____
(Thomas M. Rickenbach, Ph.D)

COMMITTEE MEMBER: _____
(Rosana Nieto Ferreira, Ph.D.)

COMMITTEE MEMBER: _____
(Scott Curtis, Ph.D.)

CHAIR OF THE DEPARTMENT
OF GEOGRAPHY, PLANNING, AND
ENVIRONMENT:_____
(Thad Wasklewicz, Ph.D.)

DEAN OF THE
GRADUATE SCHOOL: _____
Paul J. Gemperline, PhD

ACKNOWLEDGEMENTS

This study was funded in part by a grant (AGS-1660049) from the National Science Foundation Climate and Large-Scale Dynamics Program.

While my time at East Carolina University was filled with many personal and academic challenges, I believe my time here and overcoming these challenges made me a better student, researcher, and person. And, my success here at ECU would not have been possible without a few important people, and I would like to take this opportunity to thank them. Firstly, I would like to thank my professors at Valparaiso University, because without all of their encouragement two years ago, I never would have ended up at ECU. I would also like to thank my parents for their constant support throughout all of this, even though they don't always understand what I'm working on. I would also like to thank my advisor, Dr. Tom Rickenbach, and my committee members, Dr. Scott Curtis and Dr. Rosana Nieto-Ferreira for the advice and guidance throughout my time at ECU. I am forever grateful for all the help, advice, and mentorship they gave me with my research and other work here at ECU. I also want to thank my friends, both near and far, for always supporting me and being there for me no matter what. I would also like thank my fellow graduate students in the Department of Geography, Planning, and Environment. My time here would not have been as enjoyable without them, and I am grateful for the friendships I made while here. My experiences and memories of my time at ECU will be something I remember forever. And finally, I would like to thank Dr. Jen Golbeck and her family of 5 golden retrievers, The Golden Ratio, for always making me smile and making graduate school a little bit easier.

TABLE OF CONTENTS

LIST OF TABLES vii

LIST OF FIGURES viii

CHAPTER 1: INTRODUCTION 1

CHAPTER 2: REVIEW OF LITERATURE 5

2.1 Precipitation Variability in the Southeastern United States 5

2.2 Similarities to the Monsoon 8

2.3 North Atlantic Subtropical High 12

2.4 Other Large-Scale Atmospheric Influences 15

CHAPTER 3: QUESTIONS AND OBJECTIVES 18

CHAPTER 4: DATA AND METHODOLOGY 19

4.1 Study Area 19

4.2 Data 19

4.2.1 North American Regional Reanalysis 19

4.2.2 National Mosaic and Multi-Sensor Quantitative Precipitation Estimation 20

4.3 Data Analysis 22

4.3.1 Analysis of NMQ and NARR 23

4.3.2 Determining Onset of the Convective Season 27

4.3.3 Sensitivity Tests 28

CHAPTER 5: RESULTS AND DISCUSSION 30

5.1 Results of IPF Onset Determination 30

5.2 Results of the Sensitivity Tests of IPF Onset Date Determination 45

5.3 Onset Dates and Meteorological Conditions: 2009 59

5.5 Onset Dates and Meteorological Conditions: 2011 72

5.6 Onset Dates and Meteorological Conditions: 2012 77

5.7 Similarities in Onset Behavior 83

CHAPTER 6: CONCLUSIONS 87

REFERENCES 91

LIST OF TABLES

Table 1: Summary of criteria to determine onset and for each sensitivity test. 45

Table 2: Average onset date for the SE US & standard deviation of onset for 2009 for the Average of the Maxima, 30 Day Average, 4-year Regional Average, and Annual Regional Average. 53

Table 3: As in Table 2, but for 2010. 53

Table 4: As in Table 2, but for 2011. 54

Table 5: As in Table 2, but for 2012. 54

Table 6: Four-year (2009-2012) average onset date and standard deviation for the Average of the Maxima. 55

Table 7: As in Table 6, but for the 30 Day Average. 56

Table 8: As in Table 6, but for the 4-year Regional Average. 57

Table 9: As in Table 6, but for the Annual Regional Average. 58

Table 10: Monthly mean longitude and latitude of the NASH for 2009-2012. 86

LIST OF FIGURES

Figure 1: Annual precipitation in North Carolina, demonstrating that the SE US receives precipitation year-round. 2

Figure 2: 2009-2012 seasonal cycle composite of IPF from Rickenbach et al., 2015. 2

Figure 3: 2009-2012 seasonal cycle composite of MPF. From Rickenbach et al., 2015. 3

Figure 4: Daily average precipitation for 4 August 2009 for total, MPF, and IPF. From Rickenbach et al., 2015. 4

Figure 5: Dry period circulation at 500 hPa (a) and 850 hPa (b). Geopotential height is dark solid lines and thinner lines are anomalies (solid are positive and dashed are negative anomalies. From Diem, 2006. 7

Figure 6: Same as Fig. 5, but for wet periods. 7

Figure 7: Onset of the South American monsoon, From Nieto Ferreira and Rickenbach, 2011.. 10

Figure 8: Example of a stationary cold front over South America. From Garreaud, 2000. 10

Figure 9: 00 UTC GFS on 1 June 2017, valid for 00 UTC on 2 June 2017. The western ridge of the NASH can be seen over the SE US. Filled colors indicate temperature (°F), contours show mean sea level pressure, and the barbs indicate the 10 m wind (knots). From College of DuPage. 14

Figure 10: WSR-88D radars that will be used to study the SE US (from Rickenbach, et al., 2015). 21

Figure 11: The twenty-seven 2°x2° boxes over the SE US. 23

Figure 12: Four-year (2009-2012) averaged monthly-mean maps of IPF rain rate for the SE US for: March, April, May, June, July, and August. 24

Figure 13: Onset for 2009 in the SE US. 30

Figure 14: Time series of IPF from 1 March-31 August 2009 for the box at 25°-27° N, 80°-82 W°. Onset occurs on12 May 2009 for this box. 32
Figure 15: Same as Fig. 14, but for the box located at 31°-33° N, 86°-88° W. Onset occurs on 7 May 2009 for this box. 32
Figure 16: Same as Fig. 14 but for the box located at 35°-37° N, 84°-86° W. Onset occurs on 29 April 2009 in this box. 33
Figure 17: Onset in each box for the SE US for 2010. 34
Figure 18: Time series of IPF for March 31-August 2010 for the box located at 29°-31° N, 82°-84° W. Onset occurs in this box on 17 May 2010. 35
Figure 19: As in Fig. 18, but for 33°-35° N, 82°-84° W. Onset occurs in this box on 17 June 2010 35
Figure 20: As in Fig. 18, but for 35°-37° N, 88°-90° W. Onset occurs in this box on 22 April 2010 36
Figure 21: Onset dates for each box in the SE US in 2011 37
Figure 22: IPF time series for 1 March-31 August 2011 for 27°-29° N, 80°-82° W. Onset occurs on 15 June. 38
Figure 23: IPF time series for 1 March-31 August 2011 for 33°-35° N, 86°-88° W. Onset occurs on 10 June. 38
Figure 24: IPF time series for 1 March-31 August 2011 for 35°-37° N, 80°-82° W. Onset occurs on 10 May. 39
Figure 25: Onset dates for the SE US for 2012. 40
Figure 26: IPF time series for 1 March-31 August 2012 for the box at 25°-27° N, 80°-82° W. Onset occurs on 28 April. 41

Figure 27: As in Fig. 26, but for the box at 29°-31° N, 84°-86° W. Onset occurs on 17 May..... 42

Figure 28: As in Fig. 26, but for 35°-37° N, 76°-78° W. Onset occurs on 5 May. 42

Figure 29: Onset in the SE US for the four-year average. 43

Figure 30: IPF time series for 1 March-31 August, 2009-2012 for the box at 25°-27° N, 80°-82° W. Onset occurs on 12 May. 44

Figure 31: As in Fig. 30, but for the box at 33°-35° N, 82°-84° W. Onset occurs on 14 May..... 44

Figure 32: As in Fig. 30, but for the box at 35°-37° N, 88°-90° W. Onset occurs on April 20.... 45

Figure 33: Onset in the SE US in each box for the first sensitivity test, using the thirty day average for: 2009, 2010, 2011, 2012, and the four-year average. 47

Figure 34: Same as Fig. 33, but for the second sensitivity test using the four-year regional average of IPF. 49

Figure 35: Onset dates for each box in the SE US for the third sensitivity test using the annual average of IPF of each year for: 2009, 2010, 2011, and 2012. 51

Figure 36: Specific humidity (g/kg, filled) and temperature (°C, contoured) for the pentads 21-25 April and 26-30 April 2009..... 60

Figure 37: CAPE (J/kg) for the pentad 26-30 April 2009. 60

Figure 39: 500 hPa geopotential height in geopotential meters (gpm) for 26-30 April 2009. 61

Figure 38: As in Fig. 36, but for MSLP (hPa) and 850 hPa wind (kt). 61

Figure 40: CAPE (J/kg) for the pentads 1-5 May and 6-10 May 2009..... 62

Figure 41: As in Fig. 40, but for specific humidity (g/kg, filled) and temperature (°C, contoured). 62

Figure 42: As in Fig. 40, but for MSLP ((hPa) and 850 hPa winds (kt). 63

Figure 43: 500 hPa geopotential height (gpm) for 6-10 May 2009. 65

Figure 44: 850 hPa wind (kt) and MSLP (hPa) for 21-25 April 2010. 66
Figure 45: CAPE (J/kg) over the SE US for 26-30 April and 1-5 May 2010. 67
Figure 46: As in Fig. 45, but for specific humidity (g/kg, filled) and temperature (°C, contoured). 67
Figure 47: 850 hPa winds (kt) and MSLP (hPa) for 1-5 May 2010. 68
Figure 48: CAPE (J/kg) for 11-15 May and 21-25 May 2010. 68
Figure 49: Specific humidity (g/kg, filled) and temperature (C, contoured) for: 6-10 May, 11-15 May, 21-25 May, 26-31 May 2010. 70
Figure 50: MSLP (hPa) and 850 hPa winds (kt) for 11-15 May and 16-20 May 2010. 71
Figure 51: CAPE (J/kg) for the pentads: 21-25 May, 26-31 May, and 1-5 June 2011. 73
Figure 52: As in Fig. 51, but for specific humidity (g/kg filled) and temperature (°C, contoured). 74
Figure 53: MSLP (hPa) and 850 hPa winds (kt) for 21-25 May and 26-31 May 2011. 76
Figure 54: As in Fig. 53, but for 6-10 June 2011. 76
Figure 55: 500 hPa geopotential height (gpm) for 1-5 June and 6-10 June 2011. 77
Figure 56: Specific humidity (g/kg, filled) and temperature (°C, contoured) for 16-20 April 2012. 77
Figure 57: As in Fig. 56, but for CAPE (J/kg). 77
Figure 58: As in Fig. 56, but for MSLP (hPa) and 850 hPa winds (kt). 78
Figure 59: As in Fig. 52, but for 500 hPa geopotential height (gpm). 79
Figure 60: CAPE (J/kg) for 1-5 May 2012. 80
Figure 61: Specific humidity (g/kg, filled) and temperature (°C, contoured) for 26-30 April and 1-5 May 2012. 80

Figure 62: As in Fig. 61, but for MSLP (hPa) and 850 hPa winds (kt). 81

Figure 63: As in Fig. 61, but for 500 hPa geopotential height (gpm). 81

Figure 64: Specific humidity (g/kg, filled), and temperature (°C, contoured) for 11-15 June 2012. 82

Figure 65: As in Fig. 64, but for CAPE (J/kg). 83

Figure 66: Four-year average of 850 hPa wind (kt) and mean sea level pressure (hPa) for 01-05 April, 01-05 May, and 11-15 June 2009-2012. 86

CHAPTER 1: INTRODUCTION

The southeastern United States (SE US) receives ample precipitation year-round (Fig. 1). In the winter, precipitation is dominated by synoptic-scale baroclinic systems, while in the summer, precipitation is also produced by locally-generated convection. Previous research in this area (Rickenbach et al., 2015) shows that the springtime transition from the winter to summer regime occurs abruptly for isolated precipitation features (IPF) (Fig. 2), with rain from mesoscale precipitation features (MPF) showing little change (Fig. 3). IPF are defined as small, short-lived, and spatially heterogeneous precipitating features, and MPF are defined as larger, well-organized, and generally longer-lived precipitating features (Fig. 4). Studying precipitation with this MPF/IPF framework is important to better understand the connection between precipitation and the large scale seasonal forcing. Previous research has found that MPF are primarily associated with larger – dynamical forcing, such as forcing associated with the frontal regions of midlatitude cyclones (Rickenbach et al., 2015). Precipitation with mesoscale organization has forcing mechanisms, internal circulations, and vertical profiles of latent heat that are distinct from precipitation without mesoscale organization (Houze, 1989). This project will explore the dynamic and thermodynamic mechanisms that cause the abrupt shift in IPF precipitation in the springtime.

While it is well-known how the atmosphere evolves dynamically and thermodynamically as spring transitions to summer, how those mechanisms work to cause this abrupt shift have not yet been studied. Although the annual precipitation cycle in the SE US has been studied extensively, Rickenbach et al. (2015) recently found that much of the wintertime precipitation comes from synoptic-scale systems and summertime precipitation being a result of much smaller scale systems, such as convection or sea breeze effects, with the spring being a

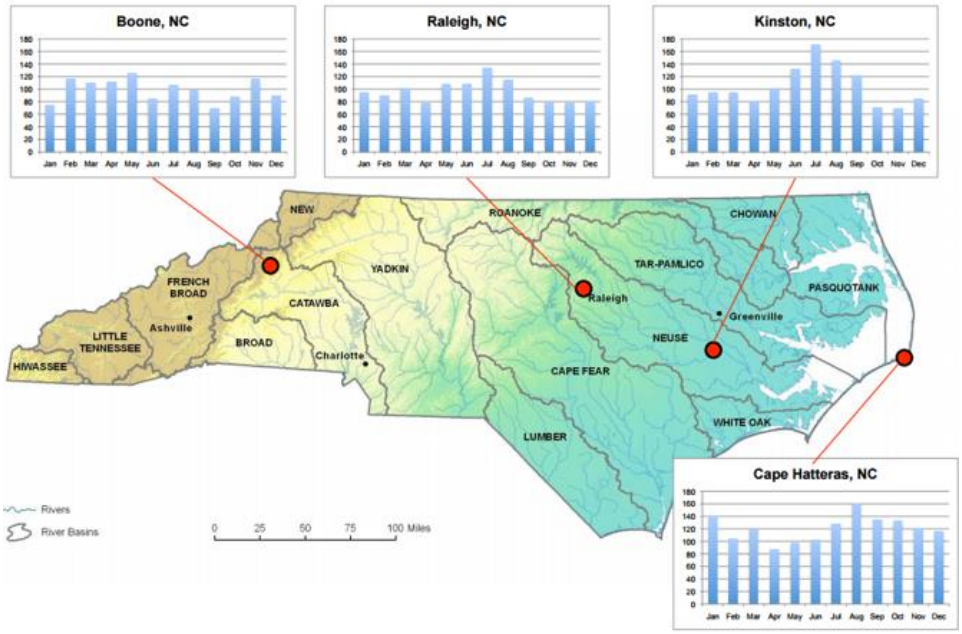

Figure 1: Annual precipitation in North Carolina, demonstrating that the SE US receives precipitation year-round.

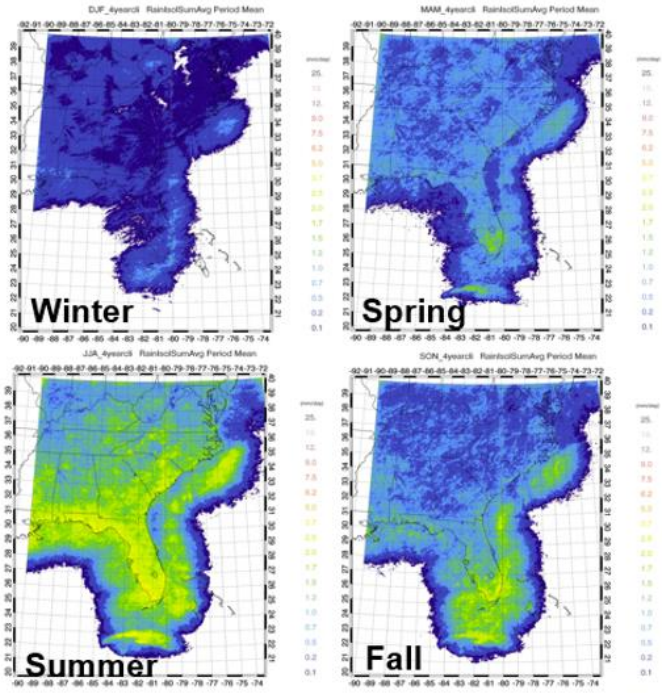

Figure 2: 2009-2012 seasonal cycle composite of IPF from Rickenbach et al., 2015.

transition period between those regimes. However, very little research has been done to study what mechanisms cause this precipitation transition to occur in the springtime in the SE US. When compared to other seasonal precipitation regimes around the globe (such as the monsoon), the SE US has received little attention. Dynamic and thermodynamic mechanisms, such as the shifting jet stream and cyclone tracks, North Atlantic Subtropical High, passage of midlatitude cyclones and their cold fronts, and increasing temperature and convectively available potential energy, will be analyzed to determine what role each plays in the transition to the onset of the convective season.

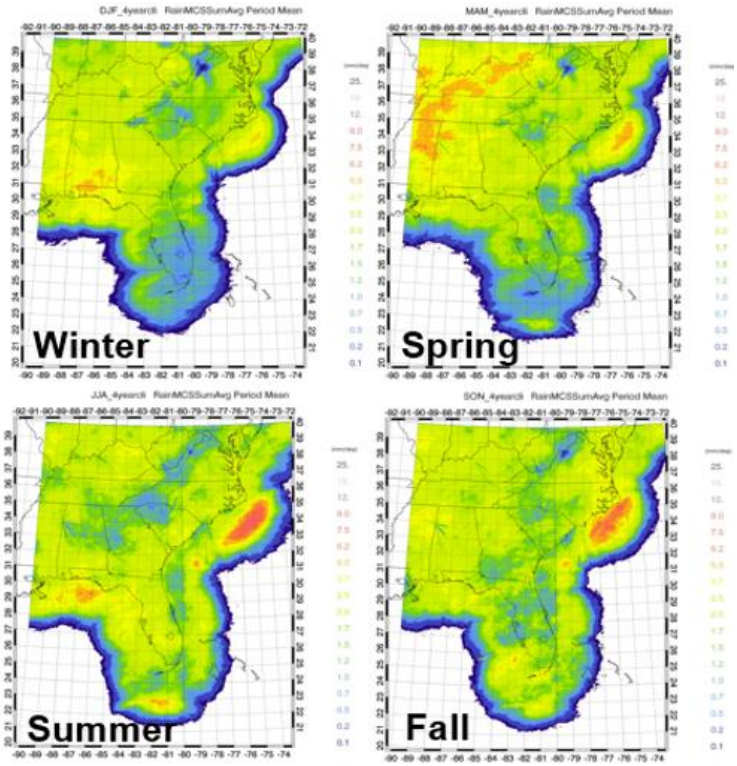

Figure 3: 2009-2012 seasonal cycle composite of MPF. From Rickenbach et al., 2015.

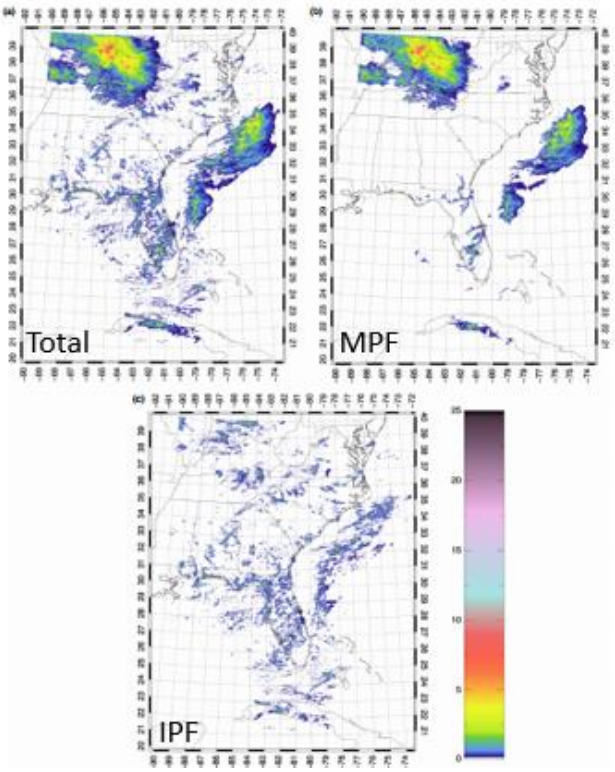

Figure 4: Daily average precipitation for 4 August 2009 for total, MPF, and IPF. From Rickenbach et al., 2015.

CHAPTER 2: REVIEW OF LITERATURE

2.1 Precipitation Variability in the Southeastern United States

There has been much research done in studying the annual cycle of precipitation and creating a precipitation climatology in the SE US. Prat and Nelson (2014) created a thirteen-year rainfall climatology for the SE US using remotely sensed data from 1998 – 2010 and studied the annual, seasonal, and diurnal patterns of rainfall. The diurnal cycle of precipitation in particular is important because it is still not very accurately represented in regional climate models and global circulation models. During the cold season in the SE US, the precipitation maximum is west of Atlanta, Georgia, and precipitation is dominated by synoptic – scale weather systems moving west to east. However, the maximum of precipitation in the warm season is along the coastal areas, likely due to effects of the sea breeze. It was also found that cold season precipitation is characterized by rain events frequently occurring during the day with no contrast between the land and ocean. On the contrary, warm season precipitation is characterized by a strong land/ocean contrast. During the warm season, precipitation tends to fall over the land in the afternoon and early evening, with morning rain occurring over the ocean (Prat and Nelson, 2014).

Rickenbach et al. (2015) created a four year precipitation climatology for the SE US using a classification of instantaneous precipitation features based on feature size. This is a different approach from most precipitation climatologies for the SE US that categorize precipitation into stratiform and convective precipitation, or into frozen versus liquid precipitation. However, a size – based classification is useful, since the size of precipitation features relates to daily and seasonal forcing (Nesbitt et al., 2006, Rickenbach et al., 2015). Precipitation features were classified as either MPF or IPF based on a feature size threshold.

Precipitation spatially larger than 100 km is categorized as mesoscale precipitation features (MPF), and precipitation spatially smaller than 100 km is categorized as isolated precipitation features (IPF). 100 km is the threshold used as that is the threshold where different forcings become important for precipitation development. At sizes larger than 100 km, larger scale synoptic forcings are important for the formation of MPF precipitation, while local – scale forcings are important below 100 km for the formation of IPF (Rickenbach et al., 2015). Isolated precipitation typically forms in response to the sea breeze, topographic circulations, or thermal circulations, and is modulated by the diurnal cycle of solar radiation (Rickenbach et al., 2015). It was found that 70 – 90% of precipitation is due to MPF, with a decrease in the summer and the southern coastal areas. MPF also has a very small seasonal cycle, and no clear diurnal cycle. However, IPF has a very prominent seasonal cycle that outlines the southeast coast in the summer. Similar to what Prat and Nelson (2014) found for warm season precipitation in the SE US, it was concluded that isolated precipitation is thermodynamically driven, forced by surface heating, thermodynamic instability, thermal circulations (i.e. the sea breeze), or a combination of those forcings. The diurnal cycle of isolated precipitation is also similar to the diurnal cycle of warm season precipitation from Prat and Nelson (2014). Isolated precipitation forms preferentially off shore at night and in the early morning, and forms onshore in the afternoon as a response to daytime heating (Rickenbach et al., 2015).

A study by Diem in 2006 examined the synoptic-scale controls on summer precipitation in the SE US, focusing on features such as the Bermuda High (also known as the North Atlantic

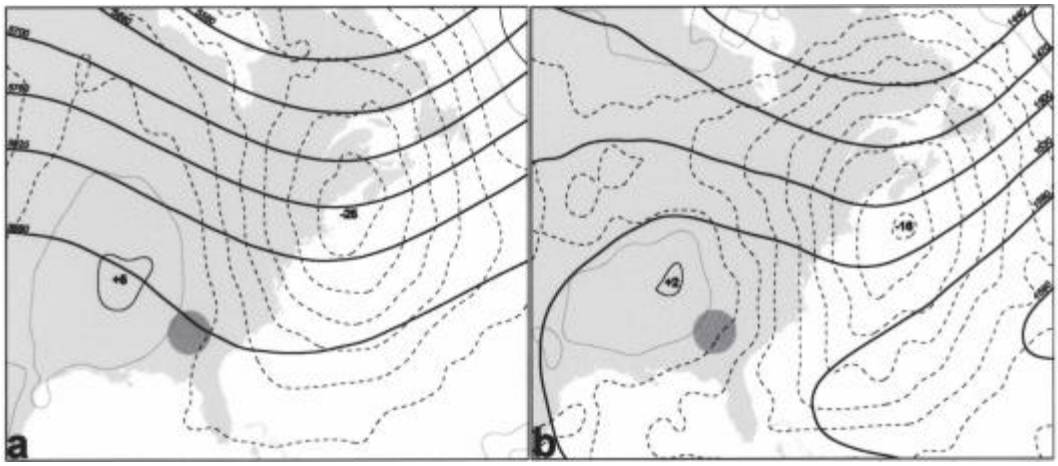

Figure 5: Dry period circulation at 500 hPa (a) and 850 hPa (b). Geopotential height is dark solid lines and thinner lines are anomalies (solid are positive and dashed are negative anomalies. From Diem, 2006.

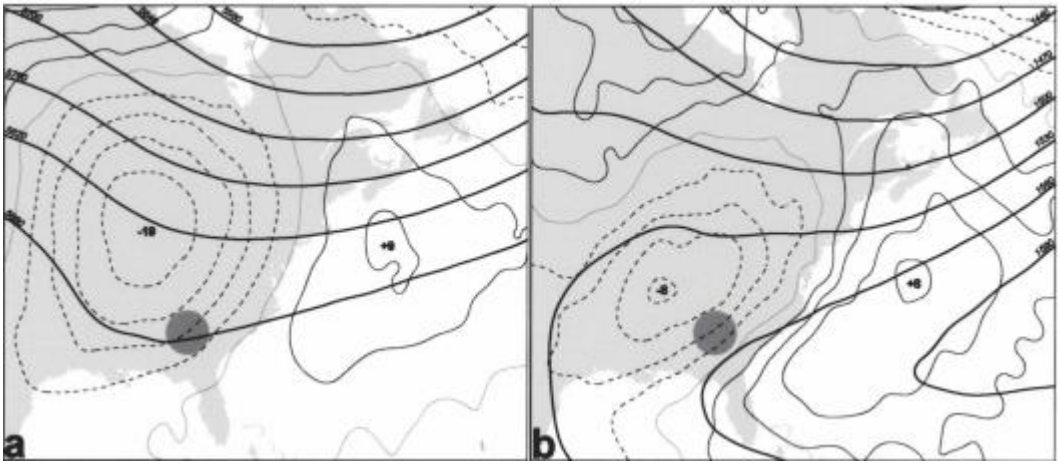

Figure 6: Same as Fig. 5, but for wet periods.

Subtropical High (NASH)) and upper-level troughs and ridges. The Bermuda High Index (BHI) measures the slope of the sea level pressure gradient from Bermuda to New Orleans, Louisiana in order to assess the presence and strength of the Bermuda High. Positive values of the BHI are indicative of enhanced southerly moisture advection and decreased stability over the SE US (Diem, 2006), and previous studies had found a significant positive correlation between the BHI

values and summer precipitation totals over the SE US (Henderson and Vega, 1996). Diem (2006) also found that wet periods in the SE US in the summer coincided with midtropospheric troughing to the west with large shifts in the low-level circulation (Fig. 6). At both 500 hPa and 850 hPa for wet periods (Fig. 6), there are positive height anomalies off the coast of the SE US. The positive height anomalies indicate high pressure at the surface, and the geopotential height at 850 hPa resembles the western ridge of the NASH or Bermuda High. These shifts in the low-level circulation at 850 hPa produce strong southwesterly flow over the SE US, leading to moisture advection from the Gulf of Mexico. It was also found that along with midtropospheric troughing, fronts were present on nearly 40% of these wet periods (Diem, 2006). For dry periods during the summer in the SE US, Diem (2006) found that midtropospheric troughing was displaced to the east, with high pressure over the Midwest and SE US that was a result of either an anticyclone or a westward expansion of the NASH (Fig. 5). The negative height anomalies off the coast of the SE US in Figure 5 indicate that the NASH is either not present or rather weak, as negative height anomalies usually correlate to lower pressure at the surface. The negative height anomalies produce weak northwesterly flow over the SE US, causing a decrease in precipitation (Diem, 2006). From this study by Diem, it is clear that the NASH plays an important role in precipitation over the SE US in the summer, with wetter summers when the NASH is present, and less precipitation when the NASH is not present.

2.2 Similarities to the Monsoon

The monsoon has traditionally been considered a seasonal reversal in the direction of the wind in certain parts of the world that is associated with an increase in precipitation during the monsoon season, such as the monsoon in Southeast Asia (Gadgil, 2003). Onset of the Asian monsoon occurs in southeast Bay of Bengal in late April, then progresses northeastward to the

Indochina Peninsula in early May, the South China Sea by mid-May, and into the subtropical western North Pacific by late May. Monsoon onset occurs in the Indian subcontinent by late May (Wang and Ho, 2002). The abrupt transition to the convective season in the SE US exhibits some similarities to the onset of the monsoon in South America. Understanding the mechanisms that cause the onset of the monsoon could be useful in determining what causes the abrupt transition to the convective season in the spring. Particularly in the South Atlantic Convergence Zone (SACZ), the onset of the monsoon season is rather abrupt (Fig 7). Monsoon onset in the SACZ typically occurs between 28 October and 1 November. In Nieto Ferreira et al. (2011), the mechanisms that cause the sudden monsoon onset in the SACZ were investigated. As the monsoon onset in this region is abrupt, the onset was hypothesized to likely be dynamically driven. During southern hemisphere spring, the jet stream begins moving poleward, and as a result, midlatitude cyclones (MLCs) form in regions of stronger anticyclonic shear that leads to upper-level thinning troughs. Near the time of onset, the anticyclonic shear reaches a critical threshold that results in a thinning trough. These troughs tilt westward as they move equatorward, sometimes becoming cut-off cyclones. Thinning troughs also favor the development of stationary cold fronts at the surface, which were concluded to be what triggered the onset of the monsoon in the SACZ (Fig. 8). Once the critical threshold for anticyclonic shear is reached, the dynamic structure of MLCs changes abruptly, and the resulting stationary cold front over the SACZ triggers the onset of the monsoon season (Nieto Ferreira et al., 2011). While onset mechanisms for the convective season in the SE US will likely be different from what causes the monsoon onset in South America, there could still be similarities. Dynamic mechanisms will likely play a role in causing onset of the convective season in the SE US, such as the position of the NASH triggering onset in a similar way to how stationary fronts trigger

onset in South America. As in the South American monsoon onset, the poleward movement of the jet and cyclone tracks over the United States during the spring could also play a role in triggering onset.

Methods of determining monsoon onset in other regions such as South America will guide the onset criteria used to determine onset of the convective season in the SE US. A study by Marengo et al. (2001) examined the onset and end of the monsoon in the Amazon Basin of Brazil from 1979 – 1996. In this study, criteria for determining onset and end of the monsoon in this region were defined, and the progression of onset based on the criteria was examined, along with the sensitivity of onset to the threshold criteria. Onset was defined as the five – day average (pentad) where precipitation exceeded 4 mm/day, given that precipitation in 6 of the 8 subsequent pentads exceeded 4.5 mm/day and precipitation in 6 of the 8 preceding pentads was below 3.5 mm/day. Based on this criteria, it was found that monsoon onset progresses toward the

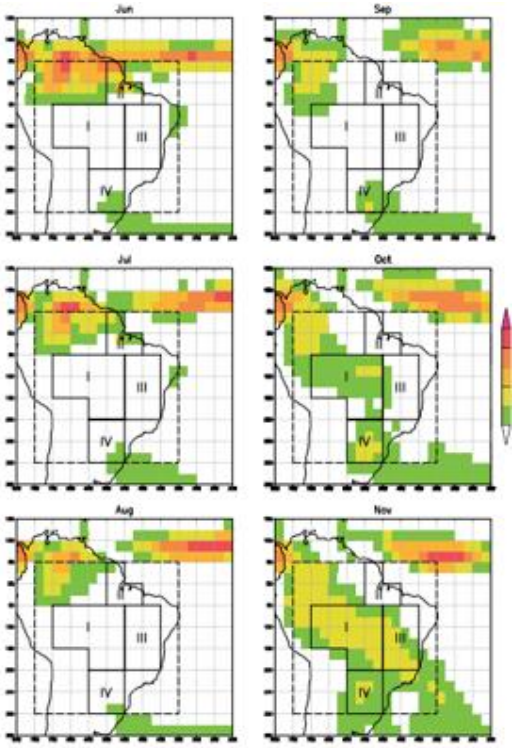

Figure 7: Onset of the South American monsoon, From Nieto Ferreira and Rickenbach, 2011.

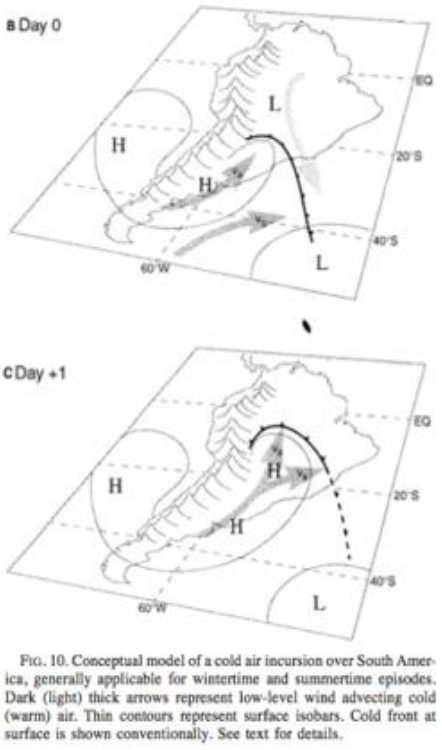

FIG. 10. Conceptual model of a cold air incursion over South America, generally applicable for wintertime and summertime episodes. Dark (light) thick arrows represent low-level wind advecting cold (warm) air. Thin contours represent surface isobars. Cold front at surface is shown conventionally. See text for details.

Figure 8: Example of a stationary cold front over South America. From Garreaud, 2000.

southeast in the Amazon Basin. It was also found that because precipitation almost always exceeds 4 mm/day in the northwest, onset is not defined there based on the threshold used. Sensitivity of onset to the precipitation threshold was also examined, and they found that a 1 mm decrease in the onset threshold resulted in approximately a twenty day lengthening of the monsoon season. Furthermore, onset becomes more clearly defined in the northwestern region of the Amazon Basin when the onset threshold is increased. And, when the onset threshold is doubled, it was found that onset was reversed and progressed toward the northwest (Marengo et al., 2001).

Nieto-Ferreira and Rickenbach (2011) examined onset of the South American monsoon, from 1979 – 2007. A constant threshold technique was used, similar to Marengo et al. (2001). The South American monsoon region was split into 5°x5° boxes, and the pentad precipitation within each box was calculated. The threshold for monsoon onset in this study was 4.6 mm/day, as that was the mean rain rate from 1979 – 2007. Similar to Marengo et al. (2001), a pentad was considered the onset date if precipitation in six of the eight subsequent pentads exceeded the threshold by at least 0.5 mm/day and precipitation in six of the eight preceding pentads was at least 0.5 mm/day below the threshold. In some of the boxes, onset could not always be defined because precipitation never exceeded the threshold or precipitation oscillated around the climatological mean threshold year – round (Nieto-Ferreira and Rickenbach, 2011).

The North American monsoon (NAM) is a warm-season phenomenon over parts of northwestern Mexico and the southwestern United States (Adams and Comrie, 1997). The NAM is characterized largely by a transition from a very dry June to a rainy July (Adams and Comrie, 1997). The development stage of the NAM occurs from May to June and is characterized as a transition period where midlatitude cyclone tracks and the jet stream move northward, along with

an amplified diurnal cycle for precipitation over the Great Plains (Higgins et al., 1997). The onset of the monsoon begins with heavy rain over southern Mexico and quickly moves northward into the southwest US by early July. Increases in precipitation over northwestern Mexico coincide with an increase in vertical moisture transport and southerly winds from the Gulf of California. Over the southwestern US, increases in precipitation coincide with the formation of an anticyclone at the jet stream level, and is known as the monsoon high (Higgins et al., 1997). The mature stage of the NAM occurs from July to August. During this stage, the NAM is fully developed, and the monsoon high is associated with enhanced upper-level divergence near and to the south with enhanced rainfall over Mexico. To the east and north of the monsoon high, the upper-level flow is convergent and rainfall decreases during this stage (Higgins et al., 1997). This stage of the NAM has also been linked to increased upper-level divergence and precipitation associated with an induced trough over the eastern US (Higgins et al., 1997). While the NAM may or may not play a role in IPF onset, the monsoon does occur over the western United States and should be taken into consideration when looking at IPF onset in the SE US.

2.3 North Atlantic Subtropical High

The North Atlantic Subtropical High (NASH) dominates the weather pattern, particularly precipitation, in the SE US in the late spring and summer. Therefore, understanding how the NASH influences precipitation in the SE US during the spring and summer will aid in understanding what, if any, role it plays in the onset of the convective season. The NASH is a semi-permanent subtropical high pressure system that weakens and intensifies and changes location throughout the year. In the spring, it migrates westward and by June, July, and August

(JJA), the NASH's surface center is near Bermuda, and its western ridge is over the eastern United States (Li et al., 2011) (Fig. 9). Li et al. (2011) define the western ridge of the NASH as the location where the 1560 gpm (geopotential meter) line at 850 hPa intersects the ridge line of the NASH. During the late spring and early summer, the NASH migrates westward and southward.

April and May are defined as the transitional months from the winter to summer pattern of the NASH (Davis et al., 1997). By May, the NASH strengthens and expands westward and the southwest to northeast flow north of the high is established (Davis et al., 1997). The exact position of the western ridge over the eastern US strongly influences precipitation patterns in the SE US. When the ridge is located further north, rainfall over the SE US decreases as the area is dominated by subsidence. Precipitation in the SE US increases when the ridge is centered further south due to southwesterly winds transporting ample moisture and warm air from the Gulf of Mexico and Atlantic Ocean (Li et al., 2011; Davis et al., 1997). Recent studies suggest that the NASH has intensified over the past thirty years, allowing for the western ridge to extend further over the eastern US (Li et al., 2011). With this intensification and further westward extent of the NASH, the north-south movement of the western ridge of the NASH over the SE US has also increased, causing the NASH to have an even greater influence on summertime precipitation (Li

et al., 2011). This indicates that likelihood of both anomalously dry and wet summers has increased in the SE US (Li et al., 2011).

Seager et al. (2003) analyzed the impact of air-sea interactions on the NASH. During the spring, sea surface temperatures (SSTs) are warmer on the western side of the NASH over the western Atlantic Ocean due to poleward flow and upward vertical motion, with cooler SSTs on the eastern side of the NASH over the eastern Atlantic Ocean resulting from equatorward flow and subsidence. This leads to a stable atmosphere on the eastern side with little convection and an unstable atmosphere with deep convection on the western side of the NASH (Seager et al., 2003). Enhanced convection on the western side of the NASH over the SE US is another way that the NASH greatly influences precipitation in the SE US. Understanding the mechanisms that produce and maintain subtropical highs can provide a better understanding of how the NASH then influences precipitation during the spring and summer in the SE US.

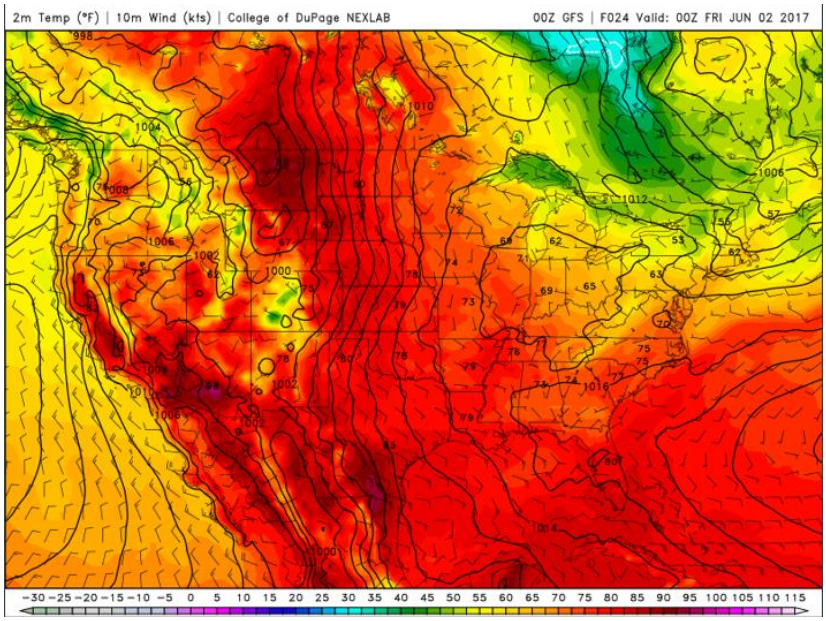

Figure 9: 00 UTC GFS on 1 June 2017, valid for 00 UTC on 2 June 2017. The western ridge of the NASH can be seen over the SE US. Filled colors indicate temperature (°F), contours show mean sea level pressure, and the barbs indicate the 10 m wind (knots). From College of DuPage.

2.4 Other Large-Scale Atmospheric Influences

The Pacific/North American (PNA) teleconnection pattern is the main mode of mid-tropospheric variability in the northern hemisphere during fall, winter, and spring. The PNA has been shown to be highly correlated with regional temperatures and precipitation in North America, with the NW and SE US having the highest correlations for temperature (Leathers et al., 1991). Temporally, the PNA is evident on time scales of days, weeks, months, seasons, and even decades (Leathers et al., 1991). A positive phase of the PNA is characterized by a trough in the east-central Pacific Ocean, ridging over the western US, and a trough over the eastern US, whereas a negative phase of the PNA will have the opposite pattern. A positive phase of the PNA generally exhibits a negative correlation on temperatures in the SE US from March – May, meaning temperatures are below average. In March, the ridge – trough system starts becoming longitudinally compressed so the most negative temperature correlation shifts west toward the southeast and Texas. In April, the longitudinal compression of the pattern continues, with the negative center shifting further west to Louisiana and East Texas. However, the pattern shifts by May, and the negative center moves northeastward and is broadly centered over the eastern portion of the SE US (Leathers et al., 1991). For precipitation, the areas with a large correlation between the PNA index and precipitation are much weaker and smaller in area when compared to the temperature. In March, the strongest negative correlation between the PNA and precipitation is centered over the Ohio Valley, and very weak positive values over the coast of the SE US. In April, the negative center shifts northward over the Dakotas, with no distinct correlation between the PNA and precipitation over the SE US. The pattern in May is spatially similar to April, however, it is weaker overall, and there are slightly higher positive values over the SE US (Leathers et al., 1991). Overall, the PNA has a strong influence on both regional

temperature and precipitation in the United States during the spring, with the PNA primarily affecting the temperatures more than precipitation in the SE US. While this study does not specifically investigate the PNA as a mechanism that causes onset of the convective season in the SE US, its influence on temperature and precipitation in the SE US could impact the timing on onset. A positive phase of the PNA in the spring could potentially cause onset to occur later, as a positive PNA generally leads to below average temperatures in the SE US.

The effects of the El Niño/Southern Oscillation (ENSO) on North American precipitation and temperature patterns were studied by Ropelewski and Halpert (1986). Monthly mean temperatures and monthly precipitation totals from weather station data spanning 1875-1980 was used (Ropelewski and Halpert, 1986). It was found that precipitation in the SE US from October-March during an El Niño year was above average due to the subtropical jet transporting moisture across the SE US. For temperature, it was concluded that El Niño events tended to result in below average temperatures in the SE US from October-March (Ropelewski and Halpert, 1986). While the influences of ENSO on precipitation and temperature patterns in the SE US are not as clear during the transition season of April and May, the above average precipitation and below average temperatures during an ENSO event could influence the onset of the convective season. ENSO also has an influence on sea surface temperatures (SST) and sea level pressure (SLP) in the Atlantic Ocean. During an El Niño event, SSTs in the tropical Atlantic basin become anomalously warm and the North Atlantic trade winds are weaker in the winter and spring months (Curtis and Hastenrath, 1995). During La Niña, SSTs in the Atlantic will be below average with enhanced northeast trade winds. These characteristics of El Niño and La Niña in the Atlantic are distinct during the spring in March to April (Curtis and Hastenrath, 1995). A study by Giannini et al. (2000) examined the relationship between ENSO and SST and SLP in the

Atlantic. The study found that when SLP is lower over the central Pacific during an El Niño event, SLP tends to be higher over the central Atlantic, with the Caribbean acting as the boundary between these positive and negative SLP anomalies. These higher than average SLP in the Atlantic can also weaken the trade winds, and increase SSTs in the season following the mature phase of an ENSO event (Giannini et al., 2000). This study also found that higher than average SLP in the North Atlantic Subtropical High is associated with positive SST anomalies on the east coast of North America (Giannini et al., 2000). The relationship between ENSO and SLP and SST in the Atlantic could influence when onset occurs in a particular year.

CHAPTER 3: QUESTIONS AND OBJECTIVES

The objective of this thesis is to improve understanding of the onset of the convective season in the SE US. In particular, the dynamic and thermodynamic mechanisms that cause the transition to the convective season will be explored, along with creating a technique for identifying onset. The following questions will be explored:

1.) How can the springtime onset of the convective season be characterized?
2.) What dynamic and thermodynamic mechanisms cause the transition to the convective season?

This project aims to improve our understanding of the mechanisms of seasonal precipitation transition in the SE US, which will improve our understanding of regional precipitation variability. The results of this research project can hopefully be used to improve model simulations of precipitation trends in a future climate. Better understanding what mechanisms cause the seasonal shift in precipitation in the SE US can be used to validate the mechanisms for precipitation variability in climate models. The techniques used analyze the onset of the convective season in the SE US could also be used to study other areas of the world with a similar seasonal shift in precipitation, for example in the subtropical fringes of monsoon regions. Finally, our results will help researches evaluate the degree to which the summertime transition to the convective season in the SE US shares characteristics with monsoon climate.

CHAPTER 4: DATA AND METHODOLOGY

4.1 Study Area

The study area focuses on the Southeast United States (SE US). The study area for this project will be the same study area from Rickenbach et al. (2015), spanning from Louisiana to the Ohio Valley in the west, and from Florida to the North Carolina-Virginia in the east. This study area was selected because the mechanisms that cause the shift from synoptic-scale wintertime precipitation to the smaller scale summertime precipitation (i.e. convection) has not been studied for the SE US. The 2009 – 2012 precipitation dataset used by Rickenbach et al. (2015) is available for the SE US, with precipitation already separated into MPF and IPF components each hour, and compiled for each day.

4.2 Data

4.2.1 North American Regional Reanalysis

The North American Regional Reanalysis (NARR) is a long-term, high resolution, and high frequency atmospheric and land surface hydrology dataset for North America that is much improved over previous reanalysis datasets (Mesinger et al. 2006). The NARR is produced by the National Centers for Environmental Prediction (NCEP), and combines NCEP Eta model data and assimilated observational data into a continuous and spatially uniform global dataset of kinematic and thermodynamic variables. NARR has a grid spacing of 32 km and is available at 3-hourly, daily, and monthly temporal resolutions. When compared to other reanalyses, NARR is much higher resolution and more accurate (Mesinger et al. 2006). Surface temperature and winds throughout the troposphere were shown to be in much closer agreement to the observations than in other reanalysis datasets (Mesinger et al. 2006). One of the main weakness of NARR is its spatial resolution as the reanalysis will not be able to resolve

meteorological phenomena smaller than approximately two times the grid spacing. Other drawbacks of the NARR dataset is that it tends does not accurately show precipitation over Canada, likely due to a limited number of rain gauges, and it tends to overestimate the strength of the Gulf of California low-level jet in summer time (Mesinger et al. 2006).

4.2.2 National Mosaic and Multi-Sensor Quantitative Precipitation Estimation

The National Mosaic and Multi-Sensor Quantitative Precipitation Estimation (QPE) (NMQ) system produces a multi-radar and multi-sensor precipitation dataset. The objectives of the NMQ system is to create high-resolution national 3D grids of radar reflectivity along with high-resolution national multi-sensor QPE (Zhang et al. 2011). To create the national grids of radar reflectivity and QPE for the coterminous United States, the NMQ system uses data from over 140 Weather Surveillance Radar-1988 Doppler (WSR-88D) and 31 Canadian C-band weather radars (Fig. 10). It also utilizes other radars such as Terminal Doppler Weather Radar (TDWR) for areas not covered by the WSR-88Ds. Along with radar data, the NMQ system also takes in lightning data, rain gauge data, and model data from the Rapid Update Cycle (RUC) (Zhang et al. 2011). NMQ data has a grid spacing of 1 km and a temporal interval of 5 minutes (Zhang et al. 2011). The dataset contains the quality controlled radar reflectivity, separated into convective and stratiform components, and also classified as liquid or ice precipitation. NMQ classifies precipitation as either convective, stratiform, or tropical using the vertical profiles of reflectivity (VPR). VPRs and assimilated sounding data are also used to classify precipitation as either liquid or ice. Precipitation rate from the radar data is determined using a reflectivity and rainfall rate (Z-R) relationship.

The precipitation data that will be used in this project are based on the analysis of Rickenbach et al. (2015), where precipitation was separated into IPF and MPF using a 100 km

size threshold on all precipitation features. Precipitation features smaller than 100 km are classified as IPF and features larger than 100 km are classified as MPF. The analysis will be based on geo-located arrays of IPF and MPF precipitation every hour. It should be noted that within this precipitation dataset, NMQ data is missing for 20 – 24 July 2011 and 11 – 13 August 2011.

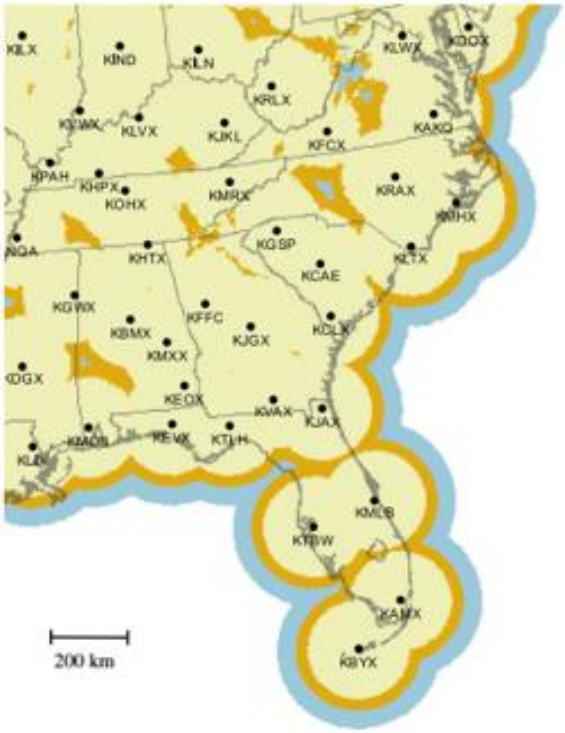

Figure 10: WSR-88D radars that will be used to study the SE US (from Rickenbach, et al., 2015).

Though it is extensively quality controlled, the NMQ system has its limitations. Some of the limitations are due to limitations of radar itself, such as issues related to beam blockage and attenuation and the fact that the vertical resolution of the beam becomes rather coarse at far ranges. Along with that, there are areas of the United States not covered by WSR-88Ds and therefore other radars (such as TDWRs) need to be used to fill in the gaps (Zhang et al. 2011). The NMQ system currently has a precipitation classification (snow versus rain) based on

temperature, and does not use polarimetric measurements to discriminate between precipitation type (Zhang et al. 2011).

4.3 Data Analysis

A method for identifying the onset of the convective season in the SE US will be designed using IPF from the NMQ precipitation dataset from Rickenbach et al. (2015), along with determining what dynamic and thermodynamic variables play a role in onset for each year using NARR data. NMQ data is analyzed from March – August for each year, along with daily composites of NARR data for May and June, and pentad composites of NARR data for April – July for each year are also analyzed. The general approach follows Nieto-Ferreira and Rickenbach (2011) and Marengo et al. (2001) who analyzed the regional evolution of onset of the South American monsoon. To aid in determining onset, the SE US was split into twenty-seven 2°x2° boxes (Fig. 11). The date of onset was determined in each box for 2009 – 2012 and the four-year average to see if onset occurs all at once in the SE US or if onset timing changes regionally (i.e. onset occurring in Florida first and slowly migrating northward). These twenty-seven boxes cover the SE US, while not including too much area over the ocean where there is less radar coverage. Along with that, these boxes were selected such that regional differences in onset timing and behavior of IPF could be analyzed (i.e. differences between coastal and inland areas, differences between southern boxes and northern boxes, etc.). The criteria for determining onset draws from monsoon literature as described earlier in Chapter 3.

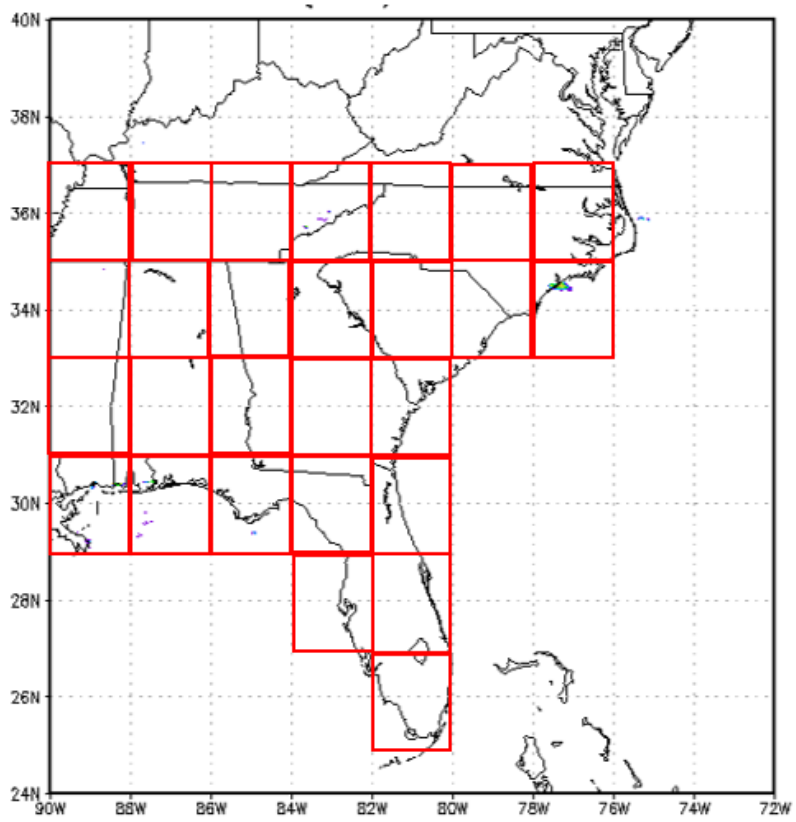

Figure 11: The twenty-seven 2°x2° boxes over the SE US.

4.3.1 Analysis of NMQ and NARR

Spatial grids of daily-averaged IPF rain rate from the NMQ dataset were created for March through August 2009 – 2012 using the Gridded Analysis and Display System (GrADS) to visualize and analyze how IPF changes over the SE US during the spring and summer months. Shown in Figure 12 are the four – year averaged monthly – mean maps of IPF rain rate for March – August. In March and April, there is very little IPF over the SE US. IPF precipitation is scattered and cover a small area in March and April. However, IPF drastically increases in May, particularly in Florida. The Atlantic coast is also outlined by IPF precipitation. Further inland, IPF coverage increases in May, though it is still relatively scattered. By the month of June, IPF has increased in spatial coverage, with nearly all

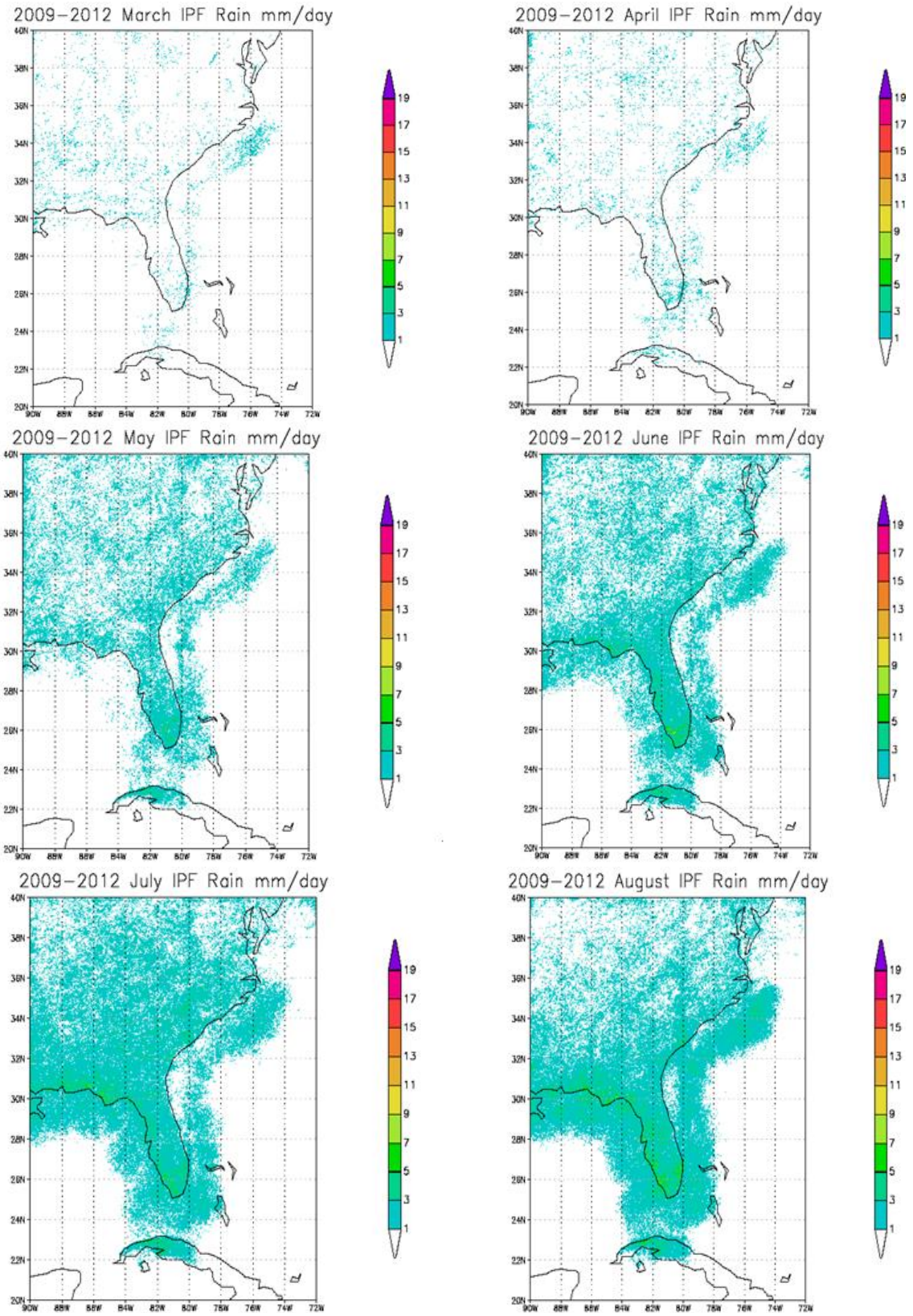

Figure 12: Four-year (2009-2012) averaged monthly-mean maps of IPF rain rate for the SE US for: March, April, May, June, July, and August.

of Florida and the coastal areas covered in IPF. IPF also outlines the entire coastline of the SE US, along with increasing in its spatial coverage of the inland areas in the SE US. IPF continues increasing in intensity and coverage during July and August, though the increase is not nearly as drastic as the increases in IPF observed in April to May and June.

Along with the daily composites, time series of IPF precipitation for each of the 2°x2° boxes were created. Using GrADS, IPF was averaged for each day to create a time series from 1 March – 31 August for each of the twenty-seven boxes in each year. Time series of the four-year average of IPF in each box were also created. These time series were used to determine regional differences in the seasonal transition of IPF rain across the SE US. After determining the daily IPF precipitation for each box and generating these time series, the mean IPF and standard deviation of IPF for each 2°x2° box were calculated. The slope of the time series curve between consecutive days was calculated to determine what days from 1 March – August 31 were local maxima, to be used in determining onset. A day was considered a maxima if the slope on that day was greater than zero and the slope for the day immediately following it was less than zero. The criteria used to determine onset date are described in the next section.

Meteorological data from NARR was analyzed using GrADS. The thermodynamic variables analyzed include convective available potential energy (CAPE), surface temperature, and specific humidity. The dynamic variables analyzed include the 500 hPa geopotential height field, mean sea level pressure (MSLP), and 850 hPa winds. MSLP and 850 hPa winds were analyzed to study the behavior the NASH and how it evolves over the SE US during the spring and summer. Using the definition of the location of the western ridge from Li et al., (2011), the 1016 hPa MSLP contour will be used to determine the location of the western ridge of the NASH as that contour generally corresponds to the 1560 gpm contour. The 500 hPa geopotential heights

were analyzed to determine when upper-level troughs and ridges moved through the SE US. The three thermodynamic variables were also analyzed to determine how each evolves over the spring and summer when onset occurs. Specific humidity is a measure of how much moisture there is in the atmosphere, and moisture, along with warm temperatures, are two of the variables needed for convection to develop. CAPE is a measure of atmospheric instability, and is directly affected by both moisture and temperature. Increases in moisture and temperature in the lower troposphere lead to an increase in CAPE, and high levels of CAPE indicate higher levels of buoyancy energy available in the atmosphere for convection to form. The CAPE is defined as (AMS Glossary),

$$CAPE = \int_{P_f}^{P_n} R_d\left(T_{vp} - T_{ve}\right) d\ln p$$

where T_{vp} is the virtual temperature of a parcel lifted moist adiabatically from the level of free convection (LFC) to the level of neutral buoyancy. T_{ve} the virtual temperature of the environment, R_d is the specific gas constant of air, P_f is the pressure at the LFC, and P_n is the pressure at the level of neutral buoyancy.

When the NASH is positioned over or near the SE US, it leads to southwesterly flow from the Gulf of Mexico over the SE US, and is a source of both increased moisture and warmer temperatures that aid in the development of convection. Daily composites of specific humidity and surface temperature, 850 hPa wind and MSLP, and CAPE were generated for the months of May and June in each year. Pentad composites of those variables were also generated for April – July for each year. This longer time period for the pentad composites allows for a better understanding of how the dynamic and thermodynamic variables change and evolve over the SE US before, during, and after onset. Once an onset date was determined from the IPF data in each 2°x2° box, the meteorological data from NARR was analyzed to determine what changes occur

around the time of onset, and if there are any similarities in the dynamic and thermodynamic conditions prior to and following onset each year.

4.3.2 Determining Onset of the Convective Season

Methods of determining monsoon onset in literature mentioned in Chapter 3 (Marengo et al., 2001; Nieto-Ferreira and Rickenbach, 2011) were used as a guide for determining onset of the convective season in the SE US. Onset of the convective season in the SE US was determined for each of the twenty-seven boxes for 2009 – 2012 and for the four-year average using the following criteria: IPF precipitation (after 1 April) at the time of onset must exceed the six-month (March-August) IPF precipitation mean for that box and be a local maximum. Next, at each box, the average of IPF maxima in the thirty days following the onset date must exceed one standard deviation above the mean of that box, and the average of IPF maxima in the thirty days preceding the onset date must be within one standard deviation of the mean. Using the average of the IPF maxima before and after onset captures the variability of individual IPF events. This method requires both daily IPF rain and daily IPF rain variability to be large after onset, which are both important changes in IPF rain behavior after onset. This will be illustrated in Section 5.1.

This method of using the mean and standard deviation of each box, rather than the constant threshold technique of Marengo et al. (2001) and Nieto-Ferreira and Rickenbach (2011), best captures the variability and behavior of IPF in each box, as IPF varies greatly across the region. In South America, the monsoon onset is much more distinct, and precipitation is generally less variable than IPF, as the monsoon marks the end of the dry season and beginning of the wet season, which means the rain at onset increases distinctly and rapidly. Therefore, a constant threshold can be used as it is a threshold only exceeded once the monsoon begins.

However, IPF is too variable over the SE US for a constant threshold to be used for the whole region. While there is a distinct increase in IPF in May and June, especially in the coastal areas of the SE US, there are still many days after onset in the SE US where there is little to no IPF, particularly in the more inland areas. Using local the mean and standard deviation of IPF for each box to determine onset in that box allows for onset to be relative to the amount of IPF in that area, which is necessary as IPF is quite variable over the SE US.

4.3.3 Sensitivity Tests

Three sensitivity tests were performed to analyze how the determination of onset date of the convective season in the SE US is sensitive to the threshold criteria, as was demonstrated in Marengo et al. (2001) for the South American monsoon.

The first sensitivity test performed is the thirty-day average, and uses the full thirty day average, rather than the thirty day average of the maxima, to characterize the sustained level of IPF rain before and after onset. The amount of IPF precipitation on the date of onset still had to exceed the mean IPF of that box and be a local maximum, with the subsequent thirty day average exceeding one standard deviation above the mean, and the preceding thirty day average was within one standard deviation of the mean. Using this criteria, onset was determined for each of the twenty-seven boxes from 2009 – 2012 and the four-year average.

The second sensitivity test was more similar to the constant threshold technique from the South American monsoon literature mentioned previously. The second sensitivity test is the four-year regional average and uses the regional mean of the four-year average (averaging the mean IPF of each box from the four-year average), and used this as the mean value IPF must exceed on onset for each box for 2009 – 2012 and the four-year average. The value for one standard deviation above the mean was adjusted accordingly based on this new mean IPF value. The thirty

day average of maxima following onset still has to exceed one standard deviation above the mean with the thirty day average of the maxima before onset within one standard deviation of the mean. Using this criteria, date of onset was determined for all twenty-seven boxes for 2009 – 2012 and the four-year average. This sensitivity test was performed to see what effect a constant threshold value has on the date of onset in the SE US.

The third sensitivity test performed on the IPF data is the annual regional average, and uses the regional average (i.e. averaging the mean IPF of each box for each year) of each year for the mean IPF. The regional mean for each year from 2009 – 2012 was calculated. The regional mean for each year was used as the threshold that the daily value of IPF rain must exceed on the date of onset for that year. The value for one standard deviation above the mean was adjusted accordingly for each box. The thirty day average of the maxima after onset still had to exceed one standard deviation above the mean, and the thirty day average of the maxima preceding onset had to be within one standard deviation of the mean. Based on this criteria, onset was determined for each of the twenty-seven boxes for all four years. The reasoning for performing this sensitivity test is similar to that of the second test. This was to see what effect a constant threshold has on the date of onset across the SE US. However, in this test, using the regional average for each year rather than the four-year regional average eliminated the year-to-year variability, since IPF varies greatly from year-to-year.

CHAPTER 5: RESULTS AND DISCUSSION

The following section presents the main results and a discussion of those results. It begins with the onset dates for each of four years (2009-2012) and for the four-year average, followed by the results of the sensitivity tests described in Chapter 4. Finally, a discussion of the NARR meteorological data for each year and how the meteorological variables play a role in onset is presented.

5.1 Results of IPF Onset Determination

Using the method described in section 4.3.2, onset in 2009 first occurs in the boxes over the northwestern region of the SE US. These boxes include most of Tennessee and parts of Mississippi and Alabama. In this area, onset occurs in the final pentad of April (26-30 April). For the rest of the SE US, onset generally occurs between 1-15 May. There are a few outliers where

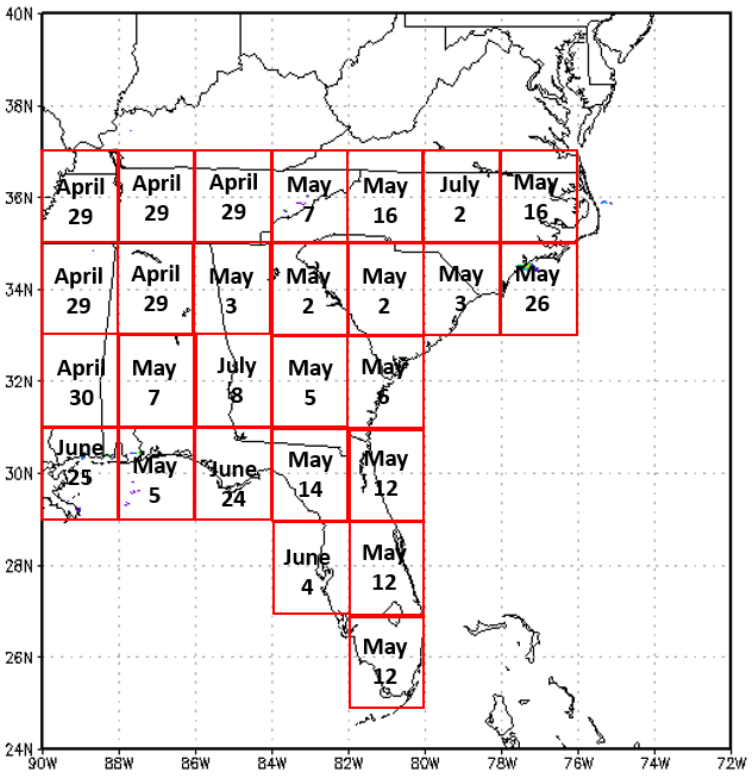

Figure 13: Onset for 2009 in the SE US.

onset does not occur in a few boxes until late June or early July (Fig. 13). However, the reason these outliers have a much later onset date compared to the surrounding boxes is because one of the onset criteria at earlier dates more similar to those of the surrounding boxes was just not met. For example, IPF precipitation on a potential earlier onset date in these later boxes may have exceeded the mean, but the thirty-day average of the maxima did not quite exceed one standard deviation over the mean, or vice versa. Beyond onset occurring in the northwestern boxes first in late April, there does not seem to be any kind of pattern or progression to when onset occurs in the SE US, as onset occurs throughout the first three pentads of May over much of the rest of the SE US.

When examining the time series of IPF from 1 March-31 August 2009 for each box in the SE US, it is clear that IPF precipitation is quite variable over the SE US. In the boxes over Florida, IPF precipitation has a rather abrupt increase in mid-May, where there is very little IPF rain before that, and suddenly in mid-May, IPF rapidly increases and generally stays high for the rest of May through August (Fig. 14). However, moving northward and further inland in the SE US, this abrupt increase in IPF precipitation is not present. Away from Florida, IPF precipitation generally does not exhibit such a drastic increase in mid – May. Rather, IPF is quite noisy and much more episodic. Instead of an abrupt increase in IPF rain, these northern and inland boxes are more characterized by increasingly larger IPF events beginning around mid – May (Fig. 15, 16). Along with IPF becoming noisier and more episodic in the more northern and inland portions of the SE US, the daily IPF precipitation maxima are smaller. In the southern boxes over Florida, daily IPF precipitation approaches and exceeds 25 mm/day (Fig. 14). However, daily IPF maxima progressively decrease toward the north, with daily precipitation from maxima in the northernmost boxes rarely exceed ~25 mm/day (Fig. 16).

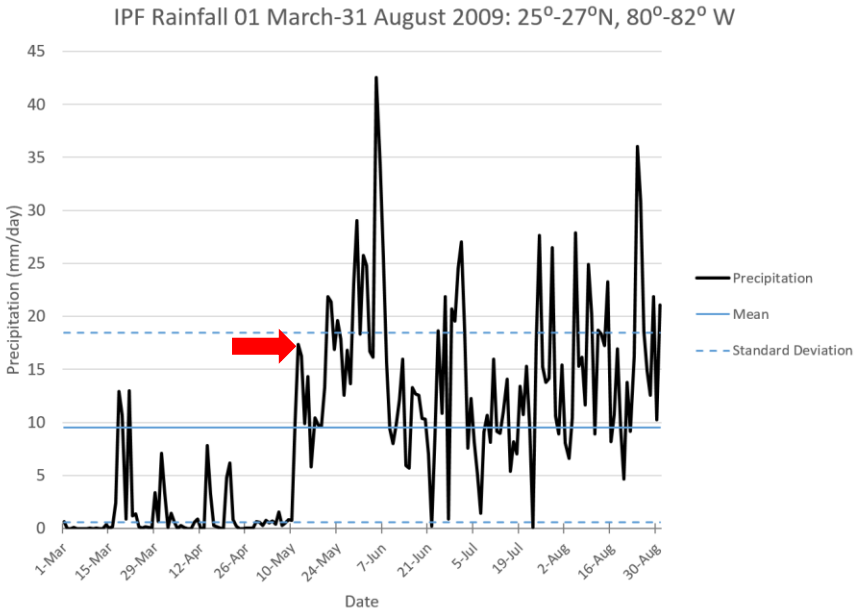

Figure 14: Time series of IPF from 1 March-31 August 2009 for the box at 25°-27° N, 80°-82 W°. Onset occurs on12 May 2009 for this box.

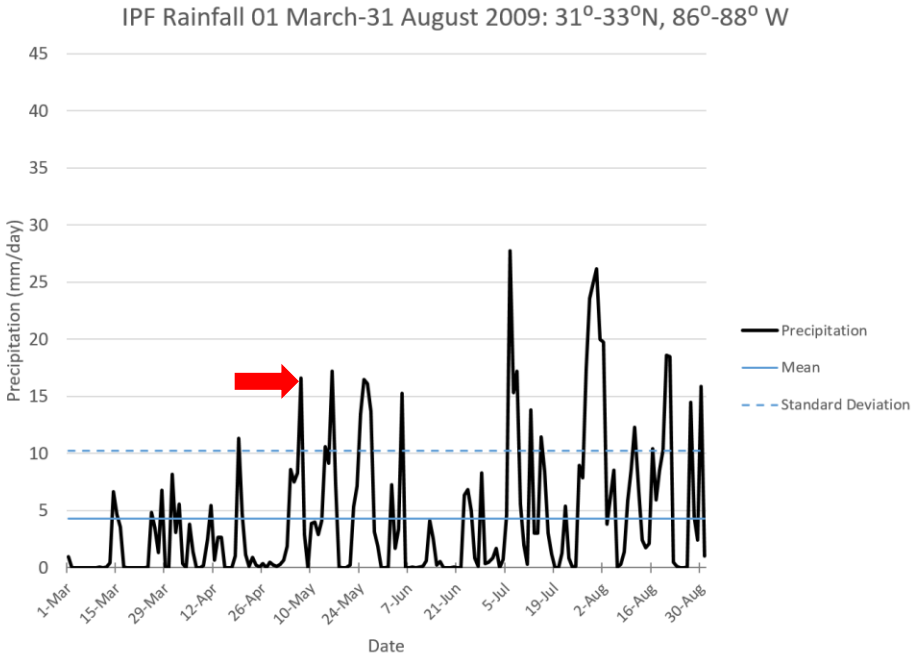

Figure 15: Same as Fig. 14, but for the box located at 31°-33° N, 86°-88° W. Onset occurs on 7 May 2009 for this box.

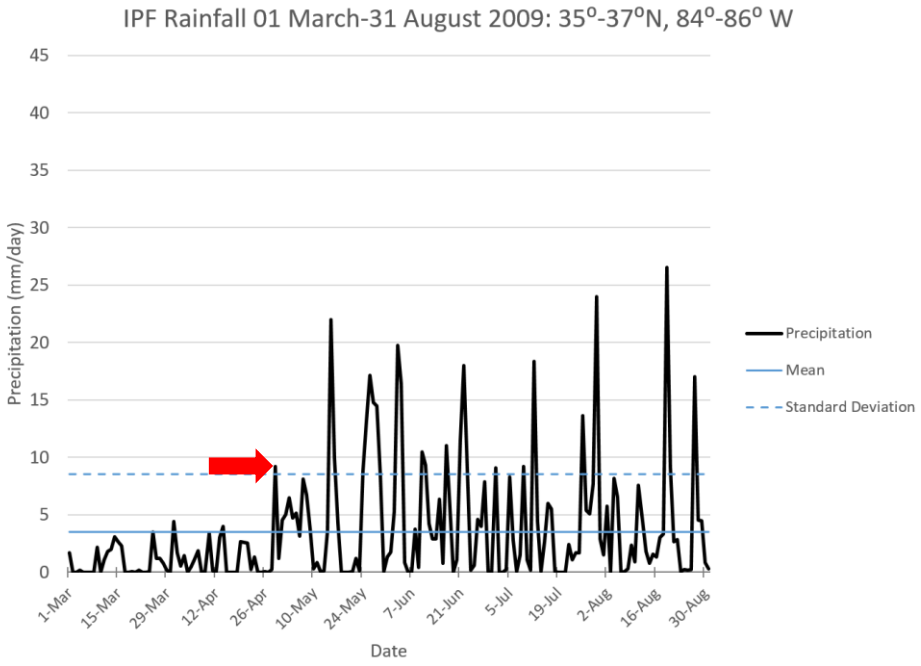

Figure 16: Same as Fig. 14 but for the box located at 35°-37° N, 84°-86° W. Onset occurs on 29 April 2009 in this box.

Onset in the SE US in 2010 broadly occurs during mid to late May (16-31 May), again with the earliest onset date in the northwestern part of the domain. Unlike 2009, only one box (the northwestern most box in Tennessee) has a late April onset date, along with only two boxes in coastal North Carolina and one on the Georgia – South Carolina border where onset occurs in early June (Fig. 17). The earliest onset date is 22 April in far western Tennessee, and onset occurs in the first pentad of May in three boxes in North Carolina, South Carolina, and coastal Georgia. Throughout the rest of the region, onset occurs in mid to late May. As with 2009, there does not seem to be any kind of regional progression or pattern as to when onset occurs.

Similar to 2009, the IPF time series from 1 March to 31 August 2010 show that IPF is quite variable in 2010 over the SE US. Similarly to 2009, time series of IPF that correspond to the southern boxes in Florida and parts of Georgia generally exhibit a sudden increase in IPF precipitation in mid-May (Fig. 18). However, that sudden increase is not as clear as in 2009. As in 2009, IPF for the northern and inland boxes of the SE US is much noisier and episodic, with

individual IPF events becoming increasingly larger beginning in mid to late May (Fig. 19, 20). The IPF maxima do not decrease much from the southern boxes to the more northern boxes in 2010, as was the case in 2009.

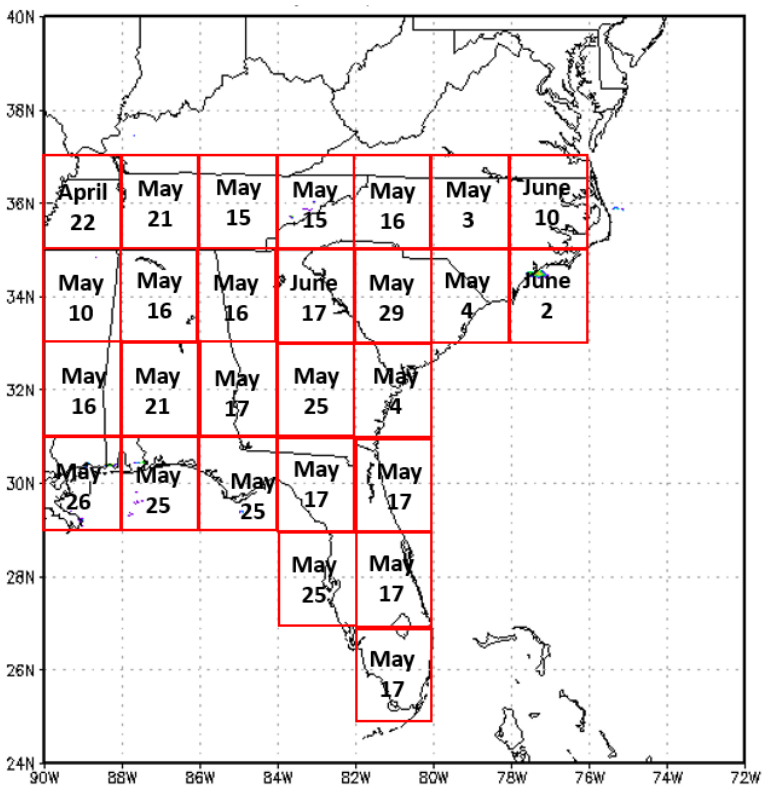

Figure 17: Onset in each box for the SE US for 2010.

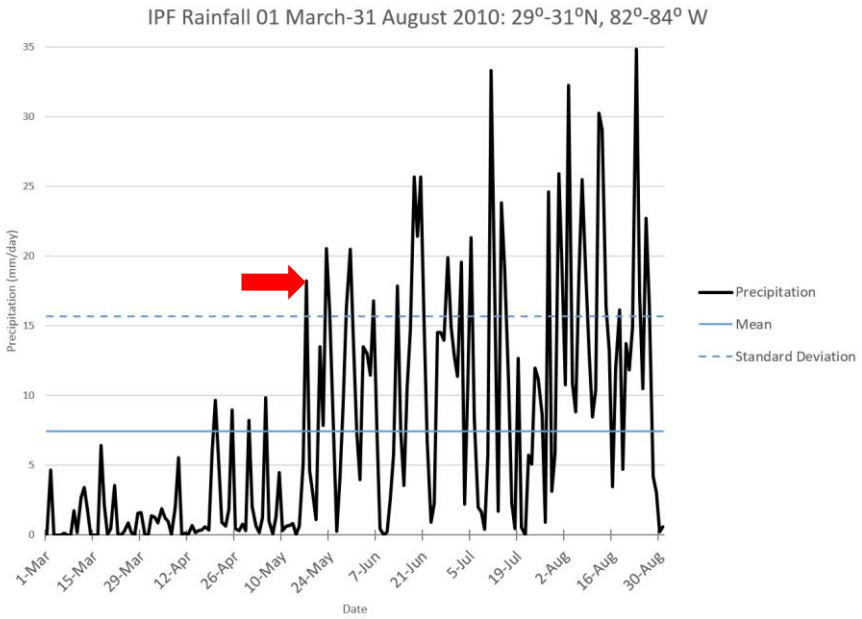

Figure 18: Time series of IPF for March 31-August 2010 for the box located at 29°-31° N, 82°-84° W. Onset occurs in this box on 17 May 2010.

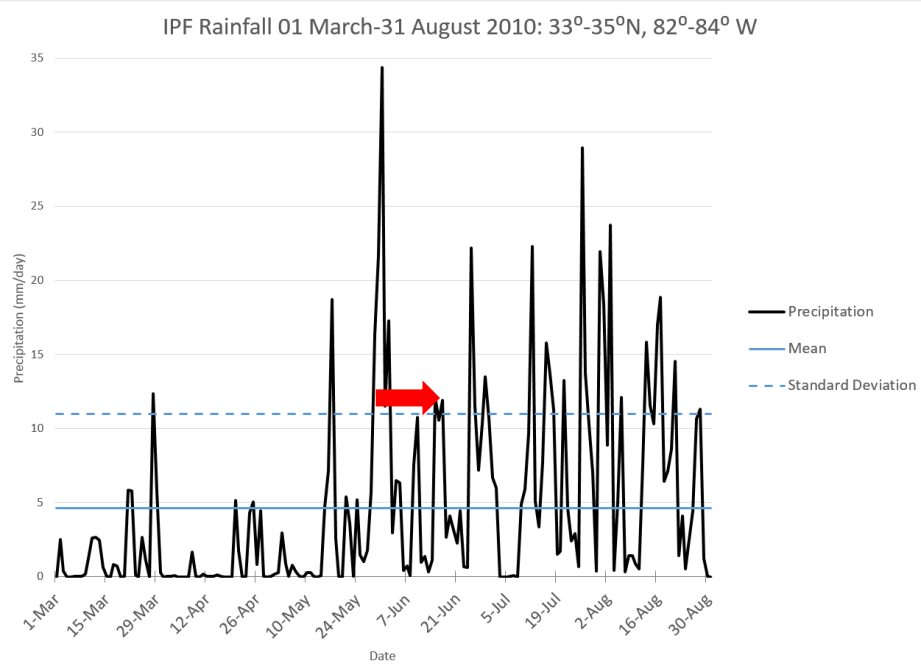

Figure 19: As in Fig. 18, but for 33°-35° N, 82°-84° W. Onset occurs in this box on 17 June 2010.

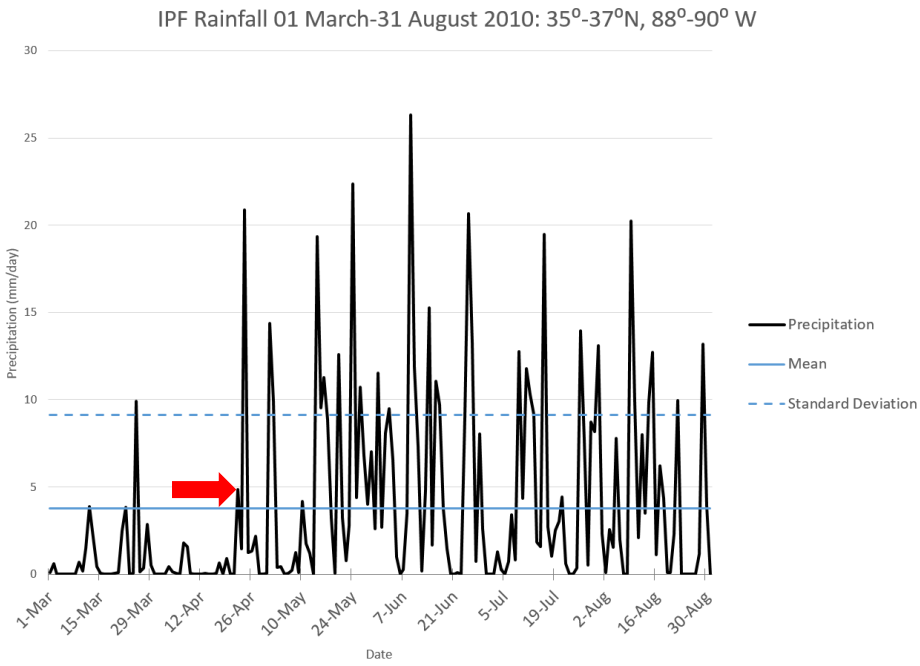

Figure 20: As in Fig. 18, but for 35°-37° N, 88°-90° W. Onset occurs in this box on 22 April 2010.

In 2011, onset across the majority of the SE US is in late May to mid-June (26 May-15 June), considerably later than onset in the two previous years. The earliest date of onset in 2011 is in the westernmost boxes over western Tennessee and northern Mississippi, where onset occurs in the first pentad of April. There is only one box along the coast of North Carolina with an onset date in late July, with this box being an outlier where one of the criteria for onset was not quite met at an earlier date more similar to the boxes surrounding it. Aside from these boxes with either a considerably earlier or later onset date, onset across the rest of the SE US in 2011 occurs in late May to mid-June (Fig. 21). Similar to previous years, onset does not exhibit any kind of pattern or progression over the SE US. It should be noted that 2011 was a La Niña year, where La Niña conditions persisted into the spring months (Climate Prediction Center), which typically leads to drier than average conditions in the SE US.

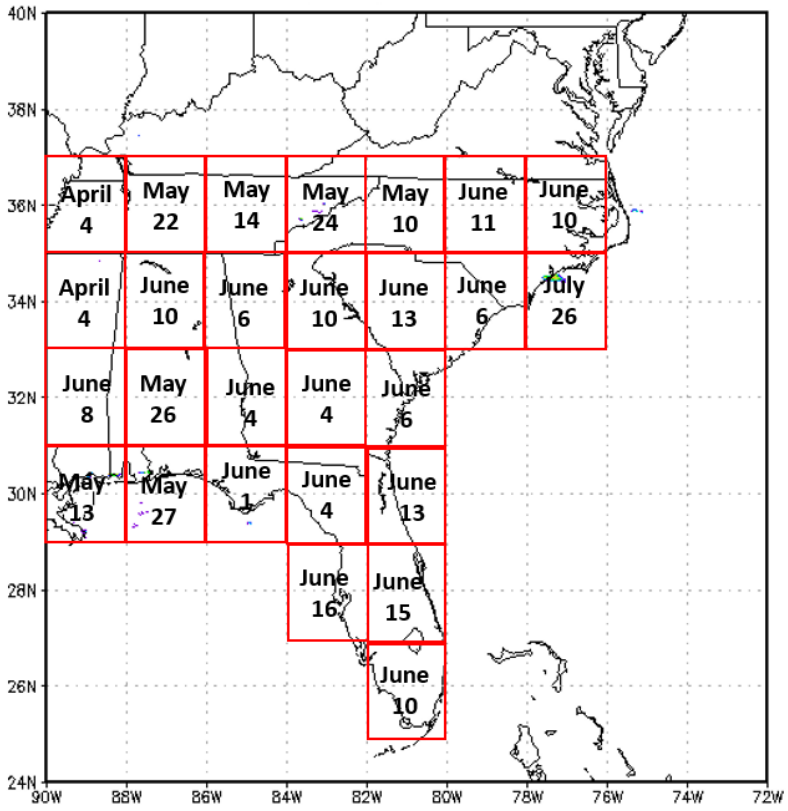

Figure 21: Onset dates for each box in the SE US in 2011.

After analyzing the IPF time series for 1 March-31 August 2011 for each box, the behavior of IPF is variable, and also quite different from the two previous years. Many of the southern boxes over Florida and the Gulf Coast do not have a drastic and abrupt increase in IPF precipitation at all (Fig. 22). Rather, the behavior in many of these southern boxes is much noisier and IPF is more episodic, with larger and more frequent IPF events in the late spring and early summer, which is more similar to what has been observed in the northern boxes of the SE US in the previous two years. There are a still a couple of southern boxes that have an abrupt increase in IPF in late May and mid-June, though IPF in many of the southern boxes is still more episodic. As in 2009 and 2010, IPF in the northern boxes is still rather episodic, with IPF events generally increasing in amount of precipitation during late May and June. However, some of the

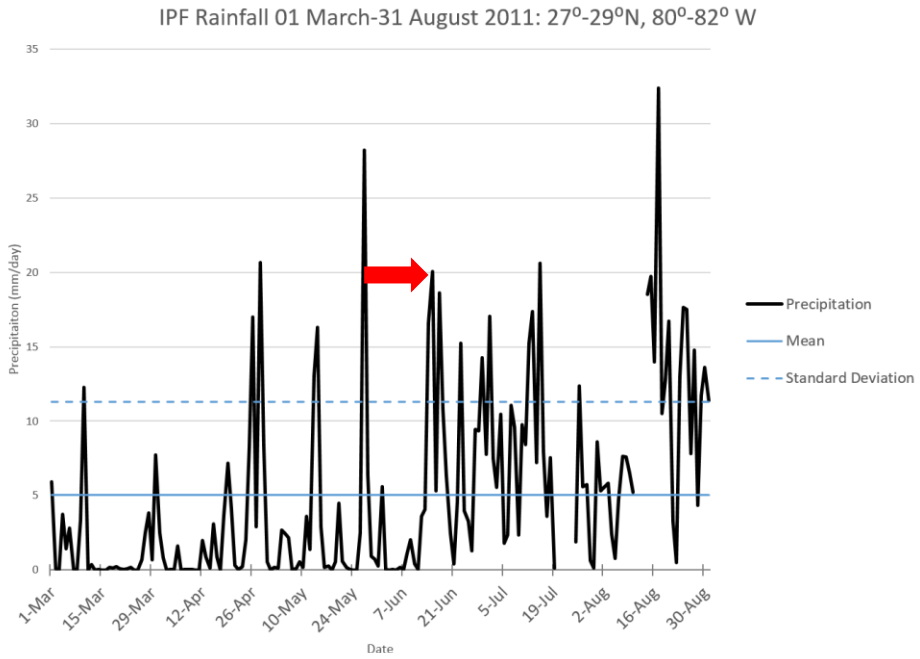

Figure 22: IPF time series for 1 March-31 August 2011 for 27°-29° N, 80°-82° W. Onset occurs on 15 June.

northern boxes have these very large IPF events that are immediately followed by multiple days with little to no IPF until the next large IPF event (Fig. 23). Other boxes in the northern region of the SE US are similar to 2009 and 2010, where IPF in those boxes is rather noisy, and best

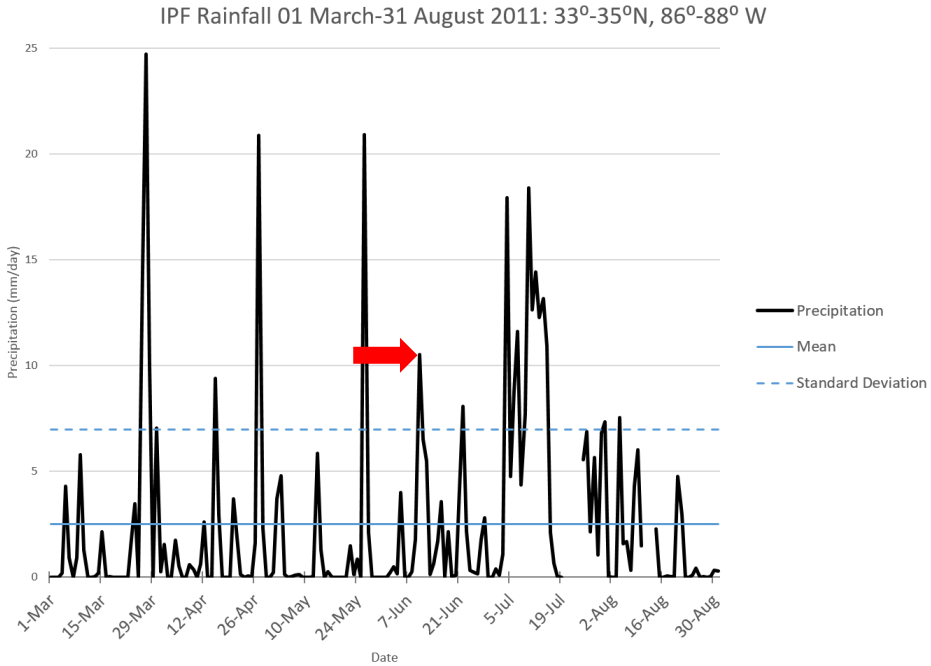

Figure 23: IPF time series for 1 March-31 August 2011 for 33°-35° N, 86°-88° W. Onset occurs on 10 June.

characterized by larger individual IPF events that also become more frequent in the late spring and summer months (Fig. 24).

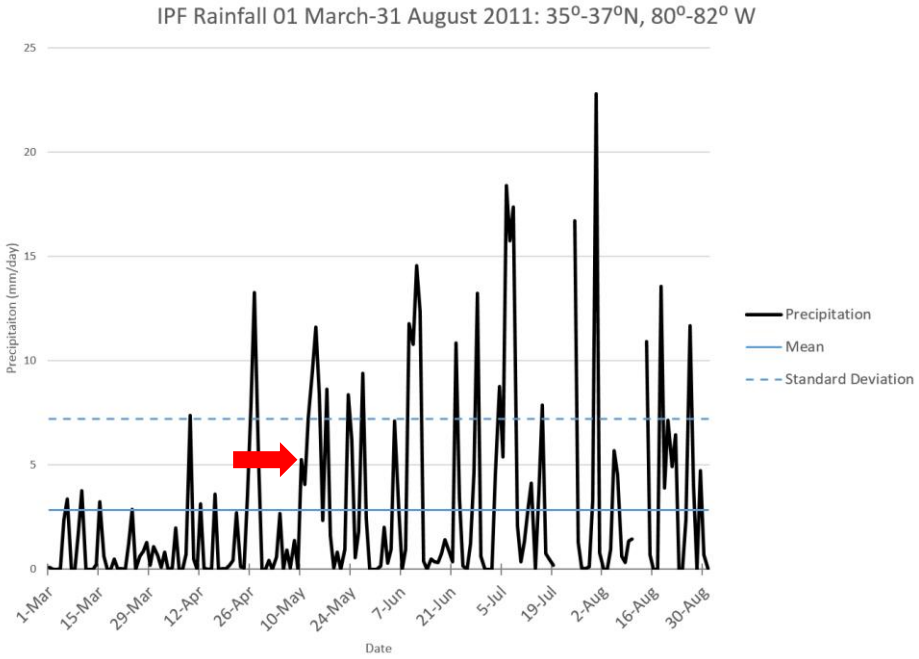

Figure 24: IPF time series for 1 March-31 August 2011 for 35°-37° N, 80°-82° W. Onset occurs on 10 May.

In 2012, onset across much of the SE US is earlier than in any of the three previous years, with onset generally occurring in late April to early May (21 April-10 May), with an area of onset dates in mid-June in the northwestern region of the SE US. There are two boxes in 2012 with considerably later onset dates than the rest of the region – one is in coastal North Carolina and the other is in central Mississippi, with onset occurring in early July (Fig. 25). As in previous years, these considerably later onset dates is the result of one of the onset criteria was not quite met at an earlier date more similar to its surrounding boxes. As was seen in the first three years, there is no discernible pattern or progression of onset in the SE US in 2012.

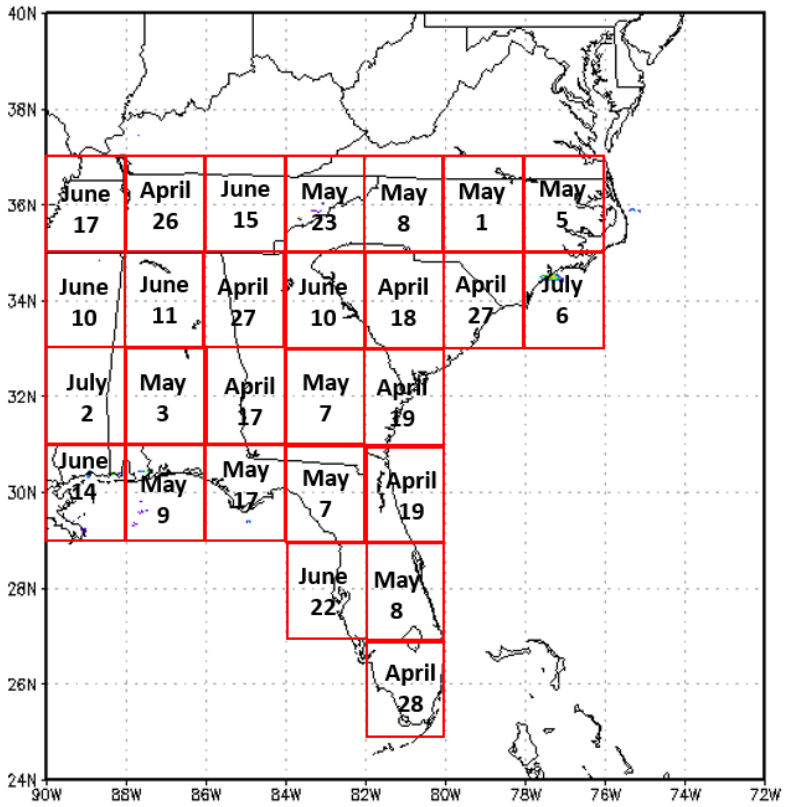

Figure 25: Onset dates for the SE US for 2012.

The IPF time series for 1 March-31 August 2012 in each box is similar to those of 2011. Many of the time series for boxes in the southern region of the SE US are rather noisy and do not have the abrupt increase in IPF in the spring or summer months. In some of the southern boxes, it is not even clear that IPF events increase in amount or frequency in the late spring and summer months (Fig. 26). However, there are some boxes in the southern area of the SE US where, while IPF is rather noisy and episodic, the individual IPF events become larger in the late spring (Fig. 27). As is seen in the previous three years, the IPF time series in the northern and inland boxes is noisy and episodic, with IPF events generally becoming larger (Fig. 28).

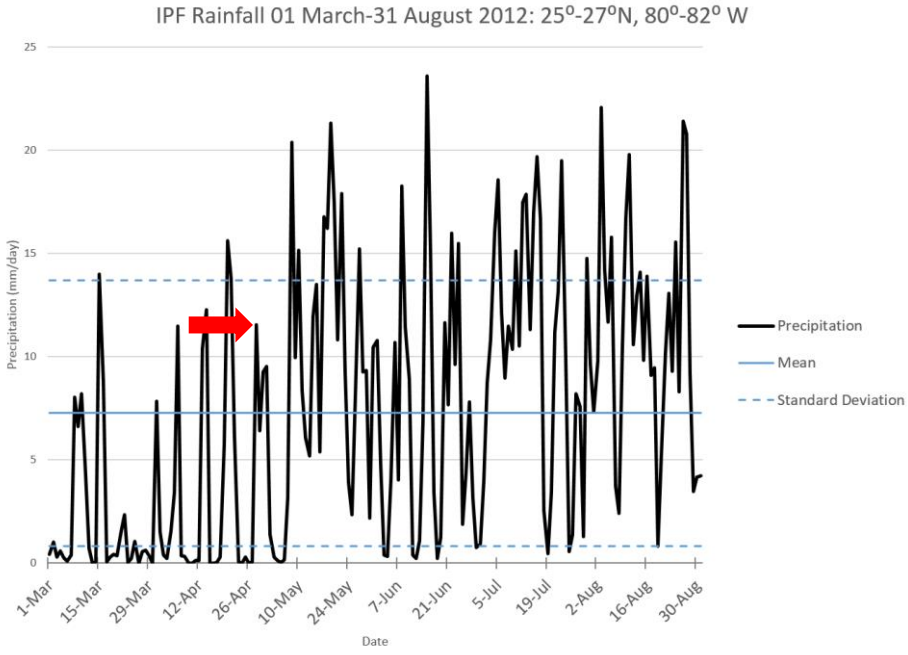

Figure 26: IPF time series for 1 March-31 August 2012 for the box at 25°-27° N, 80°-82° W. Onset occurs on 28 April.

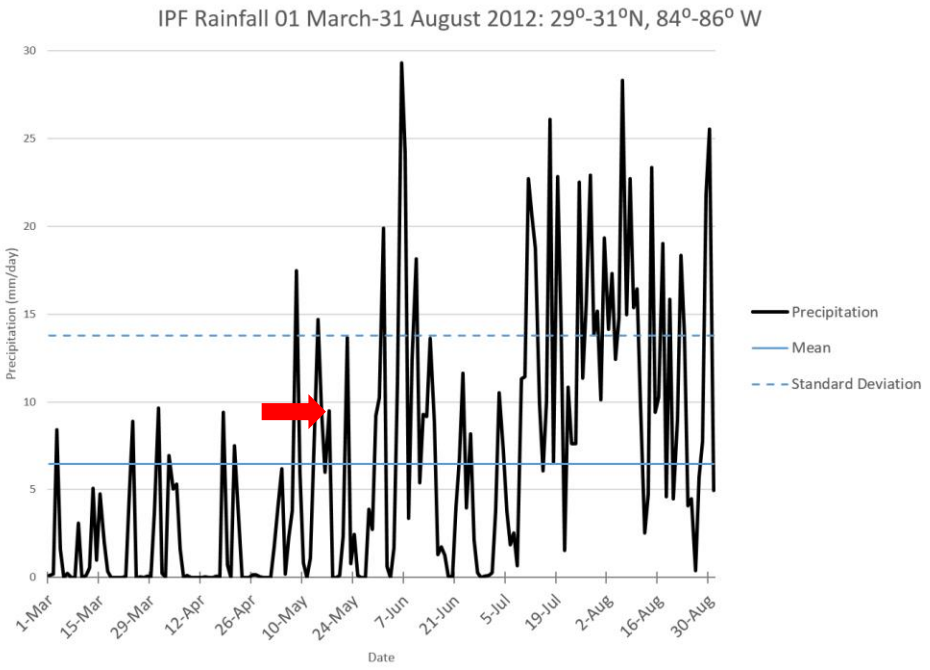

Figure 27: As in Fig. 26, but for the box at 29°-31° N, 84°-86° W. Onset occurs on 17 May.

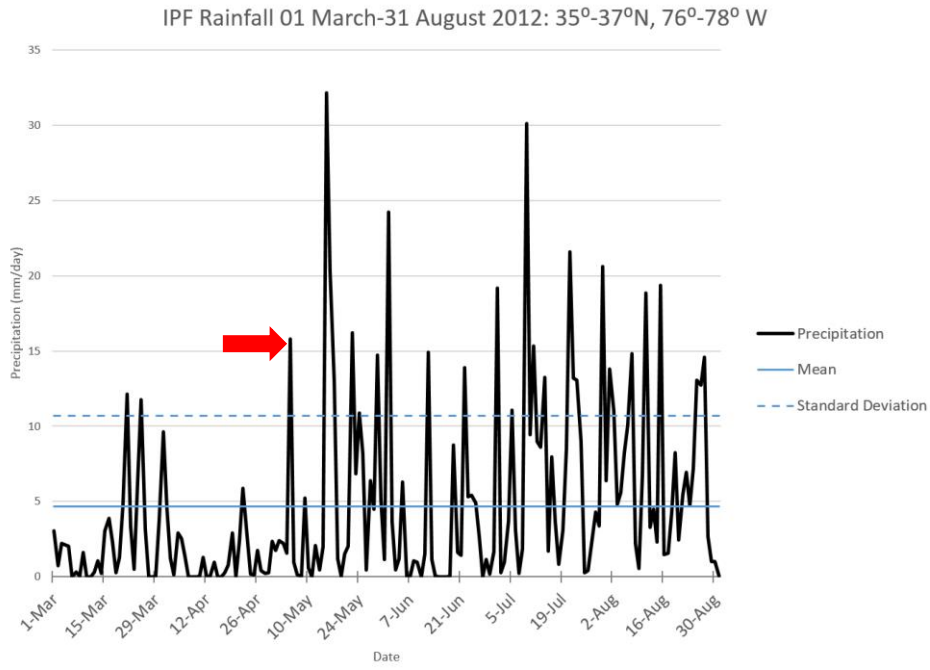

Figure 28: As in Fig. 26, but for 35°-37° N, 76°-78° W. Onset occurs on 5 May.

Onset in each box for the four-year average was determined, and IPF time series of the four-year average of each box were also created and analyzed. With the four-year average, onset was determined to occur between mid-May to mid-June for most of the SE US. As was seen in the individual years, onset in the northwestern most boxes occurs in late April (Fig. 29). The IPF time series for the four-year average across the SE US generally have a noticeable increase in IPF near and after the time of onset. The boxes in the southernmost portion of the SE US still have a more sudden increase in IPF near the time of onset (Fig. 30). The boxes further north and inland exhibit more episodic behavior of IPF, as was seen in the individual years, however, in the four-year average, the more northern and inland time series have a clearer increase in IPF. The increase in IPF is not as drastic as in the southern boxes, however, the increase in both amount of IPF precipitation and frequency of IPF events is more clearly seen in the four-year average (Fig. 31, 32).

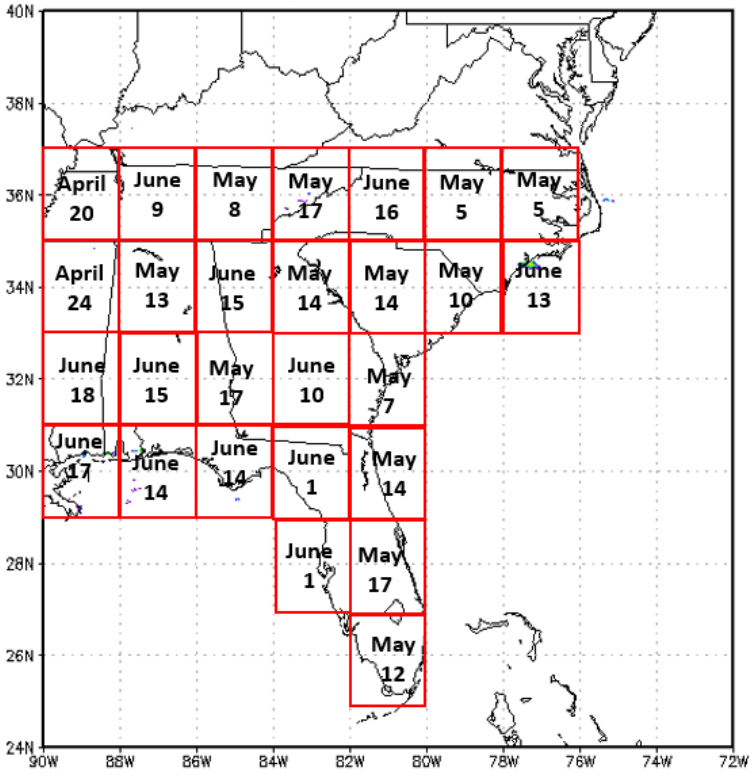

Figure 29: Onset in the SE US for the four-year average.

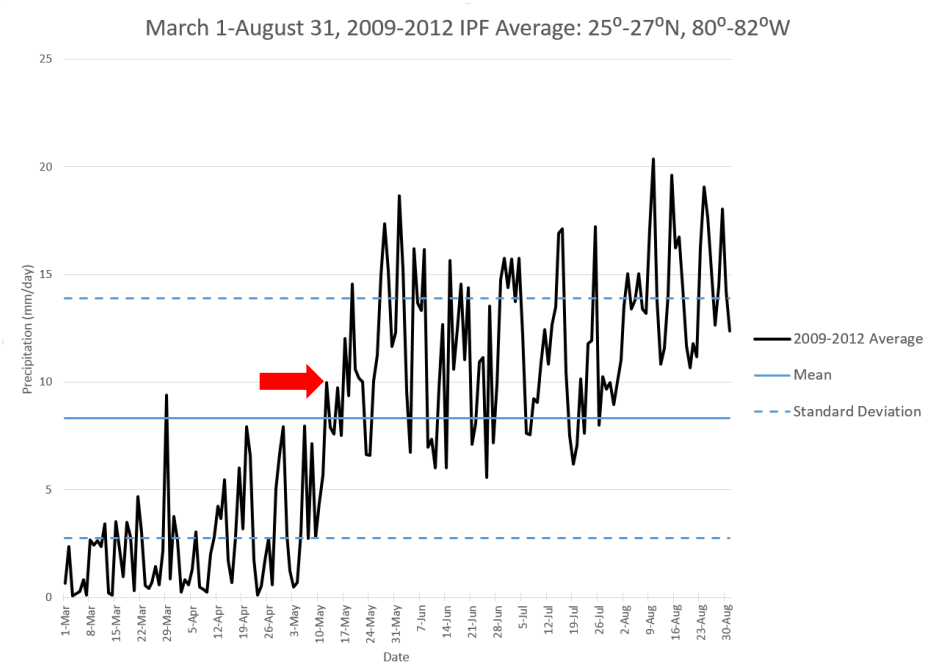

Figure 30: IPF time series for 1 March-31 August, 2009-2012 for the box at 25°-27° N, 80°-82° W. Onset occurs on 12 May.

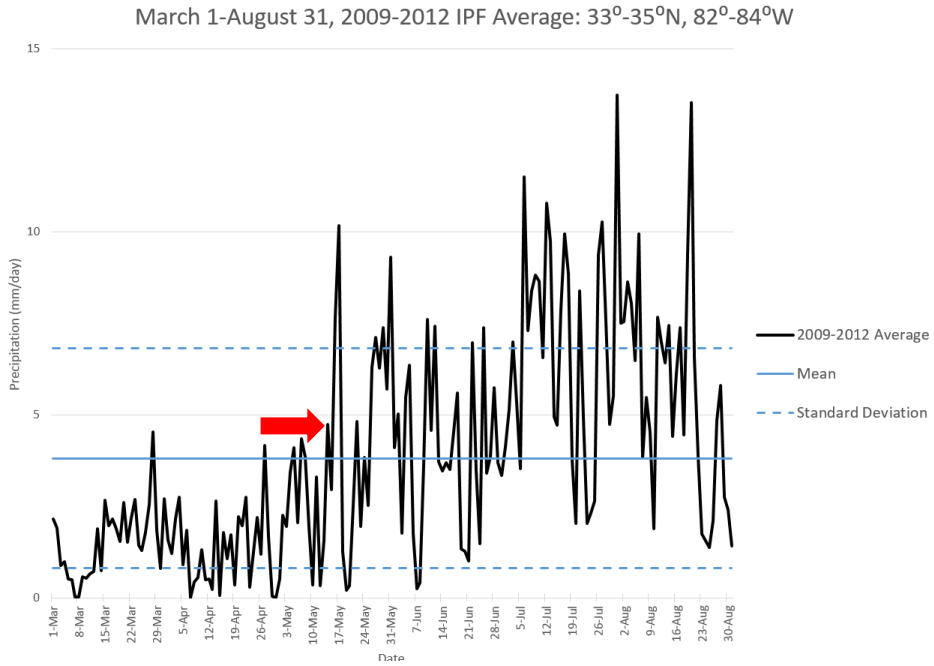

Figure 31: As in Fig. 30, but for the box at 33°-35° N, 82°-84° W. Onset occurs on 14 May.

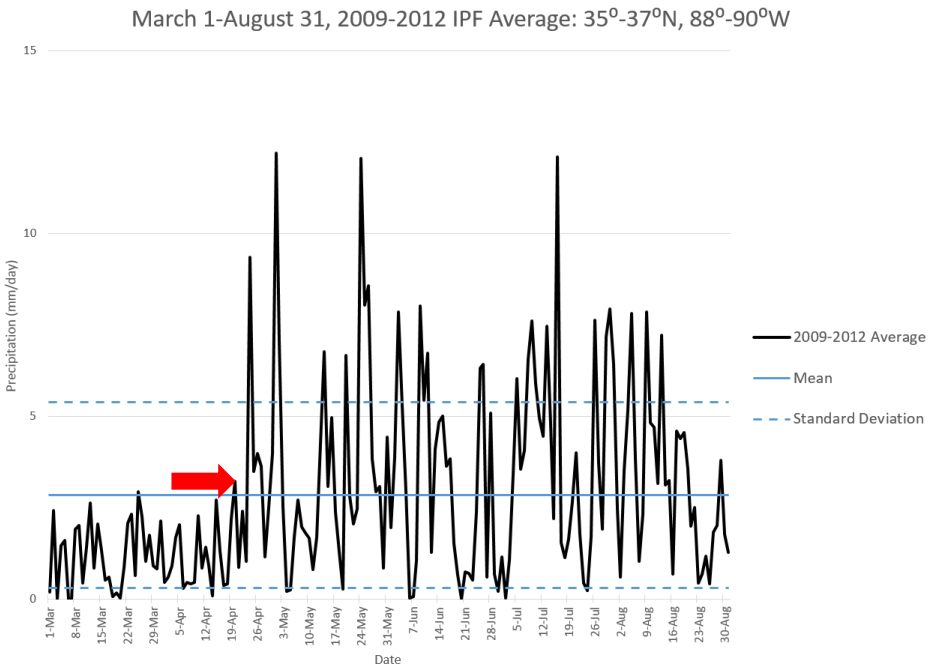

Figure 32: As in Fig. 30, but for the box at 35°-37° N, 88°-90° W. Onset occurs on April 20.

5.2 Results of the Sensitivity Tests of IPF Onset Date Determination

Test	Precipitation Threshold	Average Used
Average of the Maxima	IPF exceeds average of that box on onset	Average of the IPF maxima 30 days before & after onset
30 Day Average	IPF exceeds average of that box on onset	Average of IPF 30 days before & after onset
4-Year Regional Average	IPF exceeds the 4-year regional average on onset	Average of the IPF maxima 30 days before & after onset
Annual Regional Average	IPF exceeds the annual regional average on onset	Average of the IPF maxima 30 days before & after onset

Table 1: Summary of criteria to determine onset and for each sensitivity test.

The criteria for determining onset (average of the maxima) utilized the average of the IPF maxima thirty days before and after onset, along with using the March-August mean IPF of each box. The first sensitivity test, the thirty-day average, used the full thirty day average of IPF before and after onset, the second one, the four-year regional average, used the four-year mean of

IPF in the SE US as the value IPF rain had to exceed at onset, and the third test, the annual regional average, used the annual regional average of each year as the value IPF rain must exceed on onset (Table 1). Using the criteria of the thirty-day average, which used the thirty-day IPF precipitation average of each box as a threshold, onset was determined in each box across the SE US for 2009 – 2012 and the four-year average. Based on the criteria of the thirty-day average, onset never occurs for much of the region in all years. Specifically, 2009 has seven boxes where an onset date was defined, 2010 only has two boxes with a defined date of onset, there are nine boxes in 2011 where onset occurred, 2012 has five boxes where onset was defined, and the four-year average has fourteen boxes where onset occurred (Fig. 29). In general, for all four years, the areas where onset is defined are the southern boxes in Florida and along the coastal areas and, the date of onset in these boxes tends to be in late July to August. These boxes over Florida and along the coast receive more IPF precipitation overall compared to the boxes further inland, which is likely why these are the boxes where onset occurs using the thirty-day average. For most of the SE US, however, the onset criteria are never met using the thirty-day average because IPF precipitation is too variable. There are many days with IPF precipitation well below the value for one standard deviation above the mean in these boxes compared to the number of days with large IPF events, so the thirty day average after potential onset dates never exceeds one standard deviation above the mean, thus leading to onset being undefined for much of the SE US. While the four-year average has more boxes with a defined onset date compared to the individual years, the onset dates are still much later in July and August.

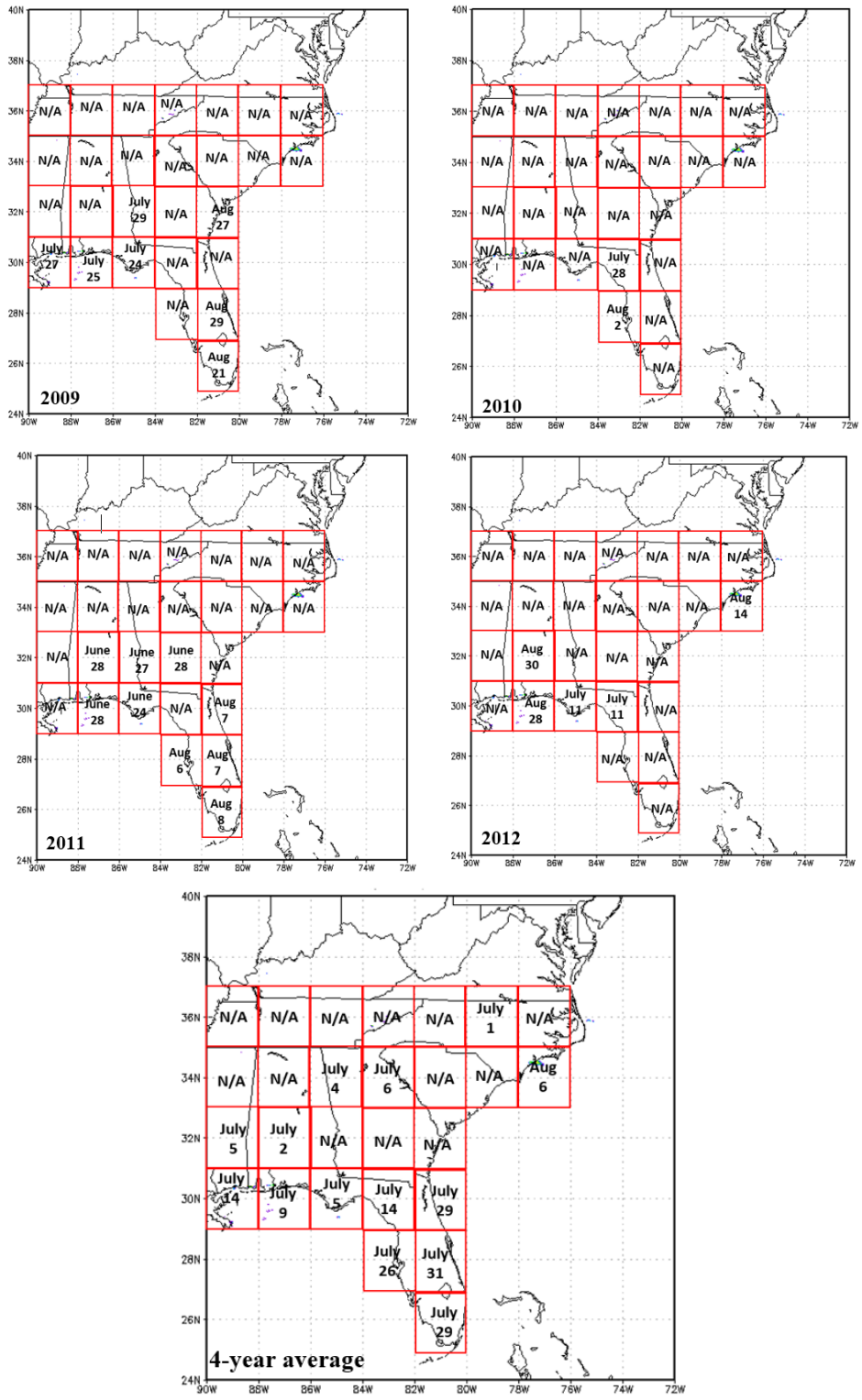

Figure 33: Onset in the SE US in each box for the first sensitivity test, using the thirty day average for: 2009, 2010, 2011, 2012, and the four-year average.

The four-year regional average, the second sensitivity test, used the four-year regional average as the IPF rain average, and IPF precipitation on the date of onset must exceed that value in each box. Using this criteria and the thirty day average of the maxima, onset was determined in each box for the SE US. In general, for all four years and the four-year average, boxes in the northern and western portions of the SE US are more likely to have a later onset date and boxes in the southern and coastal areas of the SE US are more likely to have an earlier onset date using this criteria in comparison to the baseline method used to determine onset. There are also boxes in each year and the four-year average where the date of onset did not change with this new criteria (Fig. 30). The four-year regional mean of IPF is lower than the mean IPF of the southern and coastal boxes in the SE US. As a result, the threshold for IPF precipitation to exceed on onset is lower, and the value that the thirty day average of the maxima after onset must exceed is also lower, leading to earlier onset dates in these areas. Conversely, in the northern and western boxes of the SE US, the four-year regional mean of IPF is higher than the mean IPF of each box. Therefore, the threshold that IPF precipitation must exceed at onset is increased, as is the value that the thirty day average of the maxima must exceed. This increased threshold for onset in boxes where the four-year IPF mean is higher than the IPF mean of that box leads to later onset dates in these areas.

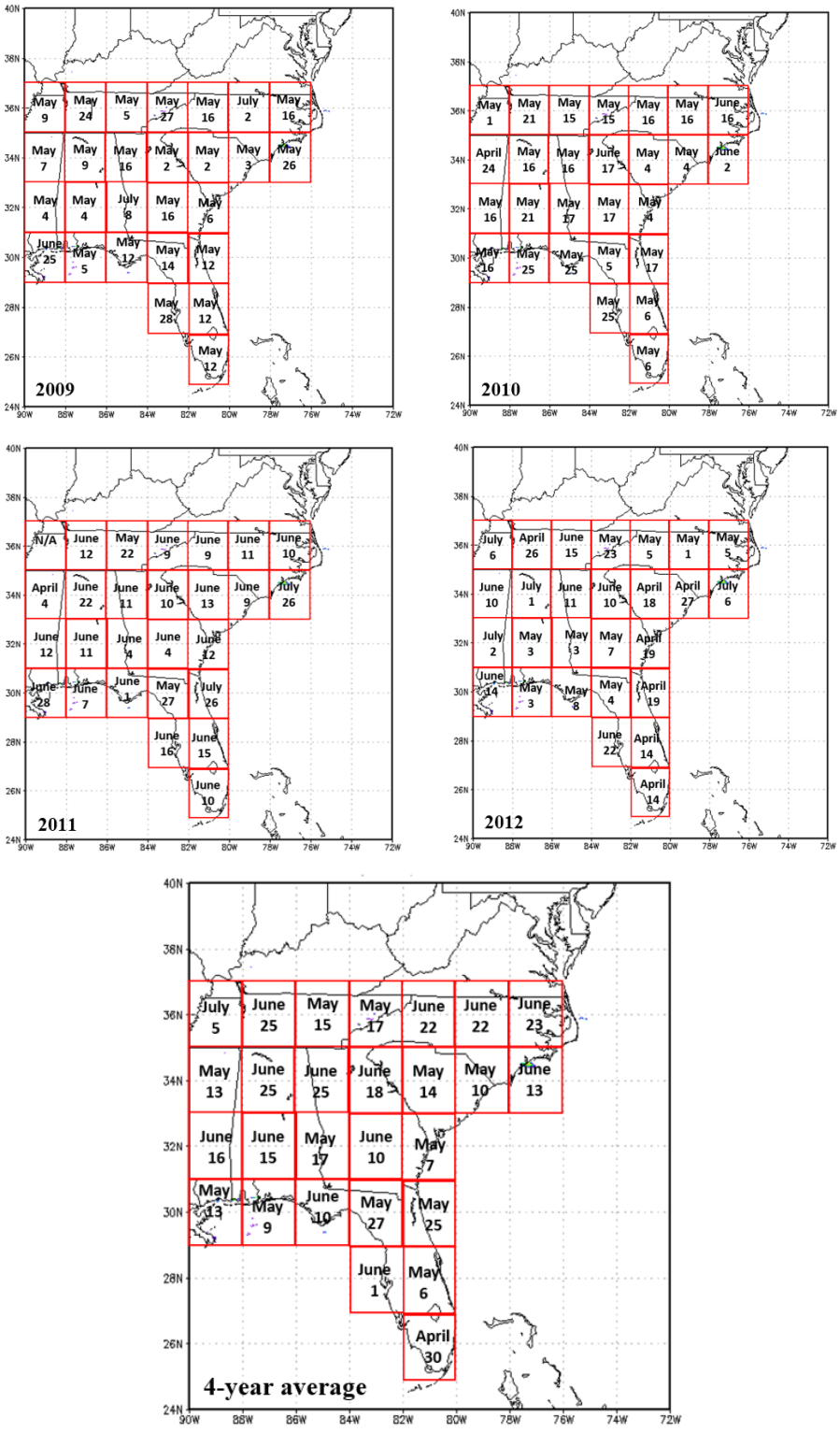

Figure 34: Same as Fig. 33, but for the second sensitivity test using the four-year regional average of IPF.

The third sensitivity test, the annual regional average, used the annual average of the region of IPF as the mean IPF rain threshold for each box in the corresponding year; that is the value that IPF precipitation must exceed on the date of onset. The date of onset was determined for each box in the SE US for 2009 – 2012 with this new threshold along with the criteria that the thirty day average of the maxima must exceed one standard deviation above the mean after onset and be within one standard deviation of the mean before onset. The results of this sensitivity test are similar to those of the four-year regional average. In general, boxes in the southern and coastal areas of the SE US tend to have an earlier onset date compared to onset determined from the original criteria, and the boxes further inland in the northern and western portions of the SE US tend to have a later onset date. There are also a number of boxes in the SE US for each year where the date of onset does not change when using the criteria of this sensitivity test (Fig. 31). The boxes with earlier onset dates are the result of the annual average of IPF being lower than the mean of IPF for that box. As a result, the thresholds that IPF must exceed on the date of onset and the thirty-day average of the maxima after onset must exceed are lower, leading to earlier dates of onset in those boxes. However, the later onset dates in some boxes are due to the annual mean of IPF being higher than the IPF mean of those boxes. As a result, the value of IPF rain that must be exceeded at onset, along with the standard deviation value that must be exceeded is also higher. Because the increased thresholds in these boxes, onset becomes later when using the annual average of IPF. Similar to the second sensitivity test, boxes where onset did not change when using the annual average of IPF were the result of the mean IPF in those boxes being very similar to the value for the annual average. Because of that, changes in the thresholds were small and did not impact when onset occurred for those areas.

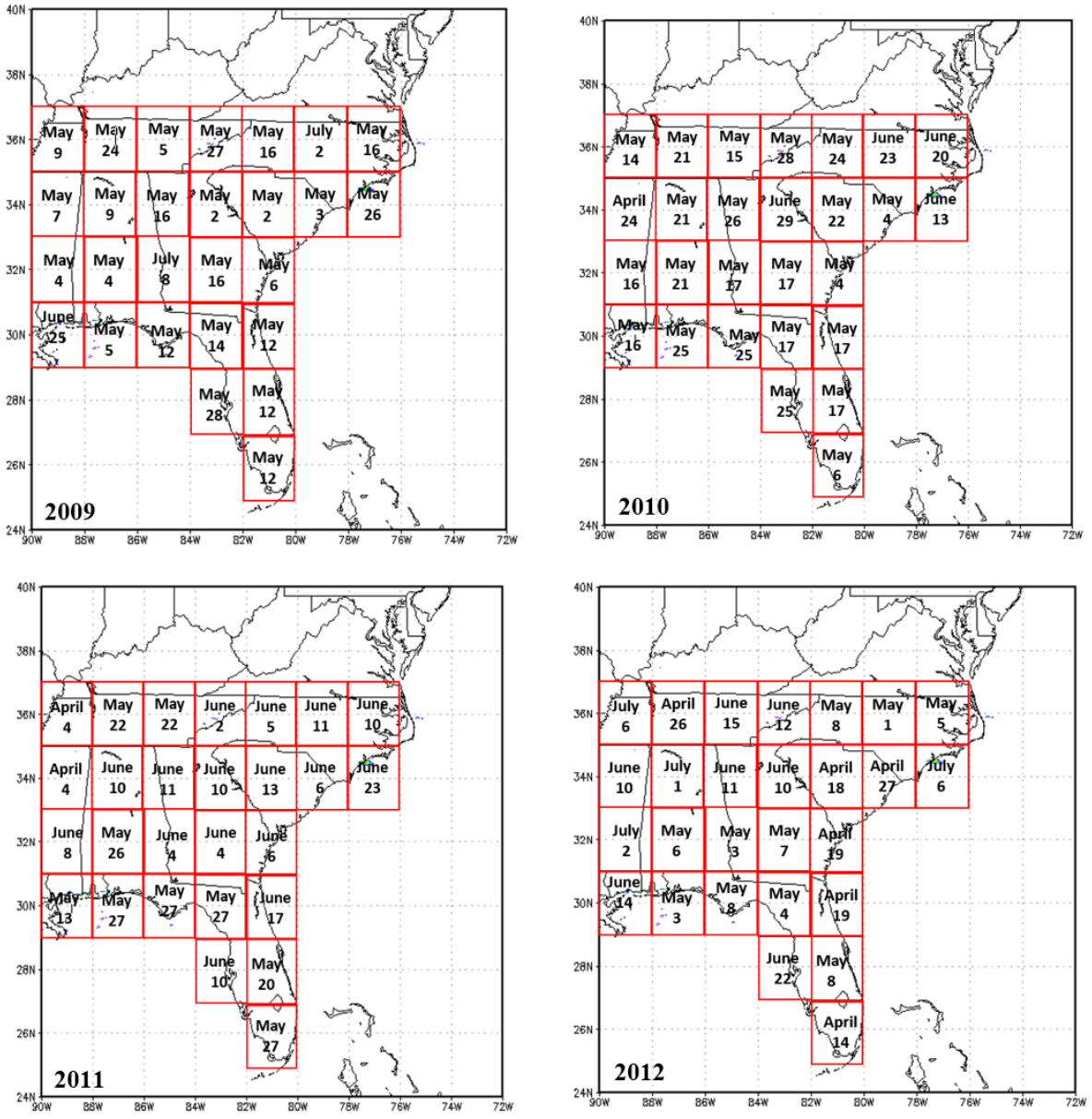

Figure 35: Onset dates for each box in the SE US for the third sensitivity test using the annual average of IPF of each year for: 2009, 2010, 2011, and 2012.

These sensitivity tests were conducted to determine if the date of onset is sensitive to the criteria used, as was indicated by Marengo et al. (2001). After conducting the three sensitivity tests described above, it can be seen that onset of the convective season in the SE US is sensitive to the criteria used. When comparing the mean onset date for the SE US in each year for the

onset criteria and the three sensitivity tests, these differences in onset can be seen. In 2009, the mean date of onset of the onset criteria (average of the maxima) was earlier than onset when using the varying thresholds of the sensitivity tests (Table 2). However, the date of onset also had the greatest spread of dates for the average of the maxima in 2009 compared to the three sensitivity tests (Table 2). Out of the four years, 2010 has the lowest standard deviation for the average of the maxima and all the sensitivity tests (Table 3). In 2010, the mean onset date for the average of the maxima was considerably earlier than the mean onset date of the thirty-day average, and a few days earlier than the annual regional average. However, mean onset for the average of the maxima was a couple days later than that of the four-year regional average (Table 3). For 2011, the mean date of onset for the average of the maxima is much earlier than the mean onset date of the thirty-day average and the four-year regional average, whereas the mean onset date for the annual regional average is a couple days earlier than the average of the maxima (Table 4). 2012 has the largest variability of onset for the average of the maxima and all the sensitivity tests (Table 5). The mean onset date of the average of the maxima is much earlier than the thirty-day average and a few days earlier than the four-year regional average and the annual regional average (Table 5). Tables 6 – 9 show the four-year mean onset date for each box in the SE US for the average of the maxima and each sensitivity test. These further show that there is no progression or pattern to when onset occurs despite different thresholds. As discussed previously, the sensitivity test using the thirty-day average is the only sensitivity test where onset greatly differs from the onset criteria (Tables 2-5, 7). When looking at the mean onset dates for the average of the maxima (Table 6), it is seen that a group of boxes in the northernmost area of the SE US have consistent onset dates over the four years, while a group of boxes in the central SE US have the greatest variability in onset date, having large standard deviations. When

comparing the mean onset date of each year, the thirty-day average is much later than the average of the maxima and the other two sensitivity tests, and Table 6 shows how onset is not defined for much of the SE US when using the thirty-day average. However, though the mean date of onset of the region for each year, and the four-year mean date of onset for each box does not vary too greatly between the average of the maxima, the four-year regional average, and the annual regional average, the criteria used for the average of the maxima is the best criteria to determine onset in the SE US. Using this criteria, over the constant thresholds of the four-year regional average and the annual regional average, onset is relative to the amount of IPF precipitation received in each box. This is an important feature to capture in the determination of onset as IPF rain is quite variable in both amounts and behavior across the SE US.

Year: 2009	**Mean Onset Date of the SE US**	**Standard Deviation of Onset Date**
Average of Maxima	15 May 2009	21.1 days
30 Day Average	8 August 2009	16.5 days
4-year Regional Average	17 May 2009	17.9 days
Annual Regional Average	17 May 2009	17.9 days

Table 2: Average onset date for the SE US & standard deviation of onset for 2009 for the Average of the Maxima, 30 Day Average, 4-year Regional Average, and Annual Regional Average.

Year: 2010	**Mean Onset Date of the SE US**	**Standard Deviation of Onset Date**
Average of Maxima	18 May 2010	11.4 days
30 Day Average	30 July 2010	3.5 days
4-year Regional Average	16 May 2010	12.4 days
Annual Regional Average	22 May 2010	15.0 days

Table 3: As in Table 2, but for 2010.

Year: 2011	Mean Onset Date of the SE US	Standard Deviation of Onset Date
Average of Maxima	31 May 2011	21.8 days
30 Day Average	15 July 2011	21.6 days
4-year Regional Average	10 June 2011	19.9 days
Annual Regional Average	29 May 2011	18.5 days

Table 4: As in Table 2, but for 2011.

Year: 2012	Mean Onset Date of the SE US	Standard Deviation of Onset Date
Average of Maxima	17 May 2012	24.9 days
30 Day Average	6 August 2012	24.8 days
4-year Regional Average	19 May 2012	28.1 days
Annual Regional Average	20 May 2012	27.6 days

Table 5: As in Table 2, but for 2012.

2°x2° Box	Four-year Mean Onset Date	Standard Deviation of Onset Date
25°-27°N, 80°-82° W	17 May	17.9 days
27°-29° N, 80°-82° W	20 May	17.2 days
27°-29° N, 82°-84° W	9 June	12.5 days
29°-31° N, 80°-82°W	15 May	22.6 days
29°-31° N, 82°-84° W	18 May	11.9 days
29°-31° N, 84°-86° W	1 June	16.4 days
29°-31° N, 86°-88° W	16 May	11.1 days
29°-31° N, 88°-90° W	4 June	19.2 days
31°-33° N, 80°-82° W	9 May	20.1 days
31°-33° N, 82°-84° W	18 May	14.5 days
31°-33° N, 84°-86° W	27 May	34.3 days
31°-33° N, 86°-88° W	14 May	10.9 days
31°-33° N, 88°-90° W	29 May	27.4 days
33°-35° N, 76°-78° W	22 June	28.8 days
33°-35° N, 78°-80° W	10 May	18.1 days
33°-35° N, 80°-82° W	15 May	25.4 days
33°-35° N, 82°-84° W	2 June	20.9 days
33°-35° N, 84°-86° W	13 May	17.7 days
33°-35° N, 86°-88° W	24 May	20.8 days
33°-35° N, 88°-90° W	6 May	27.8 days
35°-37° N, 76°-78° W	25 May	18.2 days
35°-37° N, 78°-80° W	27 May	30.4 days
35°-37° N, 80°-82° W	12 May	4.1 days
35°-37° N, 82°-84° W	17 May	7.9 days
35°-37° N, 84°-86° W	18 May	19.7 days
35°-37° N, 86°-88° W	9 May	13.9 days
35°-37° N, 88°-90° W	3 May	31.6 days

Table 6: Four-year (2009-2012) average onset date and standard deviation for the Average of the Maxima.

2°x2° Box	Four-year Mean Onset Date	Standard Deviation of Onset Date
25°-27°N, 80°-82° W	14 August	9.2 days
27°-29° N, 80°-82° W	18 August	15.6 days
27°-29° N, 82°-84° W	4 August	2.8 days
29°-31° N, 80°-82°W	7 August	N/A
29°-31° N, 82°-84° W	21 July	8.9 days
29°-31° N, 84°-86° W	10 July	15.5 days
29°-31° N, 86°-88° W	28 July	30.5 days
29°-31° N, 88°-90° W	27 August	N/A
31°-33° N, 80°-82° W	N/A	N/A
31°-33° N, 82°-84° W	13 July	21.9 days
31°-33° N, 84°-86° W	27 June	N/A
31°-33° N, 86°-88° W	29 July	44.5 days
31°-33° N, 88°-90° W	N/A	N/A
33°-35° N, 76°-78° W	14 August	N/A
33°-35° N, 78°-80° W	N/A	N/A
33°-35° N, 80°-82° W	N/A	N/A
33°-35° N, 82°-84° W	N/A	N/A
33°-35° N, 84°-86° W	N/A	N/A
33°-35° N, 86°-88° W	N/A	N/A
33°-35° N, 88°-90° W	N/A	N/A
35°-37° N, 76°-78° W	N/A	N/A
35°-37° N, 78°-80° W	N/A	N/A
35°-37° N, 80°-82° W	N/A	N/A
35°-37° N, 82°-84° W	N/A	N/A
35°-37° N, 84°-86° W	N/A	N/A
35°-37° N, 86°-88° W	N/A	N/A
35°-37° N, 88°-90° W	N/A	N/A

Table 7: As in Table 6, but for the 30 Day Average.

2°x2° Box	Four-year Mean Onset Date	Standard Deviation of Onset Date
25°-27°N, 80°-82° W	10 May	23.5 days
27°-29° N, 80°-82° W	12 May	25.7 days
27°-29° N, 82°-84° W	7 June	13.8 days
29°-31° N, 80°-82°W	26 May	42.3 days
29°-31° N, 82°-84° W	12 May	10.7 days
29°-31° N, 84°-86° W	19 May	11.2 days
29°-31° N, 86°-88° W	17 May	16.8 days
29°-31° N, 88°-90° W	13 June	19.6 days
31°-33° N, 80°-82° W	10 May	22.9 days
31°-33° N, 82°-84° W	18 May	11.7 days
31°-33° N, 84°-86° W	31 May	28.5 days
31°-33° N, 86°-88° W	17 May	18.3 days
31°-33° N, 88°-90° W	31 May	26.5 days
33°-35° N, 76°-78° W	22 June	28.8 days
33°-35° N, 78°-80° W	11 May	19.6 days
33°-35° N, 80°-82° W	9 May	24.1 days
33°-35° N, 82°-84° W	2 June	20.9 days
33°-35° N, 84°-86° W	29 May	15.0 days
33°-35° N, 86°-88° W	4 June	26.4 days
33°-35° N, 88°-90° W	4 May	28.2 days
35°-37° N, 76°-78° W	27 May	20.0 days
35°-37° N, 78°-80° W	30 May	27.5 days
35°-37° N, 80°-82° W	19 May	14.8 days
35°-37° N, 82°-84° W	26 May	10.4 days
35°-37° N, 84°-86° W	22 May	17.5 days
35°-37° N, 86°-88° W	21 May	19.3 days
35°-37° N, 88°-90° W	25 May	36.0 days

Table 8: As in Table 6, but for the 4-year Regional Average.

2°x2° Box	Four-year Mean Onset Date	Standard Deviation of Onset Date
25°-27°N, 80°-82° W	7 May	17.8 days
27°-29° N, 80°-82° W	14 May	5.3 days
27°-29° N, 82°-84° W	5 June	12.9 days
29°-31° N, 80°-82°W	16 May	24.3 days
29°-31° N, 82°-84° W	15 May	9.5 days
29°-31° N, 84°-86° W	18 May	9.4 days
29°-31° N, 86°-88° W	15 May	12.8 days
29°-31° N, 88°-90° W	1 June	21.3 days
31°-33° N, 80°-82° W	9 May	20.1 days
31°-33° N, 82°-84° W	18 May	11.7 days
31°-33° N, 84°-86° W	31 May	28.5 days
31°-33° N, 86°-88° W	14 May	10.9 days
31°-33° N, 88°-90° W	30 May	26.1 days
33°-35° N, 76°-78° W	16 June	17.3 days
33°-35° N, 78°-80° W	10 May	18.1 days
33°-35° N, 80°-82° W	14 May	24.4 days
33°-35° N, 82°-84° W	5 June	24.4 days
33°-35° N, 84°-86° W	31 May	12.8 days
33°-35° N, 86°-88° W	2 June	23.3 days
33°-35° N, 88°-90° W	4 May	28.2 days
35°-37° N, 76°-78° W	28 May	21.4 days
35°-37° N, 78°-80° W	9 June	27.4 days
35°-37° N, 80°-82° W	21 May	11.9 days
35°-37° N, 82°-84° W	1 June	7.3 days
35°-37° N, 84°-86° W	22 May	17.5 days
35°-37° N, 86°-88° W	15 May	13.2 days
35°-37° N, 88°-90° W	16 May	38.4 days

Table 9: As in Table 6, but for the Annual Regional Average.

5.3 Onset Dates and Meteorological Conditions: 2009

The pentad composites of the NARR meteorological data for 2009 were analyzed to determine what dynamic and thermodynamic variable changes occurred over the SE US near the time of onset. In the pentads before onset over the northwestern areas of the SE US, specific humidity stays in the 6-10 g/kg range, and then in the 26-30 April pentad, specific humidity increases to 12-14 g/kg, indicating a sudden increase in moisture over this area (Fig. 36). Similarly, CAPE is very low (under 500 J/kg) for all of April until 26-30 April when CAPE increases to 500- 700 J/kg over the same area where onset occurs at the end of April (Fig. 37). Meanwhile, the NASH first broadly establishes over the SE US during 21-25 April, with the 1016 hPa contour well over the SE US. The NASH is situated farther south, with the western ridge of the NASH centered over the Gulf of Mexico. This southwesterly flow from the NASH brings warm, moist air from the Gulf of Mexico into the western portion of the SE US in the pentad before onset occurs in this area of the region. By the pentad of onset (26-30 April), the NASH shifts and is centered further north (Fig. 38), with the 1016 hPa contour located well inland in the United States. This leads to strong southerly flow over the western area of the SE US at 850 hPa. This southerly flow over the western portion of the area is bringing warm, moist air into the air, aiding in increasing specific humidity and CAPE in this area. At the same time, the upper-level pattern at 500 hPa transitions from a trough in 21-25 April, to a broad ridge over the SE US during the pentad of onset (Fig. 39). With the center of the ridge located along the east coast, there is southwesterly flow in the upper levels as well over the northwestern portion of the SE US, further aiding in increasing humidity and CAPE in this area. This sudden increase in moisture and instability, likely due to the sudden westward expansion of the NASH in the pentad immediately before and during onset, coupled with the presence of an upper-level ridge,

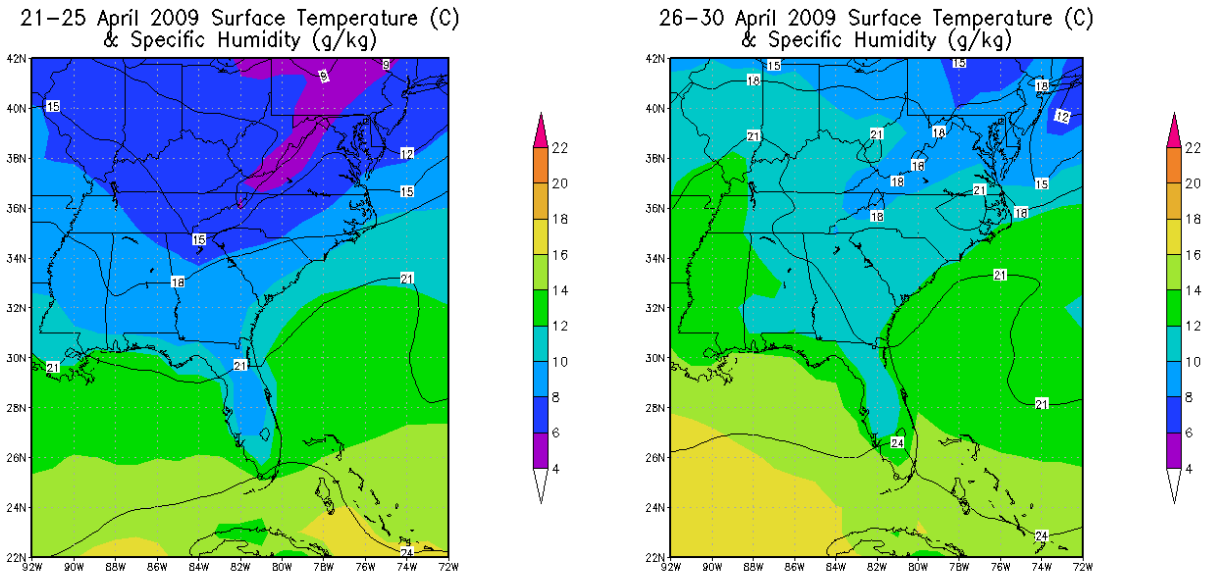

Figure 36: Specific humidity (g/kg, filled) and temperature (°C, contoured) for the pentads 21-25 April and 26-30 April 2009.

offer an explanation for why onset occurs in late April in the western area of the SE US in 2009. As onset occurs in this final pentad of April over this area, the IPF time series corresponding to the boxes in the northwestern SE US show an increase in IPF at the end of April, whereas boxes over much of the rest of the SE US have substantially less IPF during this time. Along with that,

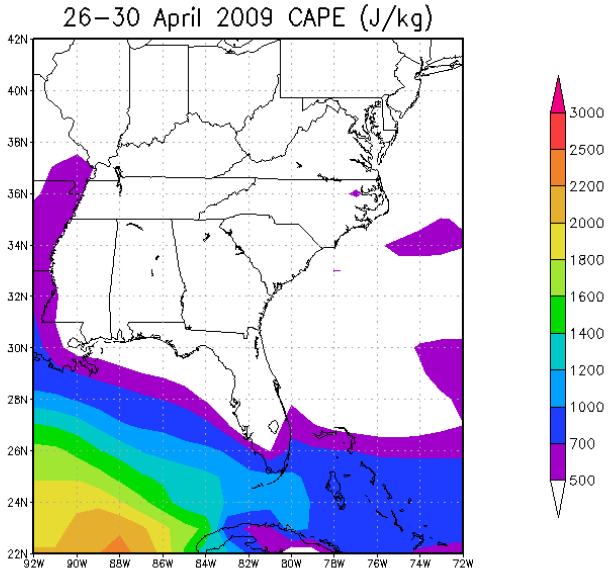

Figure 37: CAPE (J/kg) for the pentad 26-30 April 2009.

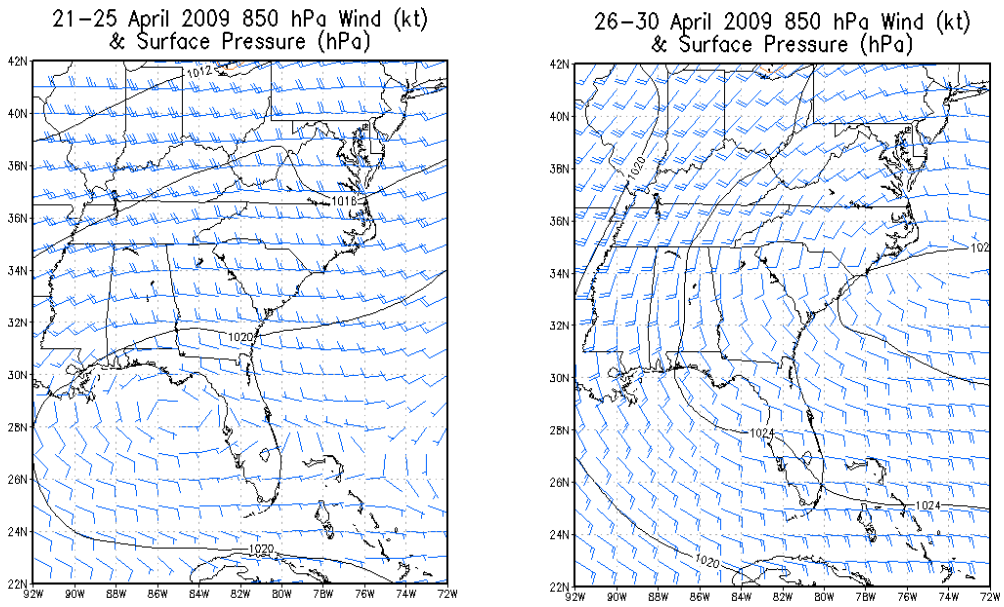

Figure 39: As in Fig. 36, but for MSLP (hPa) and 850 hPa wind (kt).

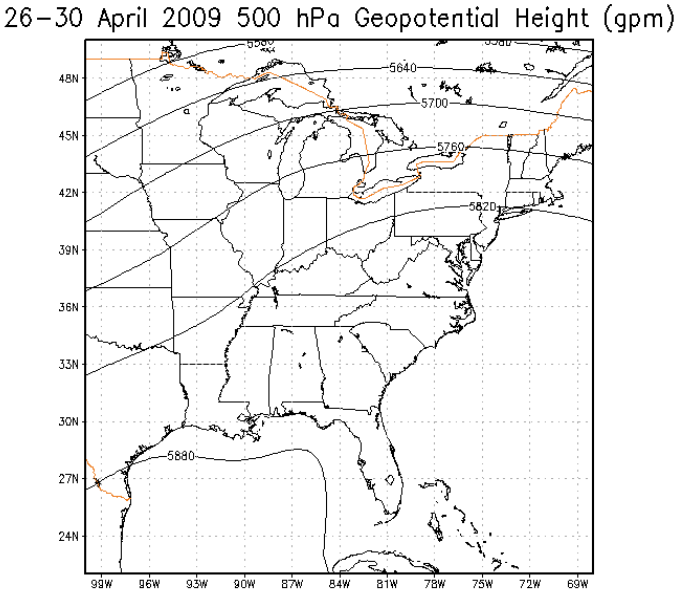

Figure 38: 500 hPa geopotential height in geopotential meters (gpm) for 26-30 April 2009.

IPF generally stays higher after onset than it was before onset in the northwestern portion of the SE US.

For the rest of the SE US, onset generally occurs during the first three pentads of May (1-15 May). During this time, CAPE increases in both amount and areal coverage of the SE US

(Fig. 40). Leading up to the beginning of May, CAPE is negligible over much of the SE US (not shown), with the only substantial amount of CAPE in April being the tongue of CAPE over the western SE US at the end of April. However, during the first pentad of May, CAPE suddenly

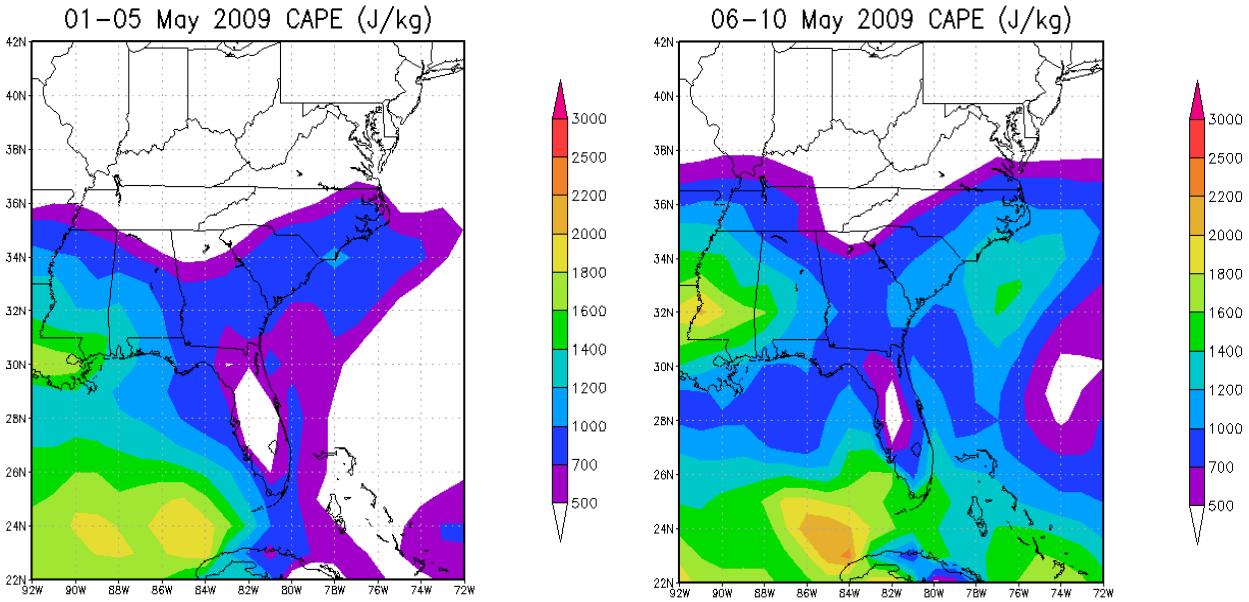

Figure 40: CAPE (J/kg) for the pentads 1-5 May and 6-10 May 2009.

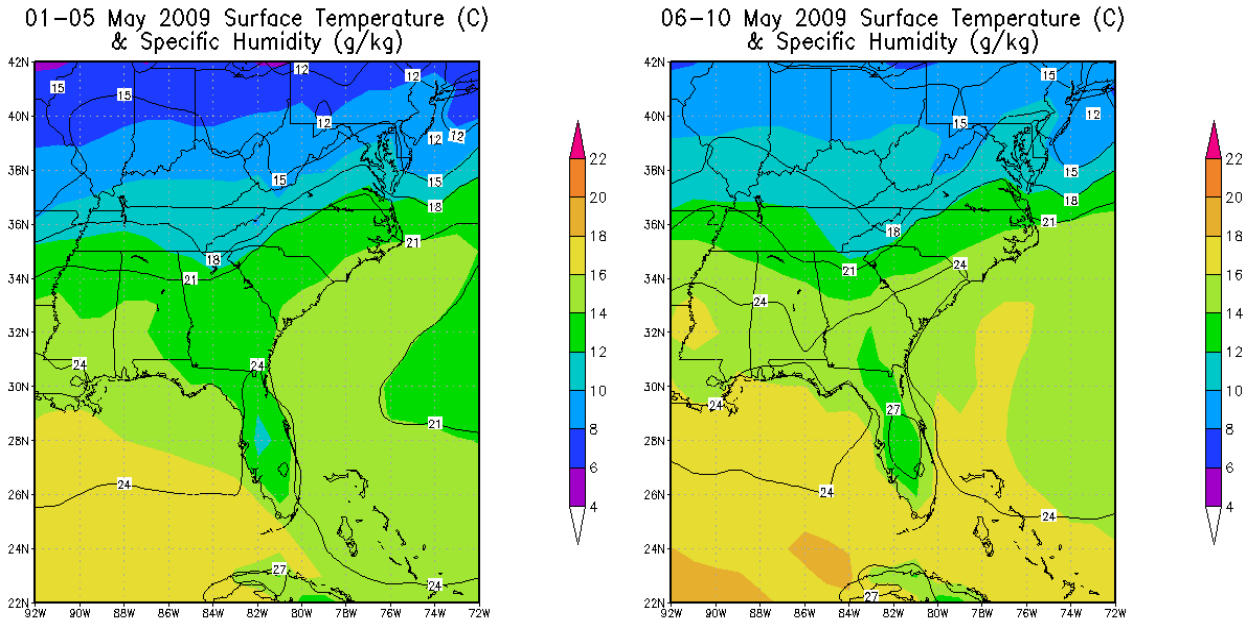

Figure 41: As in Fig. 40, but for specific humidity (g/kg, filled) and temperature (°C, contoured).

spreads over most of the SE US, with values of CAPE ranging from 500-1000 J/kg in Florida and areas along the Atlantic Coast. Over the Gulf Coast, CAPE ranges from 1000-1800 J/kg, which is a sudden increase from the previous pentads. During the next pentad of May, CAPE continues increasing in strength over the SE US (Fig. 40), indicating that instability is continuing to increase in the first two pentads of May over much of the SE US where onset is occurring. Similar to CAPE, specific humidity increases from the end of April through the first three pentads of May. During the final pentad of April, specific humidity over the rest of the SE US (excluding the western portion where onset was occurring) is in the 8-10 g/kg range, indicating that there is not much moisture over most of the SE US. However, during the first two pentads of May, specific humidity increases, and by 6-10 May, specific humidity increases to 12-14 g/kg over central Florida and to 14-18 g/kg over more of the inland areas of the SE US (Fig. 41), indicating that moisture is continuing to increase over the SE US in early May when onset is

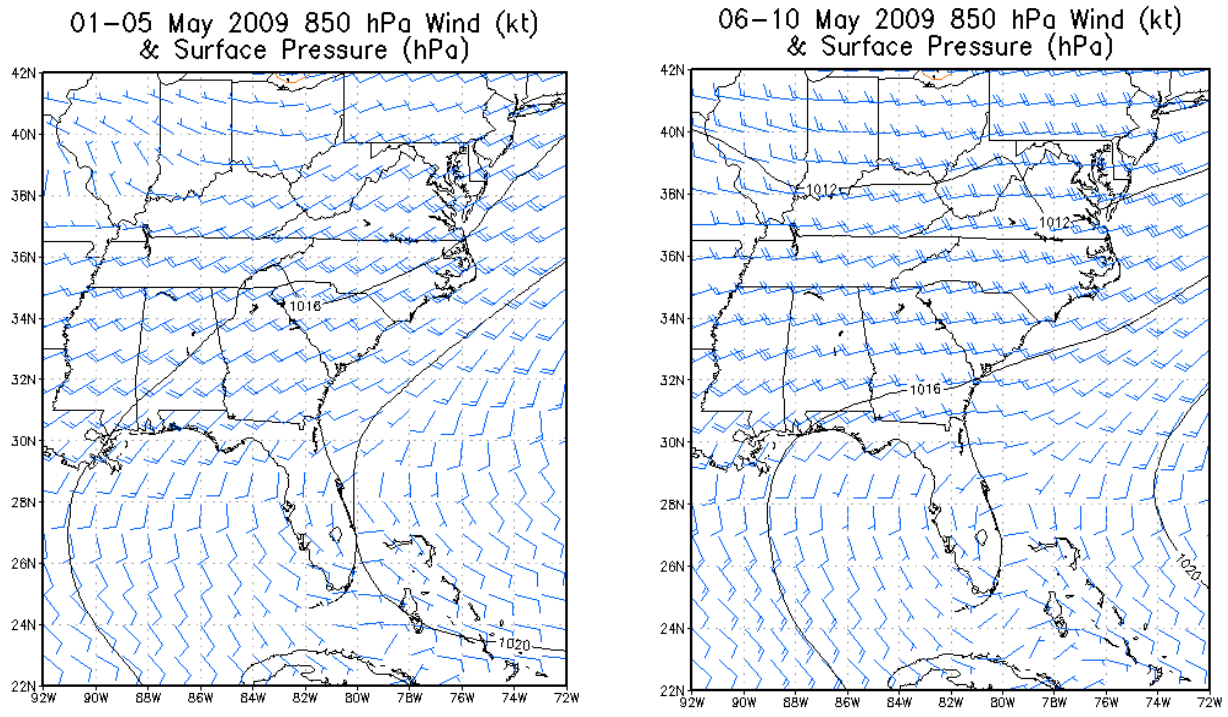

Figure 42: As in Fig. 40, but for MSLP ((hPa) and 850 hPa winds (kt).

occurring throughout the SE US. During the first pentad of May, the NASH moves southward so its western ridge is broadly located over Florida and the Gulf of Mexico, and the 1016 hPa contour is over the Gulf of Mexico and the eastern portion of the SE US. During the second pentad of May, the NASH shifts slightly eastward, though it is still broadly centered over the Gulf of Mexico and Florida. The 1016 hPa contour is largely in the same position as the previous pentad, though it has shifted slightly eastward (Fig. 42). With the NASH positioned in this location, southwesterly flow over the Gulf of Mexico is bringing moisture into much of the SE US, aiding in increasing moisture and instability. During this time at 500 hPa, there is broadly zonal flow over the SE US (Fig. 43), which aids in the NASH staying established in the lower levels during onset. When examining the IPF time series around the time of onset, IPF begins increasing in May, and then abruptly increases in mid-May around the time of onset, particularly for the boxes in Florida. Onset occurring in early to mid-May in a majority of the SE US is likely related to this more southern location of the NASH in early May, which leads to sudden increases in both specific humidity and CAPE during the first two pentads of May, with the thermodynamic and dynamic variables coming together to cause onset.

After 15 May 2009, onset has generally occurred in the SE US (with the exception of the few outlying boxes with later onset dates, as explained previously). After mid-May, the NASH is very episodic. The NASH will become established over the area for a pentad and then break down, and re-establish itself again, likely related to the passage of troughs at 500 hPa in the same pentad where the NASH is disrupted (not shown). For the rest of May and June, the pentads where the NASH is not present over the SE US correspond to pentads where there is an upper-level trough at 500 hPa over the SE US. This episodic behavior of the NASH continues for the rest of May and for much of June, with the NASH more or less staying established over the area

by July. As is expected during the late spring and summer months, CAPE and specific humidity both continue to increase over the SE US for the rest of May to July (not shown).

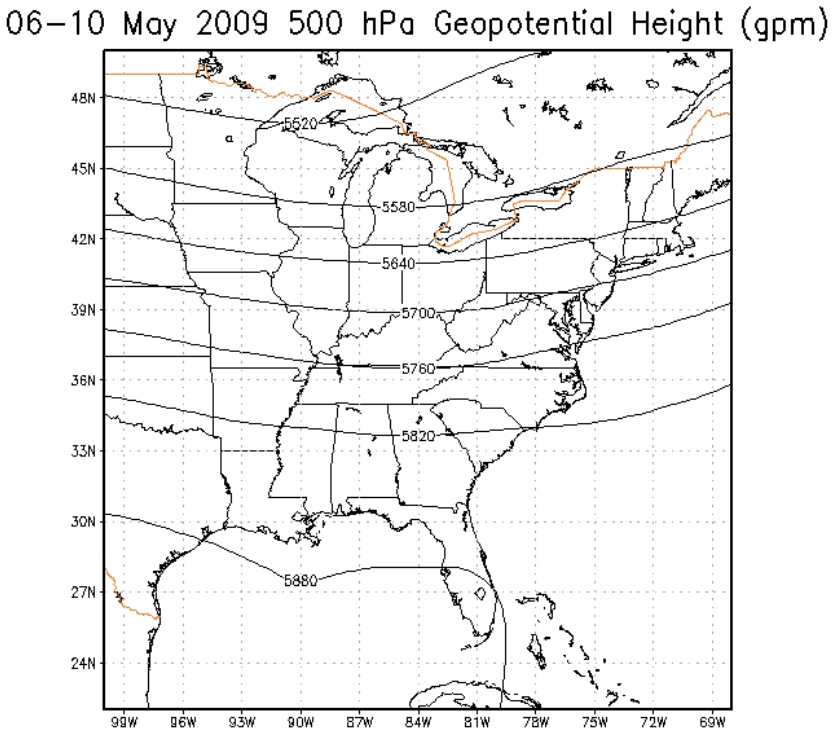

Figure 43: 500 hPa geopotential height (gpm) for 6-10 May 2009.

5.4 Onset Dates and Meteorological Conditions: 2010

When first analyzing the NARR data in relation to the late April onset date in western Tennessee, CAPE and specific humidity are quite low (CAPE is less than 500 J/kg and specific humidity is in the 6-8 g/kg range, not shown). However, there is southwesterly flow over western Tennessee that could be playing a role in triggering onset in late April there (Fig. 44). In North Carolina, South Carolina, and coastal Georgia, where onset occurs in the first pentad of May, CAPE increases from below 500 J/kg in the final pentad of April to 500-1000 J/kg in the first pentad of May (Fig. 45), indicating a sudden increase in instability. Along with that, specific humidity increases from 8-10 g/kg in this area during the final pentad of April to 14-16 g/kg in the first pentad of May when onset occurs (Fig. 46). This abrupt increase in moisture and instability over North and South Carolina and Georgia is likely due to the NASH setting up over SE US during the first pentad of May, (Fig. 47). The western ridge of the NASH is broadly centered over Florida, and extends fairly far inland over the SE US, with the 1016 hPa contour located over Florida and Atlantic coast of the SE US. With the NASH

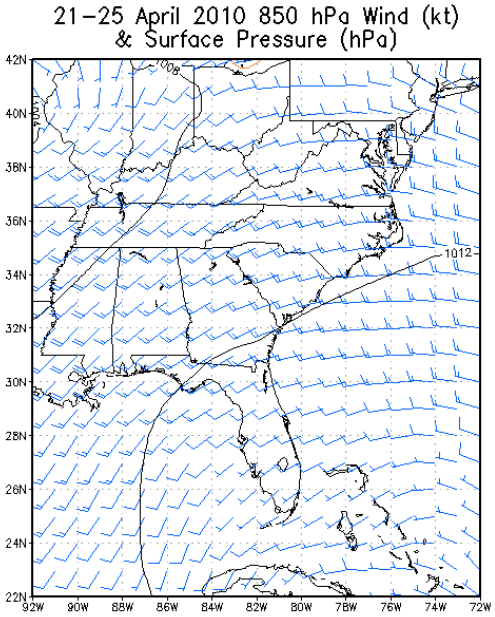

Figure 44: 850 hPa wind (kt) and MSLP (hPa) for 21-25 April 2010.

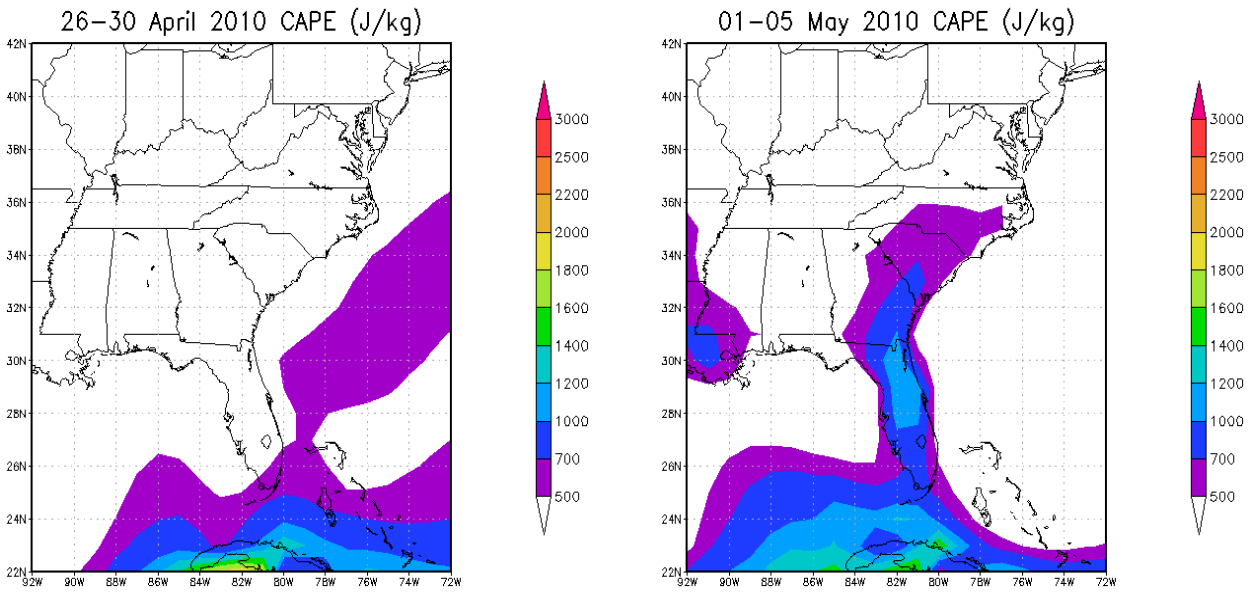

Figure 45: CAPE (J/kg) over the SE US for 26-30 April and 1-5 May 2010.

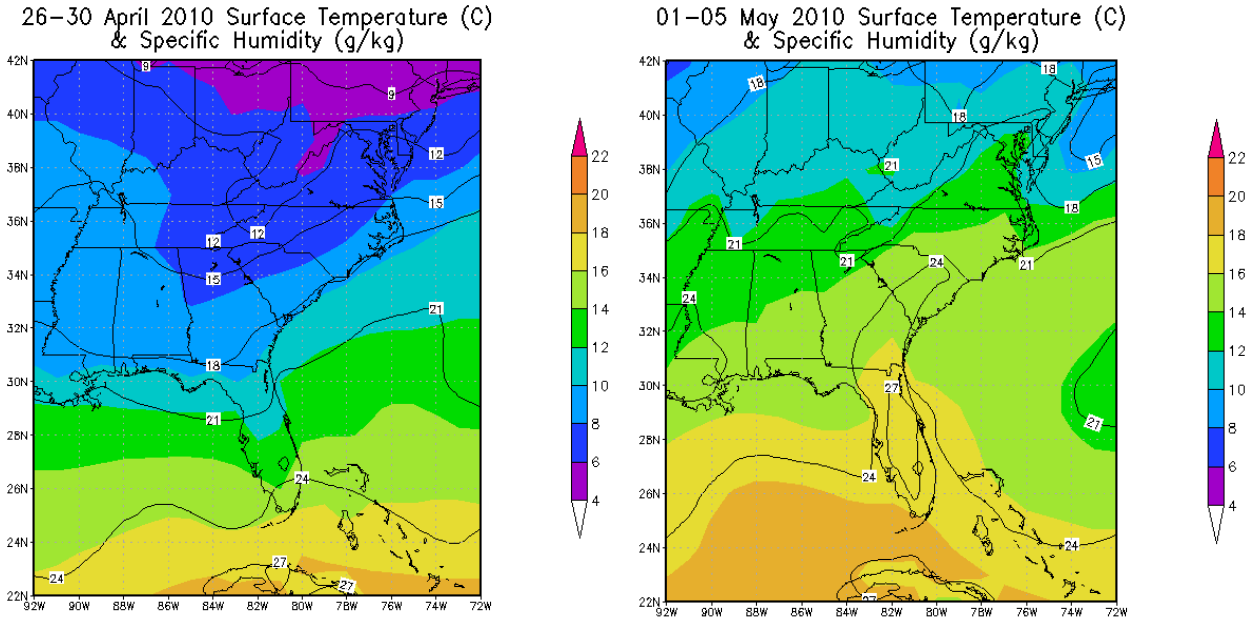

Figure 46: As in Fig. 45, but for specific humidity (g/kg, filled) and temperature (°C, contoured).

located in this position, it leads to southwest flow over this area and brings in warm and moist air that increases humidity and CAPE, leading to onset in these three boxes in the first pentad of

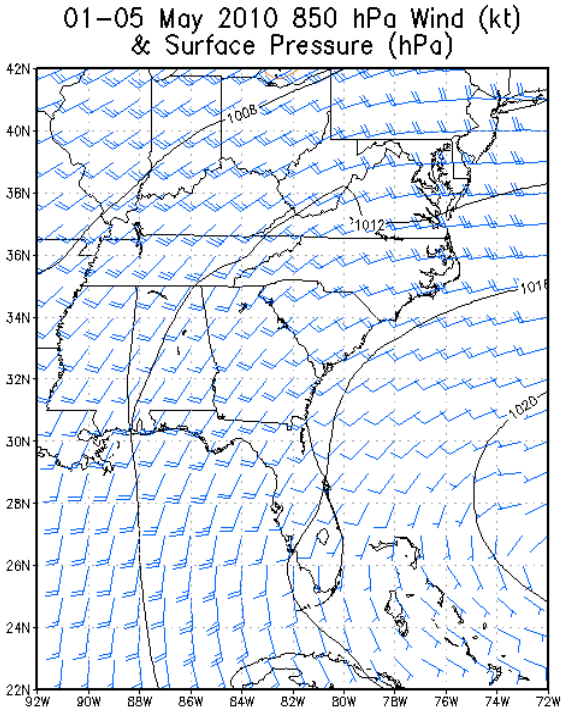

Figure 47: 850 hPa winds (kt) and MSLP (hPa) for 1-5 May 2010.

May. Onset occurring during the first pentad of May in these boxes in North and South Carolina and Georgia also corresponds to a spike in IPF in the beginning of May in these same boxes.

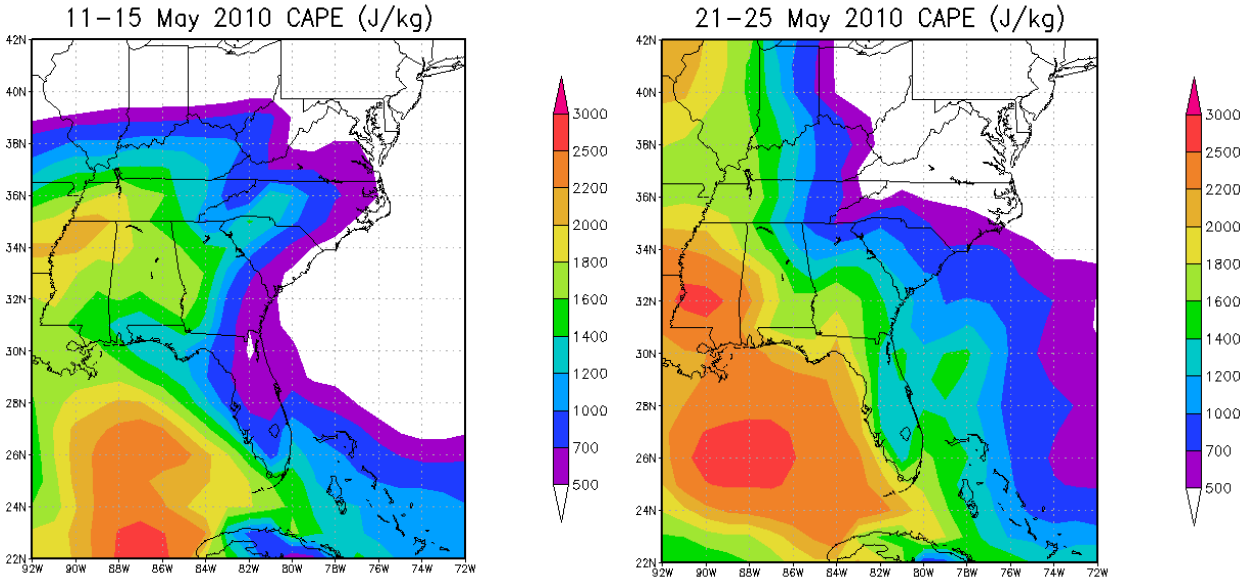

Figure 48: CAPE (J/kg) for 11-15 May and 21-25 May 2010.

For the rest of the SE US, onset occurs during mid to late May. CAPE stays below 500 J/kg for all of April, with specific humidity staying below 12 g/kg for most of the SE US in April, and the NASH does not really set up over the SE US during April. However, during the first three pentads of May leading up to onset, CAPE continues to increase across the SE US, in both strength and areal coverage. In the first pentad of May, CAPE is confined to Florida, along the coast of Georgia, North Carolina, and South Carolina, and in the far western portion of the SE US in Louisiana, with the values of CAPE ranging from 500-1200 J/kg. By the third pentad of May (11-15 May), CAPE has increased considerably over the SE US, and when analyzing the IPF time series, IPF begins increasing over much of this same area during this time. CAPE values in the western region of the SE US range from 1400-2200 J/kg, with values in the eastern half of the SE US ranging from 500-1400 J/kg (Fig. 48). During this time, boxes in the western domain receive an increased amount of IPF (corresponding to the larger values of CAPE) than the boxes in the eastern region where CAPE was lower, though IPF still increased in the eastern boxes. This rapid increase in CAPE over the first three pentads of May indicate that the atmosphere is becoming increasingly unstable leading up to onset. This increase of CAPE in mid-May is likely associated with the establishment of the NASH, rather than the passage of midlatitude cyclones as the 500 hPa flow in early to mid-May is dominated by either ridging or zonal flow. In mid to late May, CAPE continues to increase across the SE US, with areas in the western portion seeing CAPE values exceeding 2500 J/kg on 21-25 May (Fig. 44), indicating that instability is continuing to increase during the pentads of onset. Whereas CAPE had a more rapid increase in the pentads leading up to onset, specific humidity appears to fluctuate over the

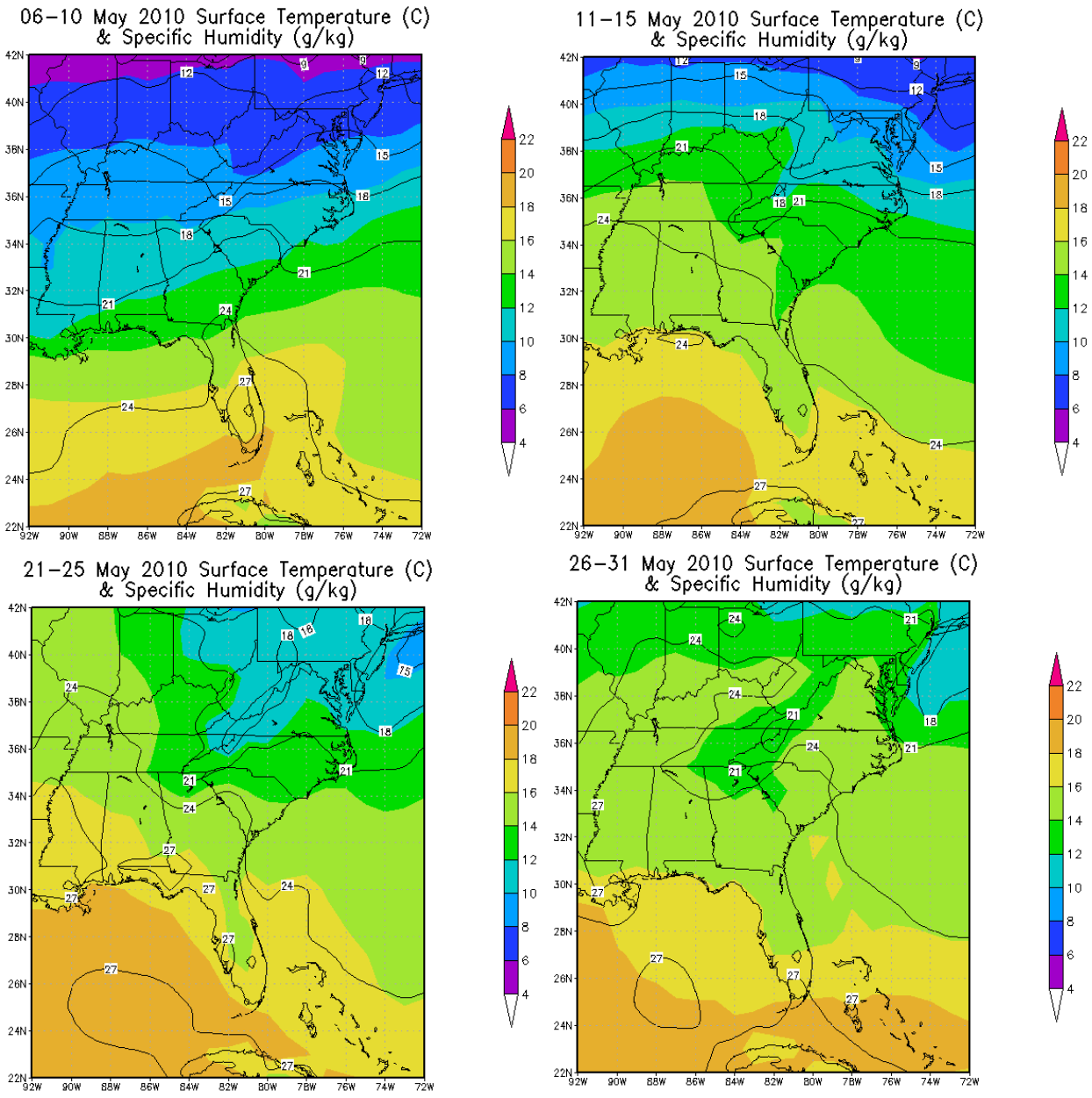

Figure 49: Specific humidity (g/kg, filled) and temperature (C, contoured) for: 6-10 May, 11-15 May, 21-25 May, 26-31 May 2010.

SE US in May. Specific humidity is in the 12-18 g/kg range in the first pentad of May over the SE US, but decreases in the next pentad, with much of the SE US in the 8-12 g/kg range. By 11-15 May, specific humidity increases again, with humidity over much of the SE US in the 12-16 g/kg range. Specific humidity continues to fluctuate during the pentads of onset in the SE US. During 16 – 20 May, humidity over Florida increases to 16-18 g/kg, then decreases to 10-14 g/kg

over the northern portions of the SE US. However, specific humidity generally increases during the last two pentads of May (Fig. 49).

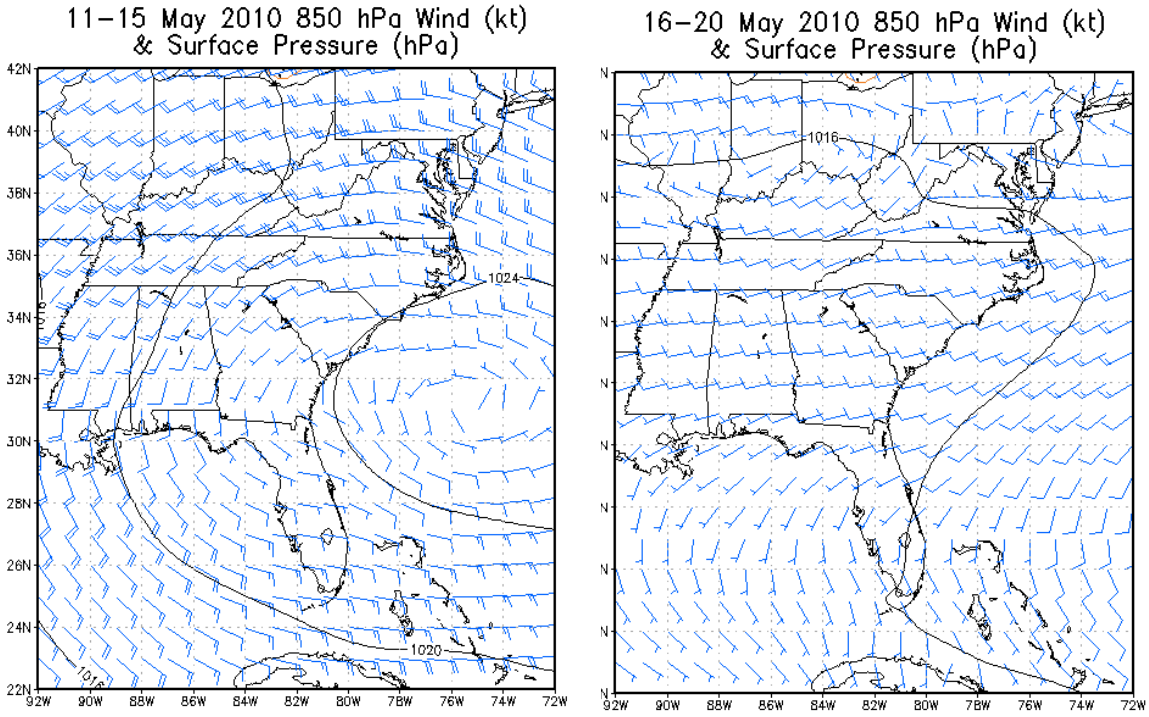

Figure 50: MSLP (hPa) and 850 hPa winds (kt) for 11-15 May and 16-20 May 2010.

The NASH exhibits rather episodic behavior over the SE US in 2010. The NASH becomes established during the first pentad of May and its western ridge is broadly centered over Florida, as discussed earlier in this section. However, in the following pentad, the NASH breaks down then re-establishes itself over the SE US in the third pentad of May, which is the pentad immediately before onset begins for much of the SE US (Fig. 50). During this third pentad of May, the 1016 hPa contour is located inland, indicating that the NASH is well-established in the SE US. During this time, the NASH is centered off the coast of South Carolina and Georgia, with the western ridge extending into Mississippi and Alabama. Fairly weak upper-level flow at 500 hPa aids in the NASH staying established during this time as there is nothing in the upper-levels

to disrupt the NASH (not shown). With the NASH in this location, southerly flow is present over the entire SE US, providing ample moisture and warm air for the region. In the following pentad (16-20 May), the NASH is not present over the SE US, though there is still weak southwest flow over portions of the SE US (Fig. 50). The southwest flow from the NASH bringing warm, moist air over the SE US, combined with increasing CAPE and specific humidity, during the pentad immediately before onset and the first pentad during onset are the most likely mechanisms causing onset in the SE US. When analyzing the IPF time series, IPF events are increasing in amount in mid to late May, corresponding to when onset is occurring for much the SE US.

After the end of May when onset has occurred over most of the SE US, CAPE and specific humidity continue to increase in June and July, as is expected during the summer months. The NASH continues to exhibit episodic behavior throughout most of June, but generally stays established over the region by July (not shown).

5.5 Onset Dates and Meteorological Conditions: 2011

In analyzing the NARR data in relation to when onset occurs, there does not seem to be any discernible changes in any of the meteorological variables in the western boxes where onset occurs in the first pentad of April. Specific humidity and CAPE are very low over that region in the beginning of April, and the NASH is not yet established over the SE US. There was a severe weather outbreak over this region that could have caused onset to occur (Storm Prediction Center). Over much of the rest of the SE US, onset occurs during the very end of May into mid-June.

In analyzing the NARR data for May leading up to when onset generally begins in 2011 in late May and early June, CAPE is variable over the SE US during the first four pentads of May (not shown). However, by the final two pentads of May (21-31 May), CAPE increases and

spreads over the SE US, with CAPE values ranging from 1000-1600 J/kg for much of the SE US, and some areas along the Atlantic Coast and Florida have CAPE values as high as 2000 J/kg (Fig. 51). In the first pentad of June, CAPE rapidly increases over much of the SE US, with values exceeding 1800 J/kg in much of the SE US, and a portion of the western region exceeding 3000 J/kg of CAPE (Fig. 51).

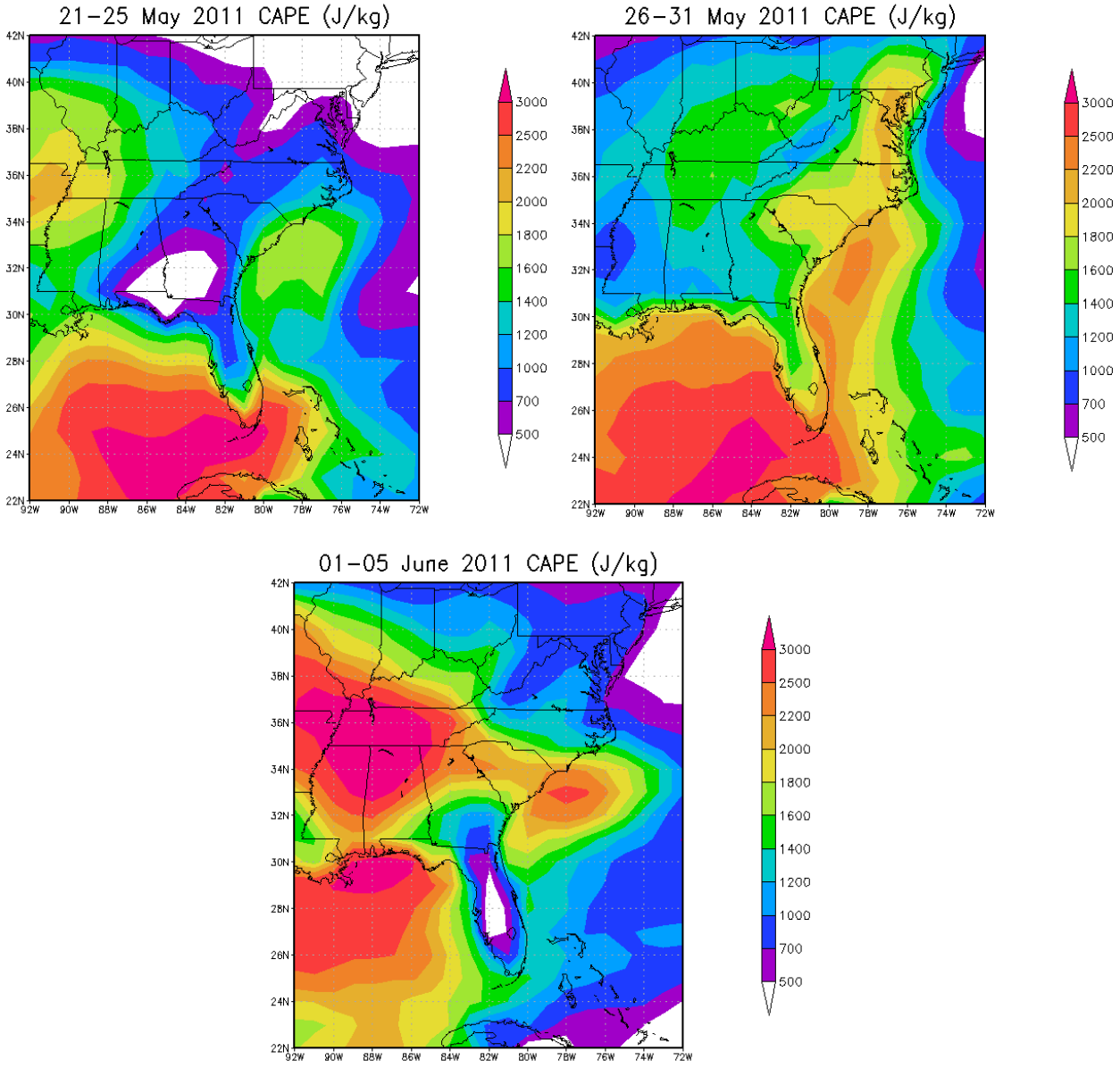

Figure 51: CAPE (J/kg) for the pentads: 21-25 May, 26-31 May, and 1-5 June 2011.

This rapid increase in CAPE indicates that the atmosphere is quickly becoming unstable during the first pentad of June. CAPE then decreases slightly during the second and third pentads of June, but increases again by the fourth pentad (16-20 June, not shown). Specific humidity stays fairly low (generally below 12 g/kg) through the middle of May. Similar to CAPE, specific humidity begins increasing during the last two pentads of May. Specific humidity increases from

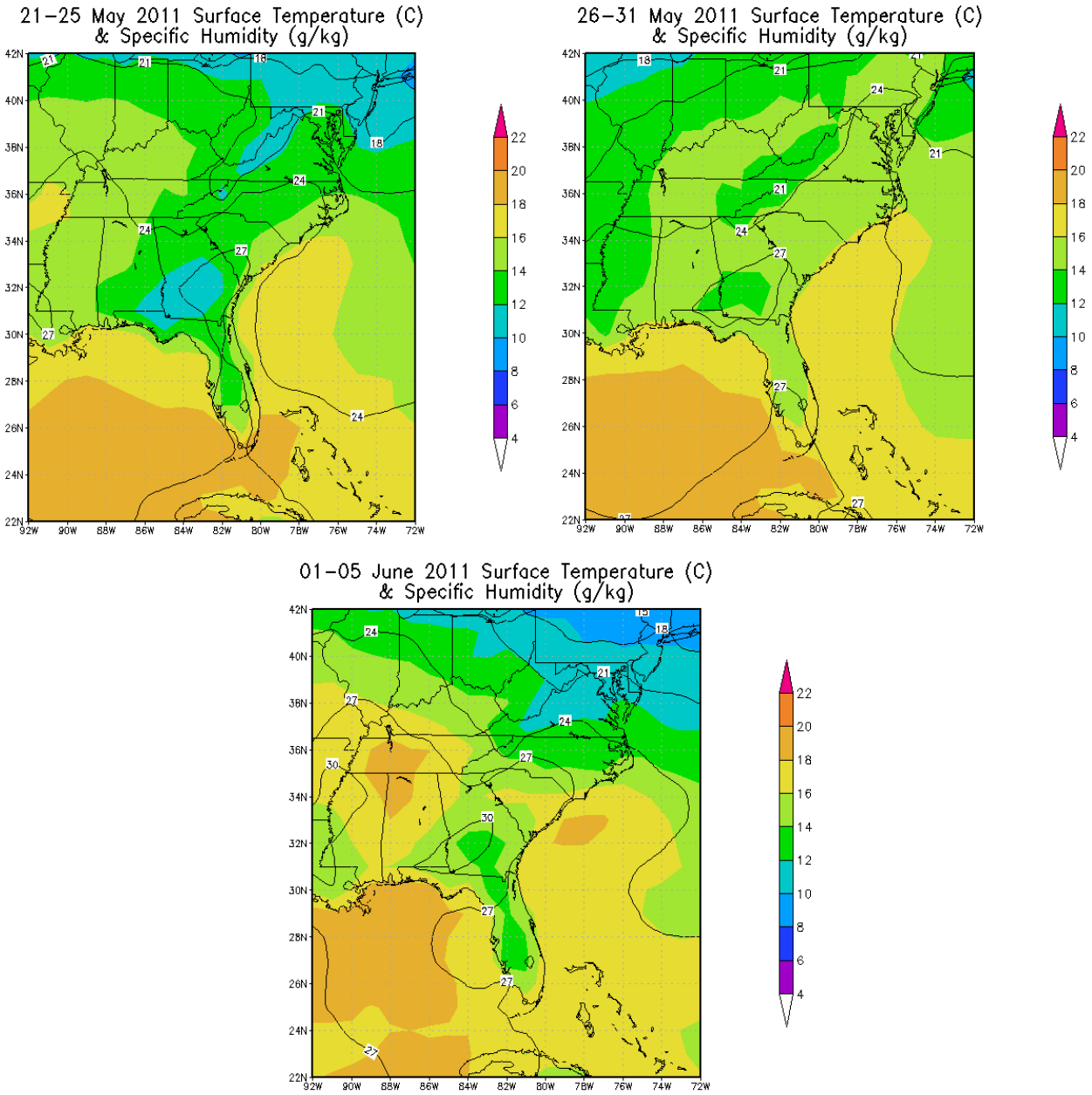

Figure 52: As in Fig. 51, but for specific humidity (g/kg filled) and temperature (°C, contoured).

less than 12 g/kg to 12-16 g/kg over most of the SE US at the end of May (Fig. 52). Similar to CAPE, specific humidity continues increasing into the beginning of June, though it does not increase quite as drastically. In the first pentad of June, specific humidity increases to 16-20 g/kg over most of the SE US (Fig. 52). The NASH is more or less present over the area for most of April, though it is not present for most of May (not shown). The NASH re-establishes itself over the SE US during the final two pentads of May, with the western ridge of the NASH centered just west of Florida (Fig. 53). The 1016 hPa contour is located over Florida and the Atlantic coast during this period. With this re-establishment of the NASH over the SE US at the end of May, there is a distinct spike in IPF rain in many of the boxes over the SE US at this time. With the NASH in this location, there is ample southwesterly flow over the SE US, bringing moisture into the area during the end of May, helping to increase both specific humidity and CAPE. The NASH is disrupted in the first pentad of June and again re-establishes itself over the area during the second pentad of June (Fig. 54), though this time the NASH is centered just off the Atlantic Coast. From the final pentad of May through the first two pentads of June, the SE US is dominated by ridging at 500 hPa (Fig. 55). The presence of this upper-level ridge at the time of onset in the SE US helps the NASH stay established. Increasing specific humidity and the rapid increase in CAPE during the first pentad of June, combined with the NASH establishing itself over the SE US at the end of May are the likely mechanisms that cause onset to occur in the SE US during late May to early June. Following onset, the NASH continues to exhibit episodic behavior where it becomes established, is disrupted, and re-establishes over the area for the rest

of June, then stays more or less established for most of July. As in the two previous years, CAPE and specific humidity continue to increase for the rest of June and into July (not shown).

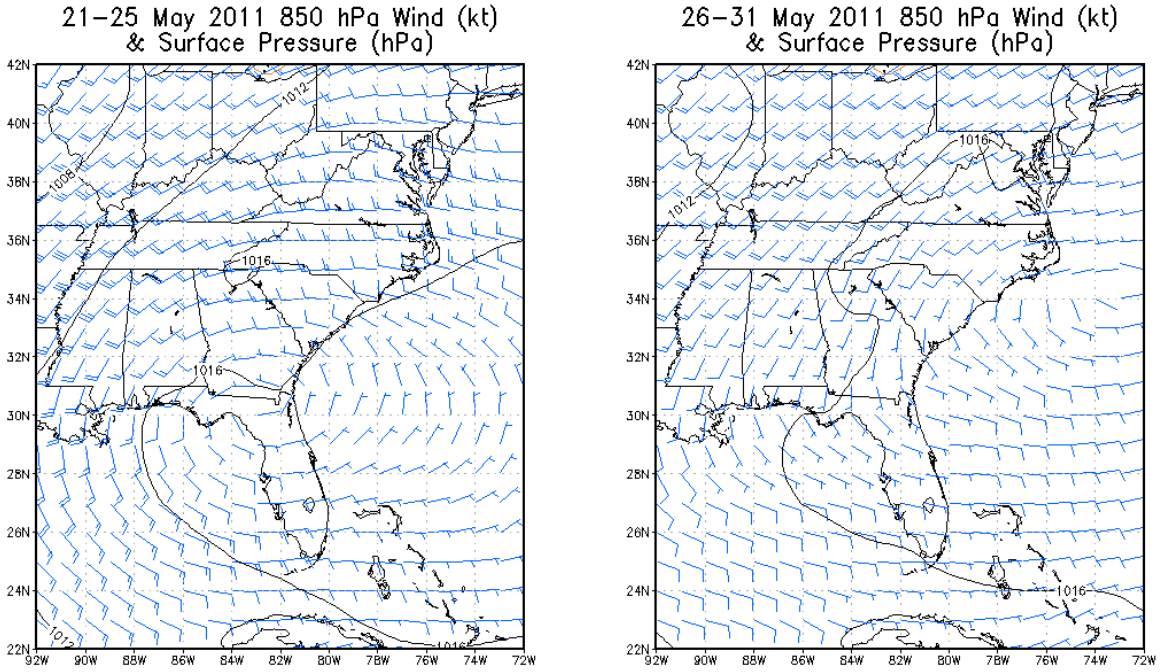

Figure 53: MSLP (hPa) and 850 hPa winds (kt) for 21-25 May and 26-31 May 2011.

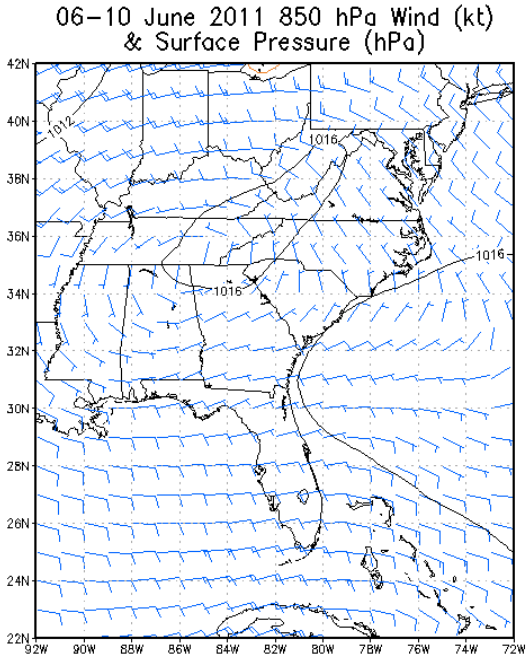

Figure 54: As in Fig. 53, but for 6-10 June 2011.

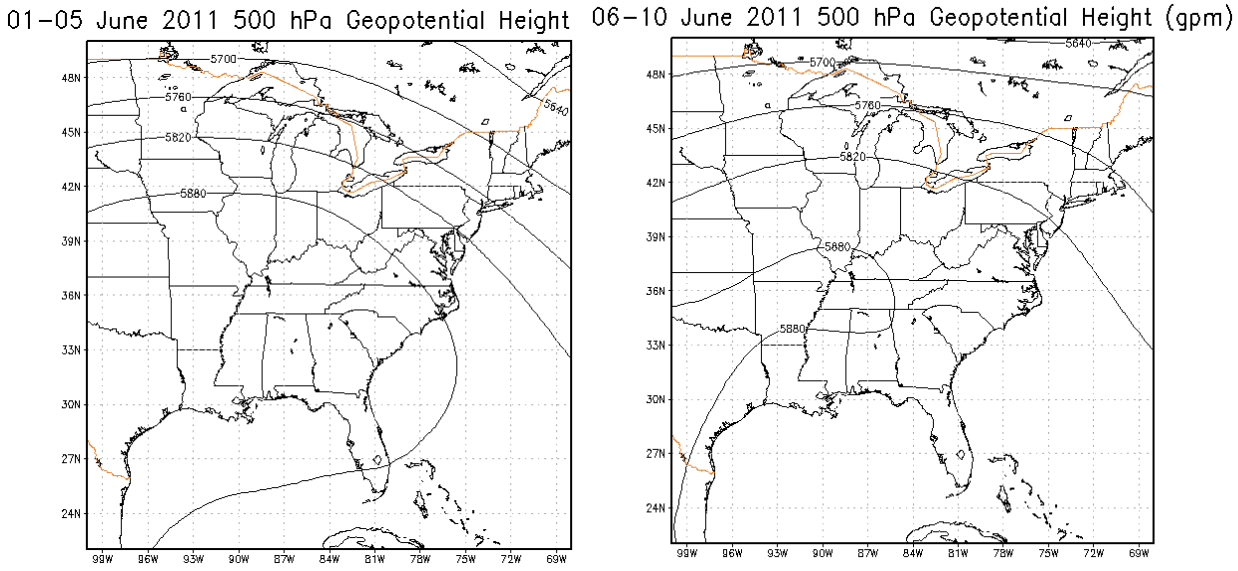

Figure 55: 500 hPa geopotential height (gpm) for 1-5 June and 6-10 June 2011.

5.6 Onset Dates and Meteorological Conditions: 2012

In southeast Georgia and northeast Florida, onset occurs during the fourth pentad of April (16-20 April). In the pentads leading up to when onset occurs in this area, specific humidity and CAPE remain rather low. However, during the pentad of onset, there is a small area of specific humidity along the coast of Georgia and northeastern Florida that ranges from 14-16 g/kg (Fig.

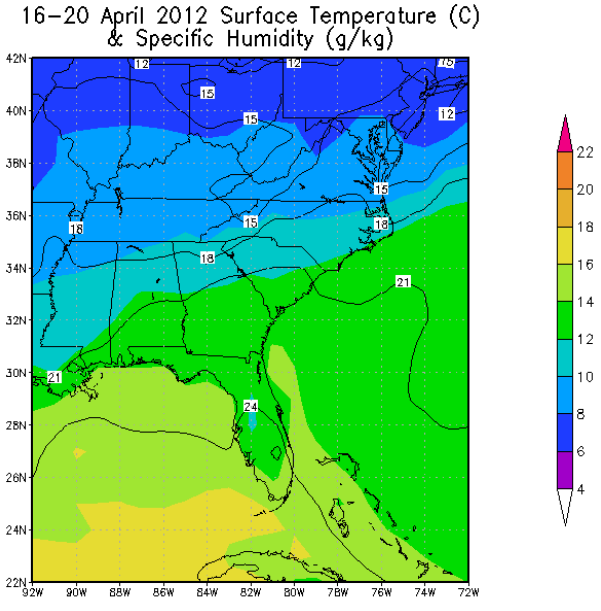

Figure 56: Specific humidity (g/kg, filled) and temperature (°C, contoured) for 16-20 April 2012.

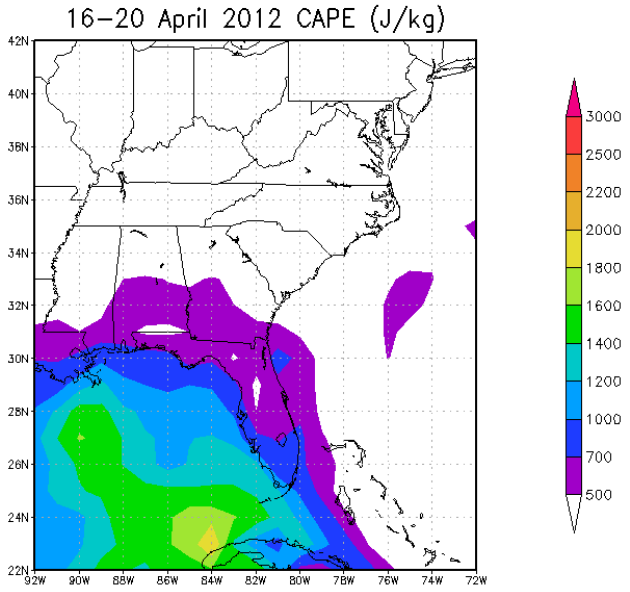

Figure 57: As in Fig. 56, but for CAPE (J/kg).

56), and CAPE values ranging from 500-1000 J/kg along the coast (Fig. 57). While the NASH is not present during this period, there is southerly flow focused over Florida and Georgia (Fig. 58), and there is a spike in IPF during this time in southeastern Georgia and northeastern Florida. Along with southerly flow during the pentad of onset, a ridge at 500 hPa is present off the coast of Florida (Fig. 59), causing southwesterly flow at the upper-levels and providing another source of moisture to this area.

Over much of the rest of the SE US, onset does not occur until later in April into early May. After onset occurs in those boxes in coastal Georgia and northeastern Florida, CAPE decreases and recedes during the following pentad (21-25 April). However, by the following pentad, CAPE increases to 500-1200 J/kg over much of the SE US (not shown). CAPE continues to increase during the first pentad of May, with CAPE values in the eastern area of the SE US ranging from 700-1400 J/kg, and from 1400-2000 J/kg in the western area of the SE US (Fig. 60), indicating that instability is quickly increasing over the SE US during onset. The western

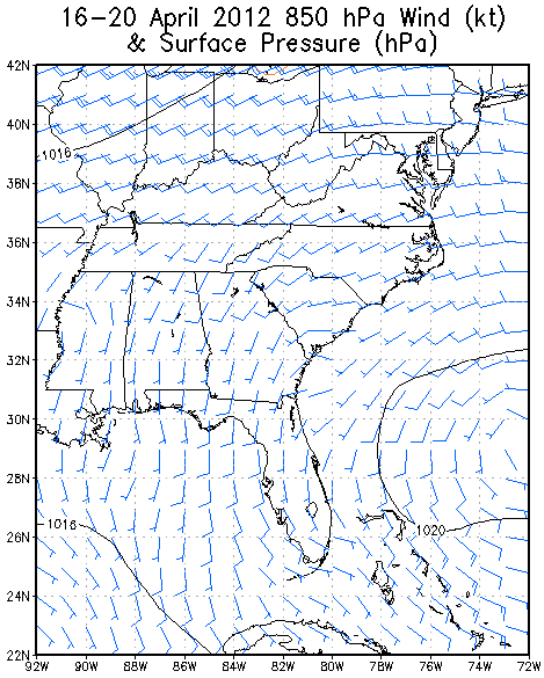

Figure 58: As in Fig. 56, but for MSLP (hPa) and 850 hPa winds (kt).

boxes where CAPE is higher compared to the eastern boxes also generally have more IPF rain than the boxes in the east where CAPE is lower. The cause for this decrease and increase in CAPE in consecutive pentads is likely related to the 500 hPa pattern transitioning from ridging to troughing, then back to ridging in consecutive pentads (not shown), with CAPE decreasing when there is an upper-level trough, and increasing under a ridge. CAPE again recedes across the SE US during the following two pentads of May, then gradually increases for the remainder of May. Similar to CAPE, specific humidity decreases across the SE US during 21-25 April, following onset in those two boxes in Georgia and Florida. As with CAPE, specific humidity then immediately increases across the region again during the final pentad of April and first pentad of May, increasing to 12-16 g/kg (Fig. 61), which is during the time of onset. After 1-5 May, specific humidity decreases for the following three pentads, then gradually increases again over the SE US. This gradual increase in specific humidity (and CAPE) is likely due to the gradual

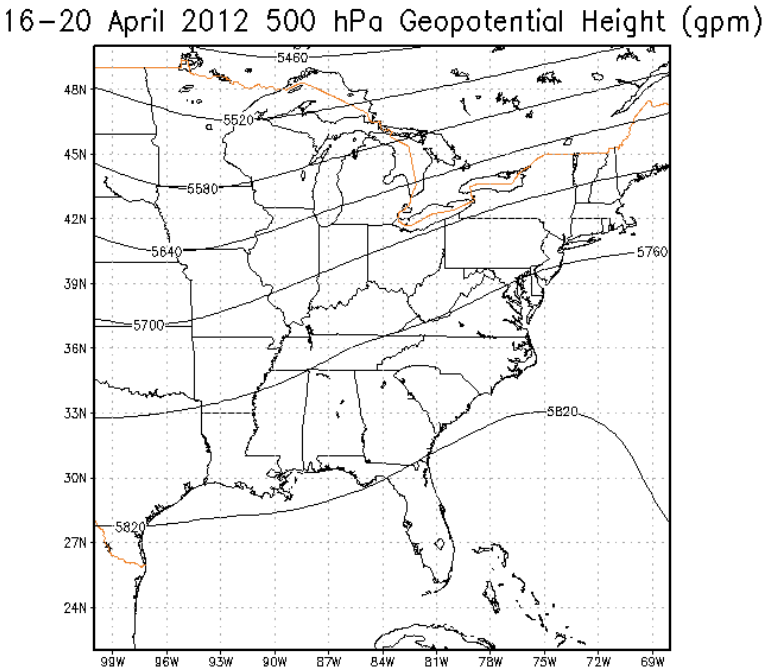

Figure 59: As in Fig. 52, but for 500 hPa geopotential height (gpm).

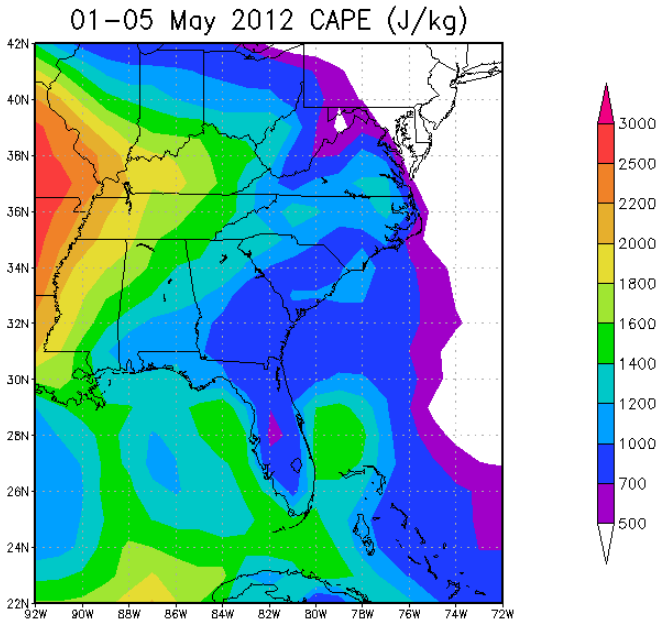

Figure 60: CAPE (J/kg) for 1-5 May 2012.

seasonal warming that occurs in the late spring. After onset in the boxes in Georgia and Florida, the NASH first becomes established over the SE US in the final pentad of April In the final pentad of April, the NASH is centered off the Florida coast, with the 1016 hPa contour located over the western portion of the SE US and the Gulf of Mexico, so the southwesterly flow from

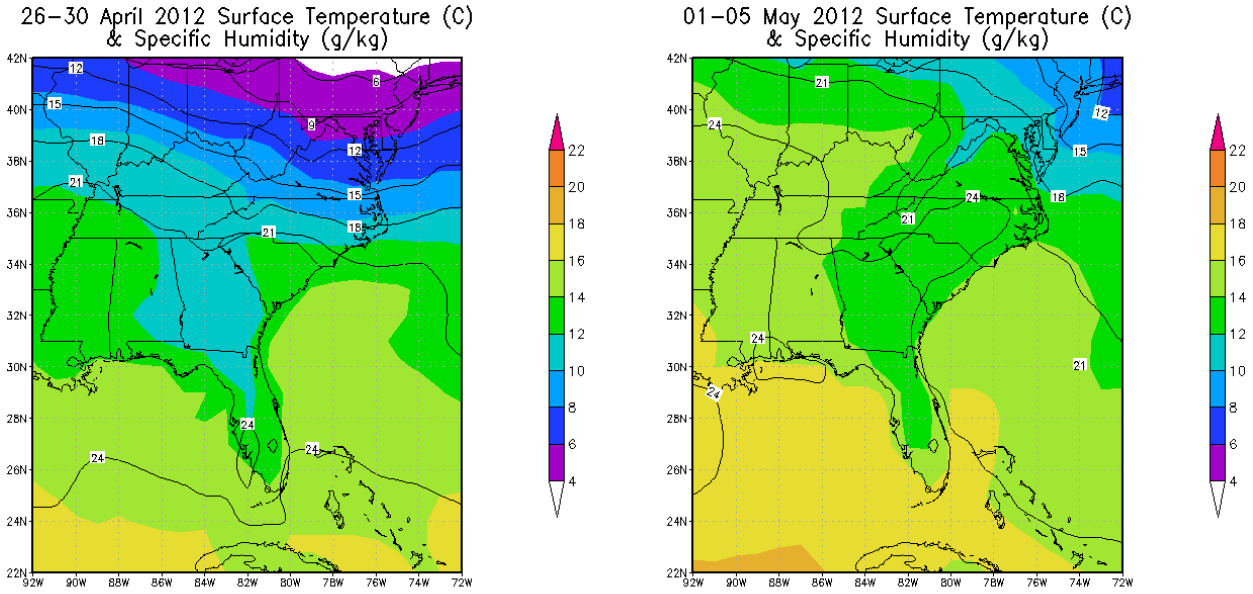

Figure 61: Specific humidity (g/kg, filled) and temperature (°C, contoured) for 26-30 April and 1-5 May 2012.

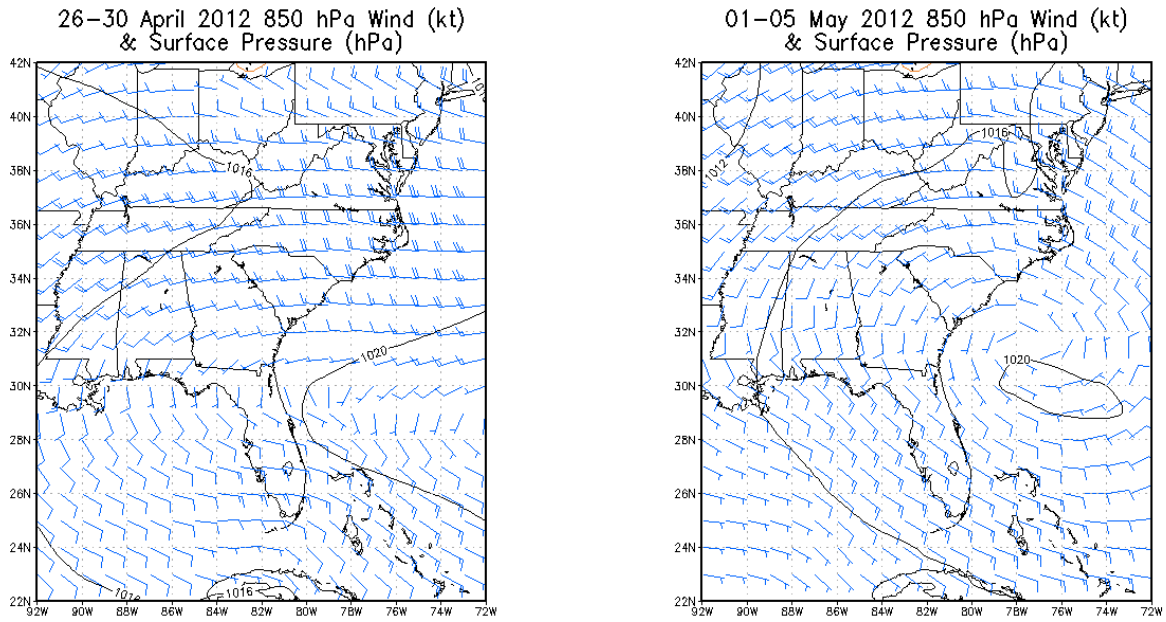

Figure 62: As in Fig. 61, but for MSLP (hPa) and 850 hPa winds (kt).

the NASH is concentrated over the Gulf Coast and Georgia. In the following pentad (1-5 May), the NASH shifts northward and eastward so the western ridge of the NASH is located more directly over the SE US (Fig. 62) and continues to bring warm, moist air from the Gulf of Mexico into the SE US in the beginning of May. At the same time that the NASH sets up over the SE US, an upper-level trough is present over the SE US for the final pentad of April and first pentad of May (Fig. 63), which then shifts to a weak zonal pattern by the second pentad of May.

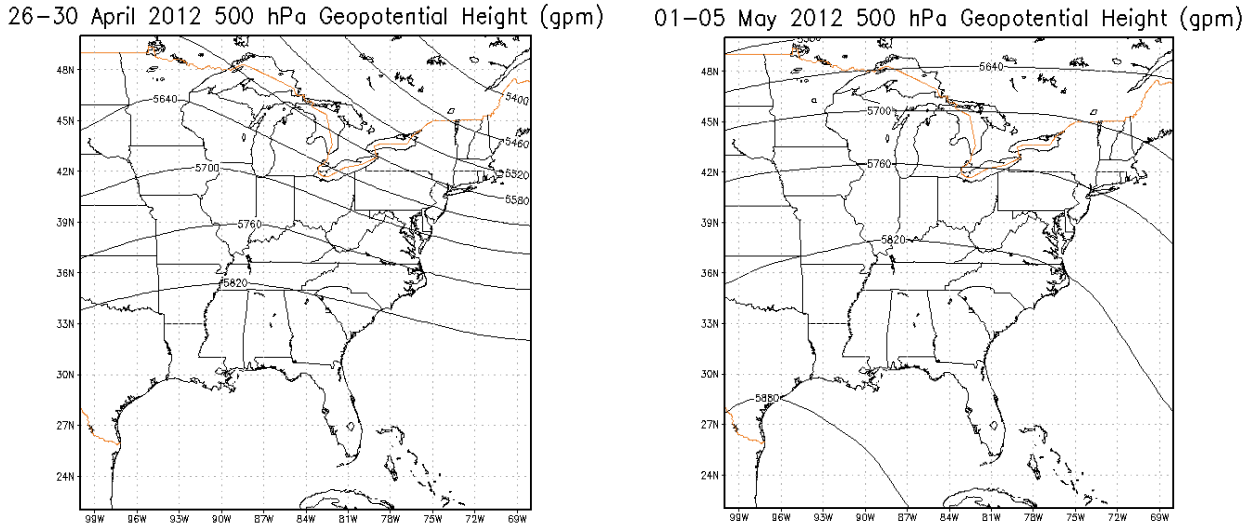

Figure 63: As in Fig. 61, but for 500 hPa geopotential height (gpm).

With the re-establishment of the NASH and onset occurring in the SE US, IPF rain increases during this period and after over the SE US. The NASH continues to show episodic behavior, as the NASH breaks down for the remainder of May and beginning of June as a series of 500 hPa troughs move through the SE US, and it becomes re-established and generally stays over the area for part of June and most of July (not shown). The combination of the NASH establishing itself at the end of April and early May, along with the increasing CAPE and specific humidity at the end of April and beginning of May work together to aid in causing onset in the SE US.

In the northwestern region of the SE US, onset occurs in early June. In the first pentad of June, there is a bit of CAPE over the region (700-1000 J/kg), which then recedes in the following pentad (not shown). During the third pentad of June, when onset occurs in this region, CAPE increases over the area to 500-1000 J/kg (Fig. 65). At the same time, specific humidity decreases from the first to second pentad of June, as did CAPE, then increases to 12-16 g/kg during the pentad of onset over the northwestern area of the SE US (Fig. 64). However, the NASH is not present over the northwestern boxes, nor is the NASH established at all over the SE US in the

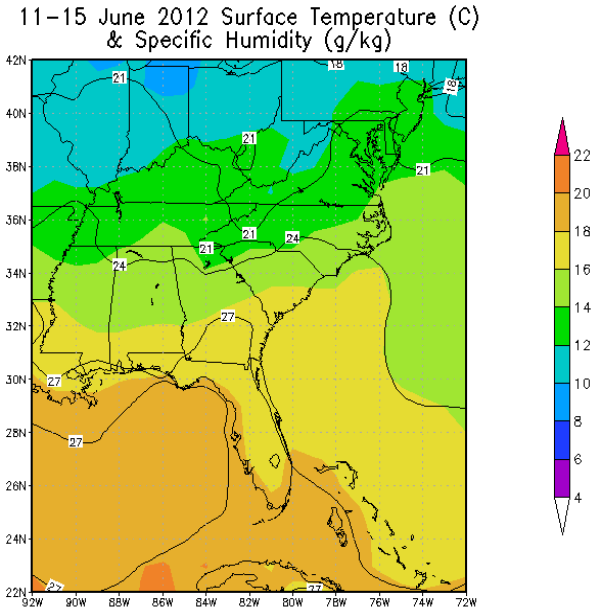

Figure 64: Specific humidity (g/kg, filled), and temperature (°C, contoured) for 11-15 June 2012.

pentads leading up to and during onset in this area. However, a weak upper-level ridge does become established over the SE US in the second and third pentads of June (not shown). In this area, onset is likely the result of increasing values of CAPE and specific humidity, and these increases in specific humidity and CAPE are likely due to the gradual warming that happens in the late spring and early summer.

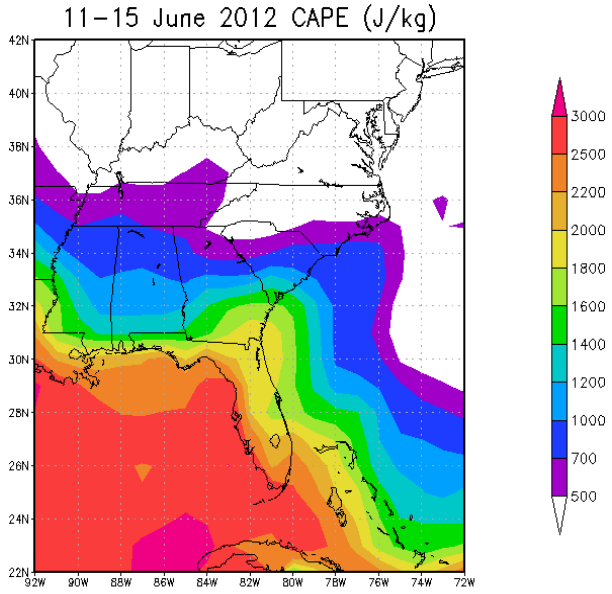

Figure 65: As in Fig. 64, but for CAPE (J/kg).

5.7 Similarities in Onset Behavior

After studying onset in each year for 2009 – 2012, there are some similarities as to what happens dynamically and thermodynamically around onset each year, despite the fact that onset happens at a different time in each year. Firstly, the NASH tends to set up over the SE US in the one to two pentads preceding onset in each year. The NASH also tends to stay established over the SE US during the first pentad of onset over the area. This behavior of the NASH indicates that the establishment of the NASH over the SE US before onset begins is important, likely because the southerly and southwesterly flow associated with the NASH provides ample moisture and warm air, thus helping to prime the atmosphere for onset to begin in the SE US.

Another similarity in onset behavior is that CAPE tends to have a drastic and sudden increase from the pentad before onset begins to the first one to two pentads of onset. These drastic increases in CAPE are sometimes associated with the upper-level pattern transitioning from a trough to a ridge, and sometimes these sudden increases in CAPE are more associated with the establishment of the NASH. In each year around the pentad where onset occurs, CAPE quickly increases, usually during the pentad of onset, from being around or below 500 J/kg, to values often exceeding 1500 J/kg, indicating that instability appears to increase rapidly in the SE US at the time of onset. Similar to CAPE, specific humidity increased during the pentad of onset in each year, though the increase was not as drastic as the increase in CAPE. Specific humidity tends to increase more gradually, and it usually begins this increase in the one to two pentads before onset, with a slightly more considerable increase in specific humidity during the pentad of onset. Specific humidity will often increase from 8-12 g/kg before onset to 14-16 g/kg or higher during the pentad of onset and after. The behavior of specific humidity over the four years indicates that moisture in the SE US seems to increase more gradually, at least when compared to how quickly CAPE increases.

Another similarity to note is the general presence of a 500 hPa ridge or zonal flow over the SE US during the periods of onset. This is important because the ridge or zonal flow helps the NASH stay established over the SE US, and the disruption of the NASH is often associated with the upper-level pattern shifting from a ridge to a trough. With these similarities in the dynamic and thermodynamic variables at the time of onset in each year, it appears that the establishment of NASH in the pentad immediately before onset, and during the first pentad of onset, works with the increasing CAPE and more gradually increasing levels of specific humidity in the SE US play a role in triggering onset in the SE US, with the presence of a ridge or zonal

flow in the upper levels aiding in the NASH staying established over the SE US. In some years, the NASH will first become established over the SE US before onset occurs. However, when that happens, specific humidity and CAPE levels are still fairly low over the SE US. This indicates that for onset to occur in the SE US, not only does the NASH generally need to be established in the SE US, but there also needs to be higher levels of CAPE and specific humidity present to trigger onset. Even in 2011, when onset was much later than the other three years, the establishment of the NASH, coupled with increasing levels of CAPE during early June were still needed to trigger onset in the SE US.

Table 10 shows the monthly mean position of the NASH for 2009-2012. It shows the westward expansion of the NASH, with the NASH moving westward from April to July. From April to May, the NASH moves from being in the Atlantic Ocean to closer to the SE US coast, and from May to June, the NASH is at nearly the same longitude, though it does move a few degrees southward. When looking at when onset occurred for the four-year average, onset largely occurs in May and June. In analyzing the four-year average of the 850 hPa winds and mean sea level pressure from NARR, this westward migration of the NASH can be observed. For much of April, the NASH, when present near the SE US, is situated further south of the SE US and further east in the Atlantic Ocean (Fig. 66). By May, the NASH expands westward and northward, with the 1016 hPa contour well over the SE US (Fig. 66). By June, the NASH shifts southward, though it stays at a similar longitude as it is at in May (Fig. 66). In the four-year average of the IPF precipitation data, onset occurs largely in May to mid-June, when the NASH is shifting westward and becoming established over the SE US.

Month	Longitude	Latitude
April	70.126°W	28.921°N
May	75.898°W	31.215°N
June	76.848°W	27.641°N
July	91.946°W	30.728°N

Table 10: Monthly mean longitude and latitude of the NASH for 2009-2012.

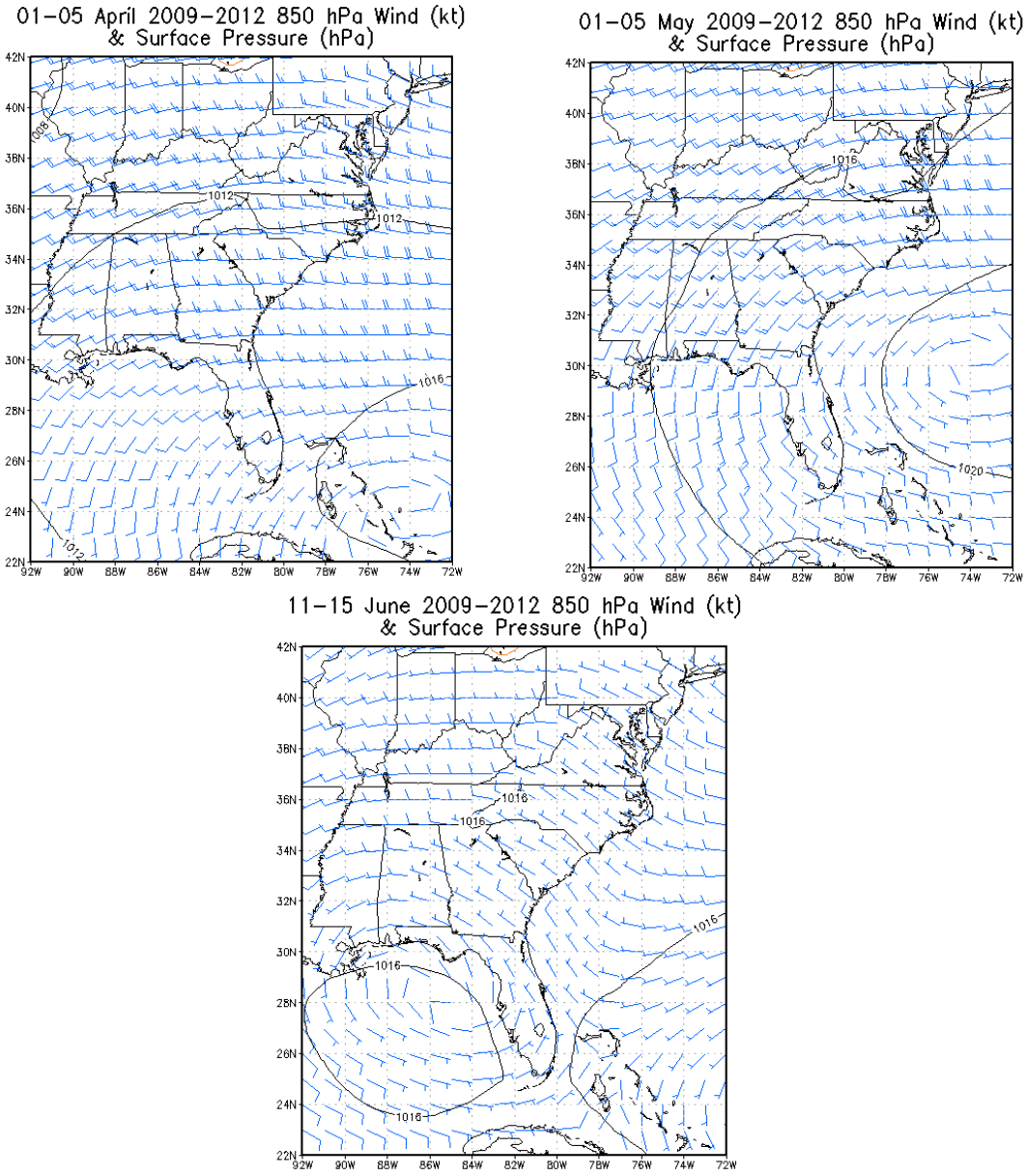

Figure 66: Four-year average of 850 hPa wind (kt) and mean sea level pressure (hPa) for 01-05 April, 01-05 May, and 11-15 June 2009-2012.

CHAPTER 6: CONCLUSIONS

This project examined possible dynamic and thermodynamic mechanisms that cause the springtime onset of the convective season in the SE US, using the MPF/IPF precipitation organization framework to analyze onset. The precipitation cycle in the SE US, along with how the atmosphere changes dynamically and thermodynamically in the spring have been studied independently, but how these mechanisms work to cause the abrupt springtime shift in IPF rain had not been studied. An objective method for determining onset of the convective season in the SE US was created, and three sensitivity tests related to determining onset were also evaluated. The meteorological conditions leading up to and immediately following onset were examined to determine possible onset mechanisms. The initial hypothesis for the cause of IPF onset is that the NASH becomes well established in late spring or early, priming the atmosphere for onset as levels of CAPE and specific humidity increase in the southerly low-level wind circulation associated with the western ridge of the NASH.

The date of onset of the convective season in the SE US was objectively determined based on the IPF precipitation in each 2°x2° box. Using the criteria, onset was determined in each box for 2009 – 2012 and the four-year average. As the results of the three sensitivity tests show, the date of onset in the SE US is sensitive to the criteria used to determine onset. Depending on the criteria used, onset can occur earlier or later, or not occur at all. The criteria used to determine onset in the SE US is better than the criteria used in the sensitivity tests at determining onset. This is because the onset criteria is relative to the amount of IPF rain received in each box, and is an important feature for the onset criteria to capture as IPF rain is rather variable in both amount and behavior across the SE US. With the criteria used to determine onset in the SE US, there was no progression of onset across the region. An initial

hypothesis for the behavior of onset was that it would occur in the south first, over Florida, and then progress northward. However, after determining onset in all boxes for each year, there was no discernible consistent pattern or progression of regional differences in onset across the SE US. An analysis of the time series of IPF in each box over the SE US shows IPF varies greatly. Despite this variability, there are still some noticeable patterns in IPF behavior in the SE US. The southern boxes are more likely to exhibit an abrupt increase in IPF precipitation in May or June, whereas boxes further north in the SE US have no clear and systematic increase, and are more characterized by larger individual IPF events.

Analysis of the NARR data shows potential dynamic and thermodynamic mechanisms that cause onset in the SE US. When analyzing CAPE, specific humidity and temperature, and MSLP and 850 hPa winds, it was determined that the same kinds of changes were occurring in the pentads immediately before and during onset. These changes relate to the NASH extending over the SE US, along with increases in CAPE and specific humidity. The NASH generally establishes itself over the SE US in at least the pentad before onset occurs. This establishment of the NASH immediately before and during onset happened in each year, indicating that the south/southwesterly flow produced by the NASH plays an important role in triggering onset. In 2011, when onset occurred much later than in the other three years, the NASH was present over the SE US for parts of April, and did not re-establish over the SE US again until the end of May, when onset finally occurred for much of the region, further indicating that the NASH plays an important role in triggering onset. At the same time, CAPE rapidly increases over the SE US during the pentad of onset, while specific humidity increases more gradually during onset. The southwesterly flow of the NASH leads to warm and moist air advection over the SE US, and this helps to prime the atmosphere for onset, with the increasing levels of CAPE and specific

humidity aid in triggering onset. The episodic and sometimes rapid increases in CAPE appear to be related to both the establishment of the NASH, and when the upper-level pattern shifts from troughing to ridging, as both the NASH and an upper-level ridge bring warm and moist air into the SE US. It also seems that the presence of an upper-level ridge or zonal flow is important at onset, as it aids in the NASH staying established over the SE US. An upper-level ridge or zonal flow combined with the moist and warm air advection from the NASH favor the development of IPF, whereas large-scale divergence associated with an upper-level trough would favor the development of MPF. Along with that, zonal flow or a ridge in the upper levels also favor the establishment of the NASH as there is nothing (such as a midlatitude cyclone or trough) that could disrupt the NASH. The boxes in the northwestern area of the SE US often had onset occur in April, and in this part of the region, that was likely due to an upper-level trough, which suggests that midlatitude cyclones may influence onset farther north and prior to the summer warmth of late May.

Onset in the SE US appears to be different from onset in monsoon regions, where in the monsoon regions, onset is generally characterized with very little or no rain before onset and large amounts of precipitation afterward, and a threshold amount of precipitation being exceeded on onset. Since the SE US receives rain year-round, onset here is referring to the change in IPF precipitation in the SE US during the late spring and early summer. However, onset is still an applicable term to use, as onset of IPF indicates a date where a precipitation threshold for IPF is exceeded after that date, and IPF continues to increase in amount and frequency of events after onset. However, unlike other monsoon regions where onset occurs rapidly, onset in the SE US does not occur very rapidly. In the South American monsoon region, stationary fronts will establish over the period of a few days and trigger monsoon onset. However, in the SE US, with

the NASH appearing to be primary onset mechanism, onset is not rapid as the NASH can take multiple pentads to establish and cause onset.

Though the results of this research have begun to provide a different way to understand the precipitation cycle in the SE US, it will be necessary in the future to expand this analysis of the onset of the convective season in the SE US to more than just the four years presented here to determine if the same meteorological changes that occurred in these four years hold true for a longer time frame. It will also be useful to expand upon the meteorological variables presented here in analyzing onset to determine if more meteorological variables have a role in causing onset in the SE US. Finally, while there is no evidence of the existence of a true monsoon in the SE US, the onset of the convective season does share some similarities with onset of the monsoon in South America and other regions of the world (such as the rapid increase in IPF in May and June). Therefore, using the monsoon framework (methods of determining onset, what triggers onset, etc.) to study the onset of the convective season is useful in further understanding the connection between precipitation variability and the large-scale seasonal changes in the atmosphere.

REFERENCES

Adams, D.K., A.C. Comrie, 1997: The North American Monsoon. *Bulletin of the American Meteorological Society, 78* (10), pp. 2197-2213.

AMS Glossary, 2018: Convective Available Potential Energy, American Meteorological Society. Accessed 26 May 2018, http://glossary.ametsoc.org/wiki/Convective_available_potential_energy

Climate Prediction Center: Cold & Warm Episodes by Season. Accessed 18 June 2018, http://origin.cpc.ncep.noaa.gov/products/analysis_monitoring/ensostuff/ONI_v5.php.

Curtis, S., and S. Hastenrath, 1995: Forcing of Anomalous Sea Surface Temperature Evolution in the Tropical Atlantic During Pacific Warm Events. *Journal of Geophysical Research, 100*, 15,835-15,847.

Davis, R.E., B.P. Hayden, D.A. Gay, W.L. Phillips, G.V Jones, 1997: The North Atlantic Subtropical Anticyclone. *J. Climate, 10*(4), 728-744.

Diem, J.E., 2006: Synoptic-Scale Controls of Summer Precipitation in the Southeastern United States. *Journal of Climate, 19* (4), pp. 613-621.

Gadgil, S., 2003: The Indian Monsoon and Its Variability. *Annual Review of Earth and Planetary Sciences, 31*. 429-467.

Garreaud, R., 2000: Cold air incursions over subtropical South America: Mean structure and dynamics. *Monthly Weather Review, 128*(7), pp.2544-2559.

Giannini, A., Y. Kushnir, M.A. Cane, 2000: Interannual Variability of Caribbean Rainfall, ENSO, and the Atlantic Ocean. *Journal of Climate, 13,* 297-311.

Henderson, K.G., A.J. Vega, 1996: Regional Precipitation Variability in the Southeastern United States. *Phys. Geogr., 17*, 93-112.

Higgins R.W., Y. Yao, X.L. Wang, 1997: Influence of the North American Monsoon System on the US Summer Precipitation Regime. *J. Climate, 10* (10), pp. 2600-2622.

Houze, R., 1989: Observed Structure of Mesoscale Convective Systems and Implications for Large-Scale Heating. *Q. J. Roy. Met. Soc., 115,*425-461.

Leathers, D.J., B. Yarnal, M.A. Palecki, 1991: The Pacific/North American Teleconnection pattern and the United States Climate. Part I: Regional Temperature and Precipitation Associations. *J. Climate, 4*(5), 517-528

Li, W., L. Laifang, R. Fu, Y. Deng, H. Wang, 2011b: Changes to the North Atlantic Subtropical High and Its Role in the Intensification of Summer Rainfall Variability in the Southeastern United States. *J. Climate, 24*, 1499-1506.

Marengo, J.A., B. Liebmann, V.E. Kousky, N.P. Filizola, I.C. Wainer, 2001: Onset and End of the Rainy Season in the Brazilian Amazon Basin. *J. Climate, 14*, 833-852.

Mesinger, F., and Coauthors, 2006: North American Regional Reanalysis. *Bull. Amer. Meteor. Soc.*, 343-360

Nesbitt, S.W., R. Cifelli, S. Rutledge, 2006: Storm Morphology and Rainfall Characteristics of TRMM Precipitation Features. *Weather Rev., 134*, 2702-2721.

Nieto-Ferreira, R., T.M. Rickenbach, 2011: Regionality of Monsoon Onset in South America: a Three – Stage Conceptual Model. *Int. J. Climatol., 31*, 1309-1321.

Nieto-Ferreira, R., T.M. Rickenbach, E.A. Wright, 2011: The Role of Cold Fronts in the Onset of the Monsoon Season in the South Atlantic Convergence Zone. *Q. J. Roy. Met. Soc. 137*, 908-22.

Prat, O.P., B.R. Nelson, 2014: Characteristics of Annual, Seasonal, and Diurnal Precipitation Derived from Long-Term Remotely Sensed Data. *Atmos. Res. 144*: 4-20.

Rickenbach, T.M., R. Nieto-Ferreira, C. Zarzar, B. Nelson, 2015: A Seasonal and Diurnal Climatology of Precipitation Organization in the Southeastern United States. *Q. J. Roy. Met. Soc., 141*, 1938-1956.

Ropelewski, C.F., M.S. Halpert, 1986: North American Precipitation and Temperature Patterns Associated with the El Niño/Southern Oscillation (ENSO). *Monthly Weather Review., 114*, 2352-2362.

Seager, R., R. Murtugudde, R., N. Naik, A. Clement, N. Gordon, J. Miller, 2003: Air-Sea Interaction and the Seasonal Cycle of the Subtropical Anticyclones. *J. Climate, 16*(12), 1948-1966.

Storm Prediction Center: SPC Storm Reports for 04/04/11. Accessed 24 June 2018, https://www.spc.noaa.gov/exper/archive/event.php?date=20110404.

Wang, B., L. Ho, 2002: Rainy Season of the Asian-Pacific Summer Monsoon. *J. Climate, 15*, 386-398.

Zhang, J., Howard, K., Langston, C., Vasiloff, S., Kaney, B., Arthur, A., Dempsey, C. 2011: National Mosaic and Multi-Sensor QPE (NMQ) system: Description, results, and future plans. *Bull. Amer. Meteor. Soc., 92*(10), 1321-1338.